Solar Energetic Particles

Donald V. Reames

Institute for Physical Science and Technology

University of Maryland

College Park, MD, USA

To be published by Springer ~March 2017
Submitted October 2016

Preface

It is common for scientific texts to be organized in logical rather than historical order. Unfortunately, perhaps, nature does not always proceed in that fashion. In an actively evolving field, new ideas and observations build slowly, step by step, often reversing course, and a student should be prepared for this. Therefore, I have included much of the backing and filling, and the individual observations which have led to our present understanding.

In reading this book, it is important to keep in mind that a realistic understanding must incorporate *different kinds* of observations. No single inquiry will suffice. Like reading a murder mystery, it is normal to speculate along the way, but we must eventually consider all the evidence, which is not available early in the story. There are many pieces of evidence, of many different kinds, in this mystery. There is now a wealth of evidence on abundances of chemical elements and isotopes and their ionization states, and much on electrons; there is onset timing, radio evidence, and the streaming limit; there are injection profiles, intensity dropouts, energy spectral shapes, spectral knees, and particle reservoirs, in addition to the solar associations. All of these help us find the origin, acceleration, distribution and transport of the solar energetic particles (affectionately SEPs). This has become a rich field. Unlike the murder mystery, however, our hard-won understanding also raises new questions for future scientists to address.

The story of SEPs is actually covered in five chapters. Chapter 1 provides a background and an introduction to SEP properties. Chapters 2 and 3 present the history and much of the physical evidence for the separation of impulsive and gradual SEP events. Chapters 4 and 5 consider properties of each of these classes individually. The later chapters provide supplementary information on high energies and radiation hazards of SEPs (Chapter 6), on SEP measurements (Chapter 7), and a Summary and Conclusions (Chapter 8).

I hope students of SEPs will enjoy reading this book as much as I have enjoyed writing it.

Don Reames

Acknowledgments

First, I would like to thank those scientists who have contributed their efforts to the progress of this field and those who have contributed the figures I have used to illustrate their discoveries.

Special thanks go to Louis Barbier, Daniel Berdichevshy, Ed Cliver, Steve Kahler, Mary Ann Linzmayer, Chee Ng, Ron Turner, and Gary Zank for reading and commenting on this manuscript and for helpful discussions leading to its preparation. I would especially like to thank Chee Ng for his assistance with the theory of particle transport, wave growth, and shock acceleration.

About the Author

Born and raised in Florida, Don Reames received his education, leading in 1964 to a PhD in Nuclear Physics, at the University of California at Berkeley. He then joined a group at NASA's Goddard Space Flight Center in Maryland using sounding rockets and balloons to study galactic cosmic rays and energetic particles from the Sun. He subsequently used data from experiments on the *Gemini*, IMP, ISEE, *Helios*, *Voyager*, *Wind* and STEREO missions, as well as many related solar missions, to study those particles and their origins more extensively. He retired from NASA in 2003 to assume an Emeritus position, but also soon joined the Institute for Physical Science and Technology at the University of Maryland in College Park to become a Senior Research Scientist. His honors include the 2012 George Ellery Hale Prize from the Solar Physics Division of the American Astronomical Society for his work on the composition and transport of solar energetic particles.

Contents

List of abbreviations

CME	Coronal mass ejection
DH	Decametric-hectometric (radio-emission frequencies)
DSA	Diffusive shock acceleration
EMIC	Electromagnetic ion cyclotron (plasma waves)
ESA	*European Space Agency*
FIP	First ionization potential
GCR	Galactic cosmic ray
GLE	Ground-level event, Ground-level enhancement event
GSFC	Goddard Space Flight Center
ICME	Interplanetary CME
LSSA	Large-scale shock acceleration
NASA	*National Aeronautics and Space Administration*
NOAA	*National Oceanic and Atmospheric Administration*
QLT	Quasi-linear theory
SEP	Solar energetic particle
SPR	Solar particle release (time at the Sun)
TAC	Time-to-amplitude converter
UV	Ultraviolet

Instruments:

AIA	*Atmospheric Imaging Assembly*, on SDO
AMS	*Alpha Magnetic Spectrometer,* on *International Space Station*
EIT	*Extreme-Ultraviolet Imaging Telescope*, on SOHO
EPS	*Energetic-Particle Sensor*, on GOES
LASCO	*Large-Angle and Spectrometric Coronagraph*, on SOHO
HEPAD	*High-Energy Proton and Alpha Detector*, on GOES
LEMT	*Low-Energy Matrix Telescope*, on *Wind*
SIS	*Solar Isotope Spectrometer*, on ACE
SIT	*Suprathermal Ion Telescope,* on STEREO
STEP	*SupraThermal Energetic Particle*, on *Wind*
ULEIS	*Ultra Low-Energy Isotope Spectrometer*, on ACE

Spacecraft:

ACE	*Advanced Composition Explorer*
GOES	*Geostationary Operational Environmental Satellites*
IMP	*Interplanetary Monitoring Platform*
ISEE	*International Sun-Earth Explorer*
PAMELA	*Payload for Antimatter Exploration and Light-nuclei Astrophysics*
SDO	*Solar Dynamics Observatory*
SOHO	*Solar and Heliospheric Observatory*
STEREO	*Solar Terrestrial Relations Observatory*

1. Introduction

Abstract The structure of the Sun, with its energy generation and heating, creates convection and differential rotation of the outer solar plasma. This convection and rotation generates the solar magnetic field. The field and its variations spawn all of the solar activity: solar active regions, flares, jets, and coronal mass ejections (CMEs). Solar activity provides the origin and environment for both the impulsive and gradual solar energetic particle (SEP) events. This chapter introduces the background environment and some basic properties of SEP events, time durations, abundances, and solar cycle variations.

We tend to think of the Sun as an image of its disk. Recent years have brought increasingly sophisticated images of that disk in single spectral lines and images of active emissions from its corona. However, we have no such images of solar energetic particles (SEPs). In a photon-dominated discipline, SEPs are stealthy and obscure; they do not brighten the solar sky. While photons travel line-of-sight, SEPs are guided out to us along magnetic field lines. We must identify, measure, and count SEPs one by one. Only in recent years have we overcome the limitations so our observations now begin to bear richer fruit. This is the story of that development.

Solar energetic particles (SEPs) come as bursts of high-energy particles from the direction of the Sun lasting for hours or sometimes days. The particle energies range from about 10 keV (kilo electron volts) to relativistic energies of several GeV, particle speeds 90% of the speed of light. In addition to the dominant protons and electrons, most of the other chemical elements from He through Pb have now been measured. The relative abundances of these elements and their isotopes have been a powerful resource in our quest for understanding of the physical processes of acceleration and interplanetary transport of SEPs.

In this chapter we introduce properties of SEPs after reviewing some properties of the solar and interplanetary environment in which they are found.

1.1 The Structure of the Sun

With a mass of 1.989×10^{33} g, the Sun consists of gaseous, ionized plasma where the inner *core* (see Figure 1.1) reaches temperatures of 15 million degrees Kelvin (MK) where some of the protons have enough energy to tunnel the Coulomb barrier of the nuclear charge. As they penetrate H, C, and N nuclei, they cause the nuclear reactions that catalyze the conversion of H into He. The energy released in this process is radiated and reabsorbed as it diffuses outward across the *radiative zone*, creating sufficient heat and pressure to balance the gravitational force trying to collapse the star.

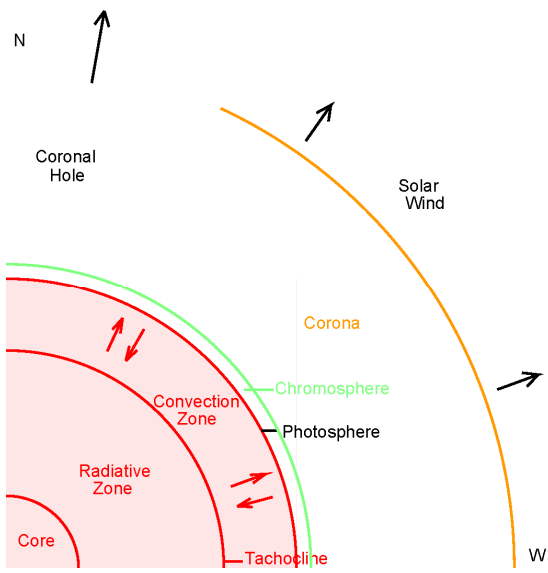

Fig. 1.1 A cross section of the Sun shows its major radial structure from the core to the evaporating solar wind. (If we look at the Sun with North at the top and South at the bottom, West is to the *right* and East to the *left*. The solar *limb* is the edge of the visible disk.)

Circulation of the hot plasma across the *convection zone* brings energy to the *photosphere*, that surface where overlying material is too thin to absorb radiation or prevent its escape out into space. Here radiation of energy cools just above the photosphere to ~4000 K. At this temperature, elements with a first ionization potential (FIP) below about 10 eV, just below that of H at 13.6 eV, remain ionized, while those with higher FIP capture and retain electrons to become neutral atoms.

Above the photosphere lies the narrow *chromosphere* where the temperature rapidly rises again to over 1 MK in the solar *corona* which extends outward another solar radius or so. The corona is probably heated by absorption of Alfvén waves, plasma waves created in the turbulent layers below, and is largely contained by closed magnetic loops. The outer layer of the corona evaporates to become the 400 – 800 km s^{-1} *solar wind* which continues to blow past the Earth at 1 AU and far beyond the planets to nearly 100 AU. Properties of the solar wind were predicted by Parker (1963) before it was observed.

Inside the *tachocline*, which lies at the base of the convective zone, the Sun rotates like a rigid body, but throughout the convective zone the Sun rotates *differentially*, faster at the equator than at the poles. The sidereal period of solar rotation at the equator is 24.47 days but it is 25% longer at latitude 60^{o}. Azimuthal surfaces of constant rotation-speed run radially through the convection zone forming conical shells about the rotation axis that extend only to the tachocline and not to their apex at the center of the Sun.

1.2 The Solar Magnetic Field

The Sun has a magnetic field that is generally dipolar in nature, although its origin is still not perfectly understood (see Parker 2009; Sheeley 2005). Magnetic fields,

produced in the extreme rotational sheer at the tachocline, are buoyant and produce omega (Ω) loops that rise through the convection zone and emerge through the photosphere to form *sunspots* and *active regions* (Figure 1.2) as they are sheared and reconnected by the *differential rotation*. Active regions tend to occur at mid-latitudes on the Sun where the effect of differential rotation on field generation is greatest. When oppositely directed fields reconnect in a largely collisionless regime of the corona, the magnetic energy can be converted to energy of SEPs, with especially copious electrons. On closed magnetic loops, this can result in sudden heating and X-ray production, mainly by electron Bremstrahlung, which is seen as a solar *flare*. Similar reconnection on *open* field lines, *jets*, can release electrons and ions into space, *i.e.* accelerate an impulsive SEP event, without the trapping or heating, as we shall see. As electrons stream out along open field lines they produce fast-drift type-III radio bursts.

Figure 1.2 shows an image of the Sun in ultraviolet (UV) light taken by the *Atmospheric Imaging Assembly* (AIA) on the NASA spacecraft *Solar Dynamics Observatory* (SDO; http://sdo.gsfc.nasa.gov/). Complex, bright areas in Figure 1.2 are active regions while the large dark region on the solar image is a *coronal hole*. Coronal holes, often seen near the poles, are regions of *open* magnetic field lines extending into the outer heliosphere, stretched out by the plasma of the solar wind. The bright regions contain locally *closed* field lines, *i.e.* loops, where any accelerated particles are contained and interact so that heating is greatly increased.

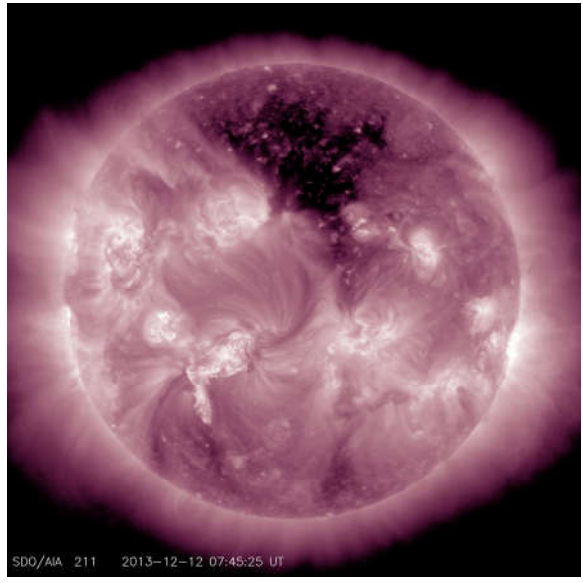

Fig. 1.2. An image of the Sun in 211 Å UV light, taken by the *Atmospheric Imaging Assembly* on the *Solar Dynamics Observatory*, shows brightening of magnetically-complex active regions and a large, dark coronal hole.

Of course, Maxwell's Equations tell us that *all* magnetic-field lines are *closed*. However, some field lines are drawn far out into the outer heliosphere by CMEs and the solar wind. For purposes of energetic-particle flow, we describe those field lines as *open* if they can conduct charged particles out from the Sun to an observer at or beyond Earth.

The direction of the solar dipolar magnetic field reverses in a cycle of one reversal in about 11 yr and solar activity increases as the field reverses. Solar minima occur when the field axis is aligned with the solar rotation axis, in one polarity or the other, and the number and size of active regions decreases dramatically. Solar maxima occur during intermediate times and the Sun appears as in Figure 1.2 late in 2013. During solar minimum the northern hemisphere contains nearly radial field lines of one polarity while the southern hemisphere contains the other; the hemispheres are separated by a plane (or wavy) current sheet, between the opposite field polarities, extending out into interplanetary space near the equator. High-speed solar wind (~700–800 km s^{-1}) emerges from the polar coronal holes.

1.3 Coronal Mass Ejections (CMEs)

Magnetic reconnection can lead to the ejection of large filaments containing 10^{14} – 10^{16} g mass and helical magnetic field with total kinetic energies of 10^{27} – 10^{32} ergs, carrying most of the energy in solar eruptions. CME speeds can be as low as that of the solar wind or can exceed 3000 km s^{-1}. Figure 1.3 shows a large CME imaged by the *Large Angle and Spectrometric Coronagraph* (LASCO) on the *Solar and Heliospheric Observatory* (SOHO; http://sohowww.nascom.nasa.gov/) with a 304 Å image from the *Extreme Ultraviolet Imaging Telescope* (EIT) near the same time scaled onto the coronagraph occulting disk. CME theory and models have been reviewed by Forbes *et al.* (2006).

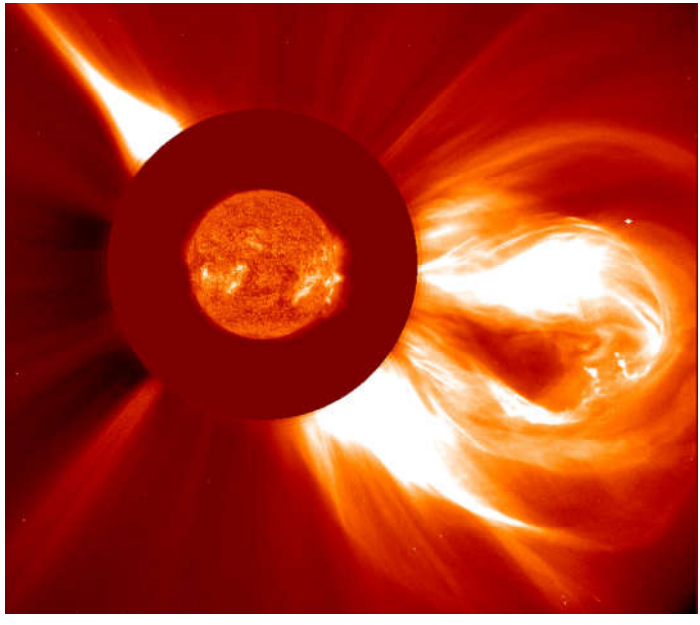

Fig. 1.3. A composite image from the EIT and LASCO telescopes on the NASA/ESA SOHO spacecraft shows a large CME being ejected to the southwest.

Filaments are irregular linear structures of cool, dense, chromospheric plasma magnetically suspended in the corona lying parallel to the solar surface, supported at oppositely-directed magnetic fields beneath an arcade of coronal loops (Martin 1998). They appear dark in Hα images and can hang above the photosphere for days. Filaments that project beyond the solar limb are called *prominences*. Filaments are often ejected as the core of CMEs. In some cases filaments that are present for many days, are suddenly ejected as a CME. These *disappearing-filament* events may drive shock waves and produce SEPs but they lack an associated flare.

When the speed of a CME exceeds the speed of waves in the plasma of the corona or solar wind, it can drive a collisionless shock wave. We will see that fast shock waves are the primary source of acceleration of the largest SEP events.

A bright *streamer* is seen in the upper left (northeast) corner of Figure 1.3, opposite the CME. Streamers are the magnetic structures stretched behind CMEs after they move out into the heliosphere. As such, they represent newly opening field lines and contribute to the slow (~400 km s^{-1}) solar wind, although the source of the slow solar wind is not fully resolved (*e.g.* Antiochos *et al.* 2011). Thus, out-flowing CMEs contribute to the average magnetic field in the heliosphere, which is larger following strong, active solar cycles than weak ones.

1.4 Interplanetary Space

The solar wind expands nearly radially outward from the Sun carrying plasma and magnetic field. The solar-wind speed remains approximately constant with distance from the Sun. As the Sun rotates, the field line connected to a given point on its surface is drawn into a spiral pattern, the Parker spiral. In the inner heliosphere, the plasma density and magnetic-field strength decrease approximately as r^{-2} with distance r, from the Sun, and as $B \sim r^{-1.5}$ by 1 AU (Burlaga, 1995, 2001).

Near Earth the typical magnetic field B is ~10 nT, the typical plasma density is ~10 particles cm^{-3}, and the electron plasma frequency, which varies with the electron density, n_e, as $n_e^{1/2}$, is ~30 kHz. The solar radius, $R_s = 6.96 \times 10^8$ m = 696 Mm, and the Earth-Sun distance, 1 AU, is 1.50×10^{11} m = 216 R_s, often a useful number. In this spirit, plasma in the 400 km s^{-1} solar wind takes 4.3 days to travel 1 AU, a shock wave with an average speed of 1700 km s^{-1} takes one day, a 10 MeV proton or a 5 keV electron takes an hour, and a photon of light takes 8.3 min. Thus, it is not surprising that particles accelerated by a shock wave near the Sun arrive near Earth long before the arrival of the shock itself.

The plasma beta, $\beta_P = \rho kT/(B^2/8\pi)$, where ρ is the density and T the temperature, is the ratio of thermal to magnetic energy density. When $\beta_P < 1$, the field controls the plasma and B is smooth and uniform, when $\beta_P > 1$, the field becomes variable and distorted by plasma turbulence. The internal structure of CMEs is dominated by magnetic field energy, with $\beta_P < 1$.

Alfvén waves propagate through plasma with correlated variations in B and the plasma density ρ with a speed $V_A = B/(4\pi\rho)^{1/2}$. In models of V_A in the solar atmosphere above an active region (*e.g.* Mann *et al.* 2003), V_A falls rapidly with height to a value of ~200 – 500 km s^{-1} at $r \approx 1.5\ R_S$, it then rises to a broad maxi-

mum of ~ 750 km s^{-1} near 4 R_S and finally decays approximately as r^{-1} out toward Earth (Mann *et al.* 2003) where it is nominally 30 km s^{-1}. However, these values depend upon assumptions about the magnetic structure of an active region. The behavior of V_A is important since the disturbance caused by a CME must exceed the speed of Alfvén waves to form a shock wave which can accelerate SEPs.

Large CMEs can be recognized in the solar wind when they pass Earth (often called ICMEs) and lists of them, with their associated coronagraphic origin, have been published (Richardson and Cane 2010). A class of particularly regular events called *magnetic clouds* is identified by a flux-rope magnetic field that spirals slowly through a large angle (Burlaga *et al.* 1981). Shock waves driven out by CMEs can also be observed near Earth and their properties can be determined (*e.g.* Berdichevsky *et al.* 2000). Lists of properties of interplanetary shock waves spanning many years are available for shocks at the *Wind* and ACE (*Advanced Composition Explorer*) spacecraft (https://www.cfa.harvard.edu/shocks/). We will see examples of shock waves later in this book.

1.5 Solar Energetic Particles

The effort to understand the physical origin of SEP events has led to the identification of two classes of SEP events, *impulsive* and *gradual* with the sources suggested by Figure 1.4 (*e.g.* Reames 1999, 2013). The history of this journey will be discussed in Chapter 2 with further physical evidence in Chapter 3. Important differences lie in abundances of elements, isotopes and e/p ratios, as we shall see.

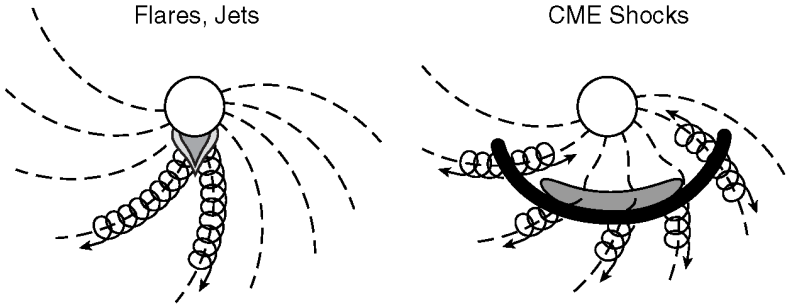

Fig. 1.4. Impulsive (left) and gradual (right) classes of SEP events are distinguished by the probable sources of particle acceleration in each case (Reames 1999). Impulsive SEP events are accelerated in magnetic-reconnection events on open field lines (*i.e.* jets) in the corona. Gradual SEP events are accelerated at shock waves (solid black) driven out from the Sun by CMEs (gray). Particles are shown as spirals along ***B*** (dashed).

The data base for many measurements from many spacecraft, including SEP intensities, from spacecraft where they were measured, is the Coordinated Data and Analysis Web site: http://cdaweb.gsfc.nasa.gov/sp_phys/. This web site has data from past and current space-physics missions.

1.5.1 Time Duration

While the terms impulsive and gradual did not originally refer to the SEP duration, it is quite often a reasonable characterization as shown by the event series in Figure 1.5.

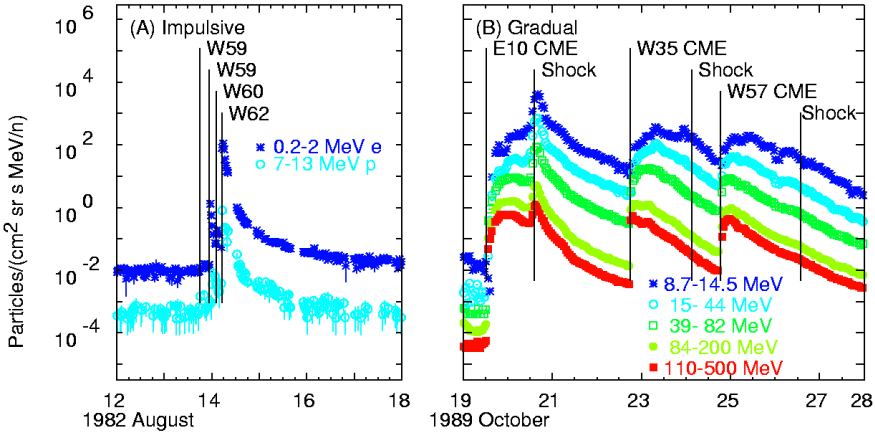

Fig. 1.5. Particle intensities are shown for a series of (A) impulsive and (B) gradual or long-duration SEP events at similar time and intensity scales. Flags labeled with the source longitude indicate the onset times of the events; also shown are the times of shock passage. Proton (or electron) energies are listed. It is difficult to obtain comparable proton energies because impulsive events are much less energetic (Reames 1999).

1.5.2 Abundances

The abundances of elements and isotopes have been powerful indicators of the origin, acceleration, and transport of SEPs. It was found (Webber 1975; Meyer 1985) that the average element abundances, in events we now call large, gradual SEP events, were a measure of the corresponding solar *coronal* abundances. These differ from abundances in the photosphere by a factor which depends on the first ionization potential (FIP) of the element as shown in Figure 1.6 and listed in Table 1.1 (Reames 1995, 2014). Low-FIP elements are ionized in the photosphere while high-FIP elements are neutral atoms. Ions are more easily transported into the corona than are neutrals (*e.g.* Laming 2009). Other measures of coronal abundances, such as in the solar wind (*e.g.* Geiss 1982), show a FIP effect that is similar but not identical (Schmelz *et al.* 2012). These SEP abundances will serve as reference abundances for all discussion of "enhancements" throughout this book.

Table 1.1 lists the photospheric (Asplund *et al.* 2009) and the reference SEP (Reames 1995, 2014) abundances that we will use. A likely correction to the reference abundance of He (He/O = 91 rather than 57), that will be discussed in Section 5.9, is shown as a red open circle in Figure 1.6. Alternative photospheric abundances by Caffau *et al.* (2011) make some difference in the FIP plot as demonstrated by Reames (2015); the differences depend on the choice of spectral lines used to obtain the photospheric abundance measurements.

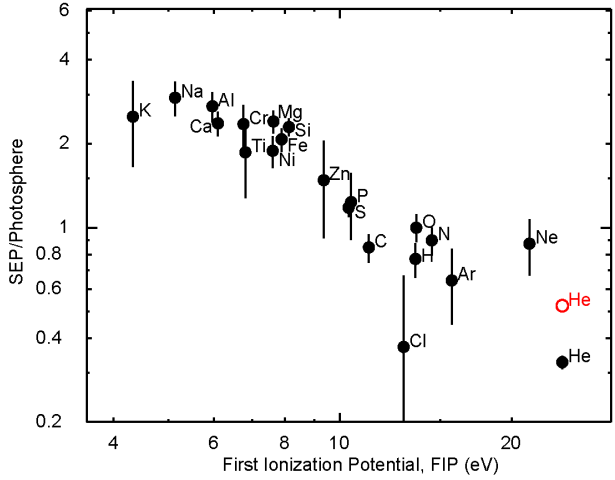

Fig 1.6. The average element abundance in gradual SEP events (Reames 1995, 2014), or reference abundance, relative to the corresponding abundance in the solar photosphere (Asplund *et al.* 2009) is plotted as a function of the FIP of the element (see text).

Table 1.1. Photospheric and SEP-Reference Abundances used in Figure 1.6

	Z	FIP [eV]	Photosphere	SEP Reference
H	1	13.6	$(2.04\pm0.05)\times10^{6}$	$(\sim1.57\pm0.22)\times10^{6}$
He	2	24.6	$(1.74\pm0.04)\times10^{5}$	57000±3000
C	6	11.3	550±63	420±10
N	7	14.5	138±16	128±8
O	8	13.6	1000±115	1000±10
Ne	10	21.6	174±40	157±10
Na	11	5.1	3.55±0.33	10.4±1.1
Mg	12	7.6	81±8	178±4
Al	13	6.0	5.75±0.40	15.7±1.6
Si	14	8.2	66.1±4.6	151±4
P	15	10.5	0.525±0.036	0.65±0.17
S	16	10.4	26.9±1.9	25±2
Cl	17	13.0	0.65±0.45	0.24±0.1
Ar	18	15.8	5.1±1.5	4.3±0.4
K	19	4.3	0.22±0.14	0.55±0.15
Ca	20	6.1	4.47±0.41	11±1
Ti	22	6.8	0.182±0.021	0.34±0.1
Cr	24	6.8	0.89±0.08	2.1±0.3
Fe	26	7.9	64.6±6.0	131±6
Ni	28	7.6	3.39±0.31	6.4±0.6
Zn	30	9.4	0.074±0.009	0.11±0.04

Abundances also distinguish *impulsive* SEP events. The earliest of these was the greatly enhanced ^{3}He/^{4}He ratio, which is ~5 × 10^{-4} in the solar wind, but can be >1 in impulsive SEP events, as seen in the examples in Figure 1.7.

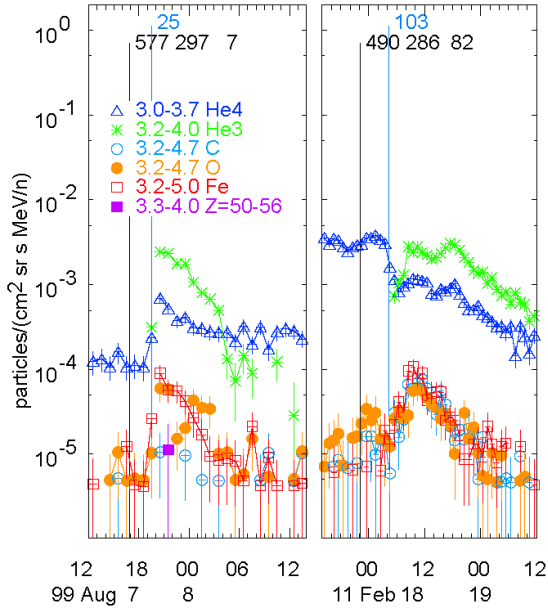

Fig. 1.7. Intensities *vs.* time are shown in impulsive SEP event numbers 25 and 103 (shown in blue flags at event onsets) from Reames, Cliver, and Kahler (2014). ^{3}He exceeds ^{4}He in these events and Fe exceeds C and O. Flags in black preceding the SEP onsets are at the associated CME onset times and list the speed (km s^{-1}), position angle (deg), and width (deg) of the CME.

These two events have event-averaged Fe/O = 1.24±0.28 and 1.34±0.20, respectively, compared with the reference value of 0.131±0.006 in Table 1.1. Enhancements of even heavier elements (*e.g.* $Z > 50$) are much greater, on average, but are difficult to measure in single small events and will be seen in Section 4.5.

1.5.3 The Solar Cycle

SEP events do not precisely follow the solar activity level of sunspots, but they do have a definite solar cycle. The upper panel of Figure 1.8 shows intensities of 120–230 MeV protons measured by the *Goddard Space Flight Center* telescope on the IMP-8 (*Interplanetary Monitoring Platform*) spacecraft. This telescope is sensitive to particles of solar and galactic origin and can observe the counter-cyclical behavior. When the Sun is active with SEP events, the greater ejection of CMEs increases the modulation that blocks and decreases the encroachment of galactic cosmic rays. The monthly sunspot number is shown in the lower panel for comparison.

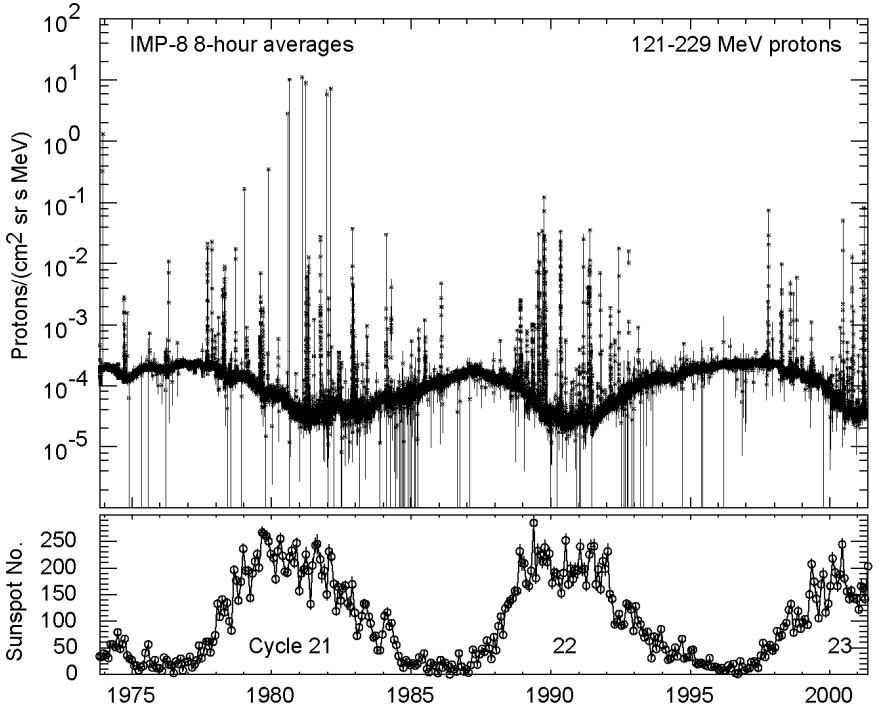

Fig. 1.8. Intensities of 120-230 MeV protons in 8-hr averages from the Goddard IMP-8 telescope are shown over 27 years in the upper panel. Spikes from individual SEP events reach a factor of 10^5 above a counter-cyclical baseline of galactic cosmic rays which the instrument also measures well. The monthly international sunspot number is shown in the lower panel for comparison.

1.5.4 Relativistic Kinematics

What we often call the particle "energy," E commonly quoted as MeV amu^{-1} is actually a measure of velocity $E = \mathcal{E}/A = M_u(\gamma - 1) \approx ½\, M_u \beta^2$, where $\mathcal{E}$ is the total kinetic energy, A is the atomic mass, $M_u = m_u c^2 = 931.494$ MeV, $\gamma = (1-\beta^2)^{-1/2}$, and $\beta = v/c$ is the particle velocity relative to the speed of light, c. Abundances of elements and isotopes are always compared at the same value of E. The total energy of a particle is $W = AM_u\gamma$ and the momentum is given by $pc = AM_u \beta\gamma$. The magnetic rigidity or momentum per unit charge is $P = pc/Qe = M_u \beta\gamma\, A/Q$ in units of MV. Note that the atomic mass unit (amu), 1/12 the mass of ^{12}C, is close enough to nucleon masses that MeV nucleon^{-1} is indistinguishable from MeV amu^{-1} for SEP studies.

We can write the Lorentz force on a single particle in the form

$$m_u \frac{d}{dt}(\gamma\, \mathbf{v}) = \frac{Q}{A} e(\mathbf{E} + \mathbf{v} \times \mathbf{B}) \qquad (1.1)$$

In a collisionless world where the electric and magnetic fields are independent of the nature of the particle, the only specific particle species dependence is Q/A.

This will be the case for most of the wave-particle interactions we will encounter during particle acceleration and transport. The exception comes when the particle interacts with matter where the electric field is that of the particle itself and depends upon Q as it scatters electrons of the stopping material. This is the case in particle detectors (Chapter 7) where the species-dependence for energy loss becomes Q^2/A. Strong enhancements observed in elements with $76 \leq Z \leq 82$ in impulsive SEPs would have been suppressed by this dependence on Q^2/A if the ions had traversed significant amounts of matter during acceleration or transport. Thus, acceleration and transport are essentially collisionless and depend upon Q/A.

Acknowledgements: We thank the SOHO and SDO projects for figures used in this chapter.

References

Antiochos, S.K., Mikić, S., Titov, V.S., Lionello, R., and Linker, J.A., A Model for the sources of the slow solar wind Astrophys. J. **731**, 112 (2011)

Asplund, M., Grevesse, N., Sauval, A.J., Scott, P., The chemical composition of the sun, Ann. Rev. Astron. Astrophys. **47**, 481 (2009)

Berdichevsky, D. B., Szabo, A., Lepping, R. P., Vinas, A. F., Mariana, F., Interplanetary fast shocks and associated drivers observed through the 23rd solar minimum by Wind over its first 2.5 years, J. Geophys. Res., **105**, 27289 (2000); Errata in J. Geophys. Res., **106**, 25133, (2001)

Burlaga, L. F., *Interplanetary Magnetohydrodynamics*, Oxford University Press, Oxford, UK (1995)

Burlaga, L.F., Magnetic fields and plasmas in the inner heliosphere: Helios results, *Planet. Space Sci.* **49**, 1619 (2001)

Burlaga, L. F., Sittler, E., Mariani, F., Schwenn, R: Magnetic loop behind an interplanetary shock: Voyager, Helios, and Imp 8 observations, J. Geophys. Res., **86**, 6673 (1981).

Caffau, E., Ludwig, H.-G., Steffen, M., Freytag, B., Bonofacio, P., Solar chemical abundances determined with a CO5BOLD 3D model atmosphere, Solar Phys. **268**, 255. (2011) doi:10.1007/s11207-010-9541-4

Forbes, T. G., Linker, J. A., Chen, J., Cid, C., Kóta, J., Lee, M. A., Mann, G., Mikic, Z., Potgieter, M. S., Schmidt, J. M., CME theory and models, Space Sci. Rev. **123**, 251 (2006)

Geiss, J., Processes affecting abundances in the solar wind, Space Sci. Rev. **33**, 201 (1982)

Laming, J. M., Non-WKB models of the first ionization potential effect: implications for solar coronal heating and the coronal helium and neon abundances, Astrophys. J. 695, 954 (2009)

Mann, G. Klassen, A. Aurass, H., Classen, H.-T., Formation and development of shock waves in the solar corona and the near-Sun interplanetary space, Astron. Astrophys. **400**, 329 (2003)

Martin, S. F., Conditions for the formation and maintenance of filaments (invited review), Solar Phys, **182**, 126 (1998)

Meyer, J. P., The baseline composition of solar energetic particles, Astrophys. J. Suppl. **57**, 151 (1985)

Parker, E.N.: *Interplanetary Dynamical Processes,* Interscience, New York (1963).

Parker, E.N.: Solar magnetism: the state of our knowledge and ignorance, Space Sci. Rev. **144**, 15 (2009).

Reames, D. V., Coronal abundances determined from energetic particles, Adv. Space Res. **15** (7), 41 (1995)

Reames, D. V.: Particle acceleration at the Sun and in the Heliosphere, Space Sci. Rev., **90**, 413 (1999)

Reames, D.V.: The two sources of solar energetic particles, Space Sci. Rev. **175**, 53 (2013)

Reames, D.V., Element abundances in solar energetic particles and the solar corona, Solar Phys., **289**, 977 (2014)

Reames, D. V., What are the sources of solar energetic particles? Element abundances and source plasma temperatures, Space Sci. Rev. **194** 303 (2015)

Reames, D.V., Cliver, E.W., Kahler, S.W., Abundance enhancements in impulsive solar energetic-particle events with associated coronal mass ejections, Solar Phys. **289**, 3817, (2014) DOI: 10.1007/s11207-014-0547-1

Richardson, I. G., Cane, H. V., Near-Earth interplanetary coronal mass ejections during solar cycle 23 (1996-2009): Catalog and summary of properties, Sol. Phys. **264**, 189 (2010)

Schmelz , J. T., Reames, D. V., von Steiger, R., Basu, S., Composition of the solar corona, solar wind, and solar energetic particles, Astrophys. J. **755**:33 (2012)

Sheeley, N. R., Jr., Surface evolution of the sun's magnetic field: a historical review of the flux-transport mechanism, Living Rev. Solar Phys., **2**, 5 (2005)

Webber, W. R., Solar and galactic cosmic ray abundances - A comparison and some comments. *Proc. 14th Int. Cos. Ray Conf, Munich*, **5**, 1597 (1975)

2. History

Abstract Large solar energetic-particle (SEP) events are clearly associated in time with eruptive phenomena on the Sun, but how? When large SEP events were first observed, flares were the only known candidate, and diffusion theory was stretched to the limit to explain how the particles could spread through space, as observed. The observation of coronal mass ejections (CMEs), and the shock waves they drive, provided better candidates later. Then small events were found with 1000-fold enhancements in ^{3}He/^{4}He that required a different kind of source – should we reconsider flares and their open-field cousins, solar jets? The ^{3}He-rich events were soon associated with the electron beams that produce type III radio bursts. It seems the radio astronomers knew of both SEP sources all along. Sometimes the distinction between the sources is blurred when shocks reaccelerate residual ^{3}He-rich impulsive suprathermal ions. Eventually, however, we would begin to measure the source-plasma temperature that better defines the SEP sources.

The first reported observation of a solar flare, that of 1118 GMT on 1 September, 1859, was published by a self-established astronomer Richard Carrington (1860) who saw the brightening of a white-light solar flare, which lasted over 5 min, while observing sunspots. The observation was confirmed by his friend Richard Hodgson. Carrington noted that the brightening did not disrupt the underlying structure. However, possibly-associated geomagnetic effects were also noticed.

2.1 The First SEPs

Some 87 yr later Scott Forbush (1946) reported the first SEPs as an increase in what we now call a ground-level event (GLE). Protons of GeV energies cause nuclear cascades through the atmosphere. Forbush was observing the intensities of the secondary particles produced by galactic cosmic rays (GCRs) using ground-level ion chambers and especially the "Forbush decreases" now known to be caused by ejecta from the Sun whose shielding reduces the intensities of the GCRs. Three large solar events beginning in February and March 1942 produced sharp intensity *increases* from SEPs prior to the Forbush decreases. Since Forbush was unaware of CMEs and the shock waves they drive, it was natural for him to assume that the SEPs had come from the associated flares, which could be *seen*.

The nuclear cascade from the large GLE of 23 February 1956 was measured by 6 neutron detectors widely spaced in geolatitude, and a balloon-borne detector which measured the atmospheric absorption mean free path of the solar protons (Meyer, Parker, and Simpson 1956). The SEP increase was associated with a Forbush decrease in GCRs that these authors regarded as a chance coincidence.

Since 1956, ground-level neutron monitors have held the promise of using the different geomagnetic cutoff rigidities at multiple sites to measure the high-energy proton spectra. Over 70 GLEs have been recorded in over 70 years (Cliver *et al.* 1982; Cliver 2006; Gopalswamy *et al.* 2012) but most of them barely rise above the GCRs. It is only recently that the neutron-monitor measurements, combined with satellite measurements have finally begun to yield rigidity spectra for 53 of the GLEs (Tylka and Dietrich 2009) as we will see in Section 6.1.

2.2 Solar Radio Bursts and Electrons

Much more sensitive ground-based evidence of SEPs was derived from the radio emission caused by streaming energetic electrons. As electrons of 10–100 keV stream out along magnetic fields from sources near the Sun, they excite Langmuir wave oscillations at the local plasma frequency. Since the plasma frequency depends upon the square root of the local plasma electron density, the emission, called a type III burst (*e.g.* Thejappa *et al.* 2012), drifts rapidly lower in frequency across the metric radio band (~10 s) as the electrons stream out from the Sun. At shock waves, electrons accelerated in the $\boldsymbol{V_S} \times \boldsymbol{B}$ electric field similarly excite local oscillations producing a type II burst (*e.g.* Ganse *et al.* 2012), but since the electrons are carried downstream of the shock soon after acceleration, the emission only drifts out with the shock speed, V_S, *i.e.* much more slowly (~10 min).

In their review of the status of solar radio measurements Wild, Smerd, and Weiss (1963) identified two sites of acceleration near the Sun:

- Impulsive bursts of electrons were accelerated to produce type III radio bursts.
- Protons were accelerated at shock waves where accompanying electrons generated type II radio bursts.

After measurements in space became possible, Lin (1970, 1974) distinguished SEP events with 40 keV electrons that were associated with type III radio bursts, optical flares, and 20-keV X-ray bursts. These differed from the large proton events in which the accompanying electrons were mainly relativistic. Lin identified "pure" impulsive electron events, meaning events in which any accompanying ions were not yet detectible, at that time. The direct measurements of electrons by Lin supported the ideas of Wild, Smerd, and Weiss (1963).

2.3 The Spatial Distribution

2.3.1 Diffusion and the Birdcage Model

"A man with only a hammer treats every problem like a nail." In early studies of large SEP events all the distributions seemed like they must be particle transport from a point-source flare and diffusion theory was the transport tool of choice. The time dependence of the proton intensities had a smooth rise and a long, slow decay. Yet events seemed to be associated with flares from such a wide span of

solar longitudes, approaching 180°. You could *see* the flares so they *must* be the source. Perhaps the particles from the flare diffused through the solar corona somehow and then out along the magnetic field lines toward Earth (Reid 1964).

In diffusion models, all of the physics of scattering is put into the diffusion coefficients, but it is when these coefficients are treated as adjustable parameters that their reality becomes tenuous. How did the particles actually cross magnetic field lines?

In fact, there was an early idea of a "fast propagation region" (Reinhard and Wibberenz 1974) of ≈60° in solar longitude after which particles diffused away more slowly. The authors did consider that the "fast propagation region" might actually be the surface of a shock wave, but could not believe it to be the actual source of the acceleration. Shock waves were generally well known in 1974.

In the birdcage model (Newkirk and Wenzel 1978) arcades of coronal loops formed structures like wires of a birdcage, spreading particles across the corona. At the footpoints of the loops the fields were somehow connected to the next series of loops, and so on across the Sun. Transport through this grid was simply assumed to be diffusive and these diffusive transport models held sway for decades.

2.3.2 Large Scale Shock Acceleration and CMEs

A direct challenge to the birdcage model came from Mason, Gloeckler, and Hovestadt (1984). They observed the abundances of low-energy H, He, C, O, and Fe ions over an extended time as connection longitudes drifted far (~120°) from the source. Relative abundances of these ions representing different magnetic rigidities were not altered by the complex journey through the coronal birdcage. The authors suggested that the ions must actually result from large-scale shock acceleration (LSSA). Shocks can easily cross magnetic field lines, accelerating particles locally across a broad surface, wherever they go. LSSA also helped explain the long duration of the gradual events, especially at low energies, where the shocks continue acceleration as they come far out from the Sun.

In the same year Kahler *et al.* (1984) found a 96% correlation between the largest energetic SEP events and fast, wide CMEs. This paper strengthened preliminary associations found during the *Skylab* mission when CME observations began to become common.

2.3.3 The Longitude Distribution

When larger numbers of gradual SEP events had been accumulated, it became possible to organize them as a function of their apparent solar source longitude. Even today with multiple spacecraft available it is difficult to study many individual events by observing each of them with multiple spacecraft at several conveniently-spaced longitudes. Cane, Reames, and von Rosenvinge (1988) did the next best thing, studying 235 proton events of >20-MeV observed on IMP and ISEE by binning them as a function of their source longitudes. The authors concluded that the most important factor organizing the time profiles of large SEP events was the

existence of an interplanetary-shock source and the curved Parker-spiral magnetic field which the particles were constrained to follow. Figure 2.1 shows a version of their findings.

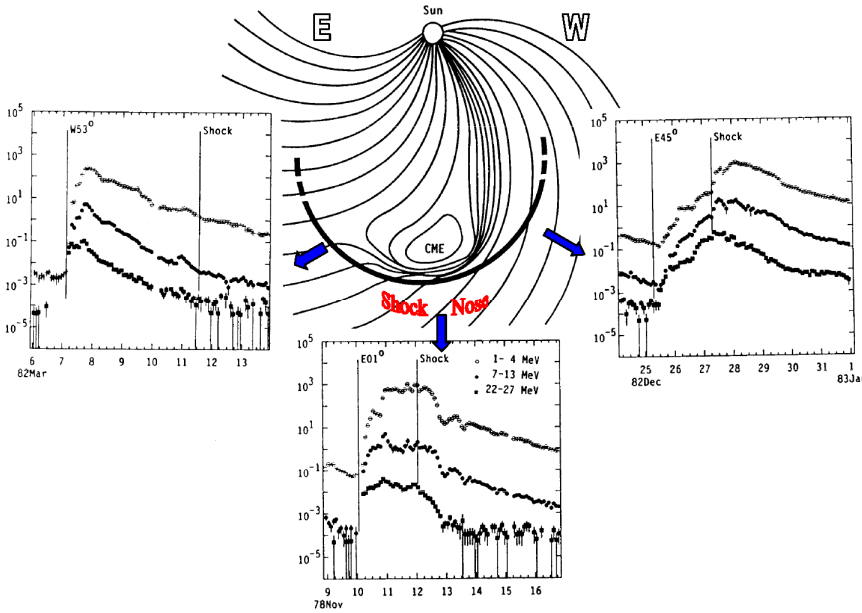

Fig. 2.1 Variation of the appearance of typical SEP events is shown as viewed from three solar longitudes (see text; after Reames 1999; see also Cane, Reames, and von Rosenvinge 1988).

In Figure 2.1, the three cases shown are described as follows:

1. A spacecraft on the East flank of the shock (a western solar-source longitude) sees a fast intensity increase early, when it is magnetically well-connected to the strongest source at the "nose" of the shock as it first appears near the Sun. At later times the intensity decreases as the magnetic connection point moves gradually around the shock toward its weaker eastern flank. When this flank of the shock would be expected to pass the spacecraft, the shock may be very weak or may have dissipated completely so far around from the nose.
2. A spacecraft observing a source near central meridian is magnetically connected far to the West of the shock nose early in the event but the intensity increases as the shock moves outward and the connection point approaches the nose. The connection to the shock nose occurs as the shock itself passes the spacecraft. Thereafter, the intensity may decline suddenly as the spacecraft passes inside the CME driving the shock.
3. A spacecraft on the West flank of the shock (an eastern source on the Sun) is poorly connected to the source but its connection and the observed intensities improve with time, reaching a maximum *behind* the shock when it encounters field lines that connect it to the nose of the shock *from behind*.

We will see that later observations of individual events from multiple spacecraft generally supported the pattern seen in Figure 2.1 (*e.g.* Figure 5.16).

2.3.4 Scatter-Free Events

Does ambient turbulence in the interplanetary medium cause pitch-angle scattering of the particles flowing out from the Sun? The classic Figure 2.2 from Mason *et al.* (1989) provides an interesting answer.

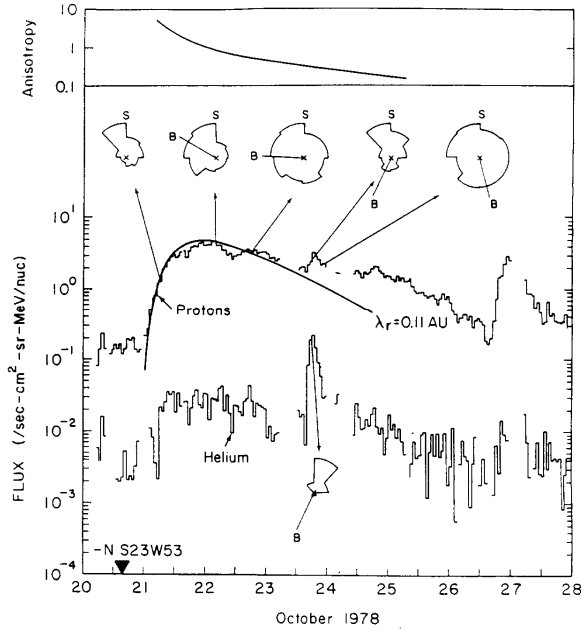

Fig. 2.2. Intensities and angular distributions of ~1 MeV amu^{-1} H and He are shown for a large SEP event of 21 October, 1978 and for the newly anisotropic flow from a small ^{3}He-rich event on 23 October. A diffusion fit, to the proton intensity is shown with a radial component of the scattering mean free path of 0.11 AU. How can scattering spread particles in time so much in the large event, but barely scatter those from the small event in its wake? (Mason *et al.* 1989)

Mason *et al.* (1989) showed that most ^{3}He-rich events (like that on 23 October 1978) actually propagate scatter free, *i.e.* with $\lambda \geq 1$ AU. We will see in Section 5.1.2 that in more intense events the streaming protons may be scattered by self-amplified waves, but the slow decrease late in gradual SEP events actually occurs when ions are adiabatically trapped in a magnetic *reservoir* (Section 5.7) behind the CME and shock. There is little scattering in the reservoir, but intensities decrease because the volume of the reservoir expands. Diffusion might be appropriate earlier in an event, but it *does not* produce the slow intensity decay of the large event, as the profile of the small scatter-free event on October 23 shows. Slow decays of SEPs are yet another misapplication of diffusion theory (see Section 5.7).

2.3.5 Field-line Random Walk

While particles do not easily cross field lines, and the field lines may not join fortuitously, as suggested by the birdcage model, their footpoints do engage in a random walk which has the effect of spreading the longitude distribution of particles

injected upon them (Jokipii and Parker 1969). The footpoints of the open field lines are imbedded in turbulent velocity fields that cause adjacent lines of force to execute a random walk relative to each other in time, as each stage of the evolving field pattern is carried out by the solar wind. Field lines are also buffeted by turbulence from the passage of CMEs Thus, even at quiet times, field lines from any small region on the Sun have a distribution that is spread about the Parker spiral so that particles from a compact impulsive SEP event have a Gaussian-like longitude (and latitude) distribution. In Figure 2.3, this contributes to the longitude spread of the impulsive events shown in the right-hand panel. In the left-hand panel, the gradual events are also spread in longitude by the spatial extent of the shock-wave source.

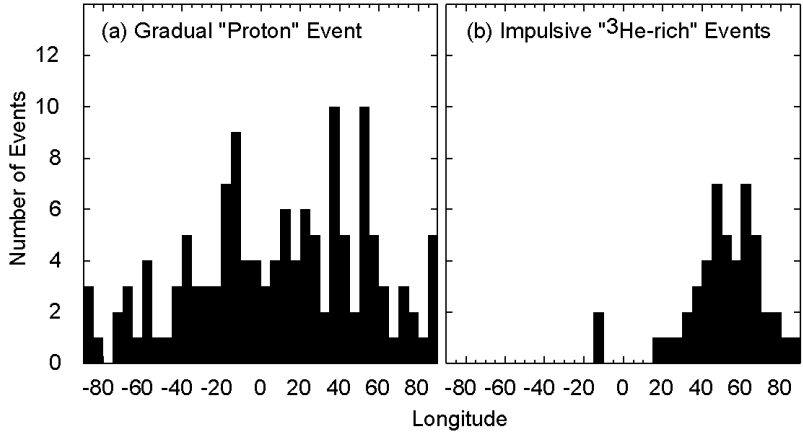

Fig. 2.3. Longitude distributions are shown for gradual SEPs (left) spread mainly because of the width of the shock source, and impulsive (right) SEP events spread by random walk of field lines and by variations in solar wind speed (Reames 1999).

2.4 Element Abundances

The earliest observations of heavier elements in SEP events were made using nuclear-emulsion detectors on sounding rockets launched into large SEP events. Fichtel and Guss (1961) observed C, N, and O nuclei above 25 MeV amu^{-1}. The observations were extended to Fe by Bertsch, Fichtel, and Reames (1969). For the early measurements, the presence of SEPs was detected by a riometer, which measures radio absorption produced by ionization of the polar cap region produced by high intensities of SEPs. The riometer was used as an indication to fire sounding rockets above the atmosphere to measure SEP abundances from Ft. Churchill in northern Canada.

2.4.1. First Ionization Potential (FIP) and A/Q

Improving measurements led to comparison of element abundances in SEP events with those in the solar corona (*e.g.* Webber 1975; Webber *et al.* 1975; Cook,

Stone, and Vogt 1984). These measurements were summarized in the review of Meyer (1985). He found two factors that influenced element abundances in large SEP events (^{3}He-rich events were excluded). There was one component, present in all events that depended upon the first ionization potential (FIP) of the elements, and a second variable component that he called "mass bias" actually depending upon the mass-to-charge ratio *A/Q* of the ions. The *A/Q* dependence differed from one event to another. The FIP dependence, that was shown in Figure 1.6, represents average abundances at the coronal origin of SEPs, relative to the corresponding photospheric abundances. Elements with FIP above about 10 eV are neutral atoms in the photosphere while lower-FIP elements are ionized. The ions are more easily swept up into the corona, as by Alfvén waves (*e.g.* Laming 2004, 2009) and thus have higher relative abundances there.

An increasing or decreasing power-law dependence on the *A/Q* ratio of the ions was clearly found by Breneman and Stone (1985) and is shown in Figure 2.4. Brenenan and Stone (1985) used the newly available ionization-state measurements of Luhn *et al.* (1984) to determine *Q*.

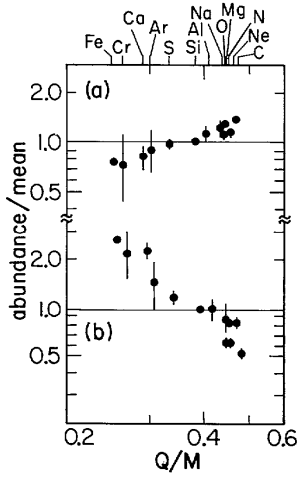

Fig. 2.4. The dependence of elemental abundances on the charge-to-mass ratio *Q/M* (our *Q/A*) of the elements is shown for two large SEP events by Breneman and Stone (1985).

After languishing for over 30 years, these power-laws have gained renewed interest. The pattern of ionization states *Q* depends upon the plasma temperature (see Figure 5.12) and it has recently been shown (Reames 2016) that the grouping of elements in enhancement *vs. A/Q* (like Figure 2.4) determine the source-plasma temperature (see Section 5.6). In fact, grouping of elements C – Mg with similar enhancements and *A/Q* in Figure 2.4 suggests a temperature of about 1.5 MK. But we are getting ahead of our story (see Section 5.6).

2.4.2. ^{3}He-rich Events

The first observation of ^{3}He/^{4}He in SEP events (Hsieh and Simpson 1970) showed some evidence of enhancement which aroused interest because of the possibility that ^{3}He could be produced in nuclear reactions, but not when Serlemitsos and Balasubrahmanyan (1975) found ^{3}He/^{4}He = 1.52 ± 0.10 but ^{3}He/^{2}H > 300. With

no significant evidence of other reaction products, like ^{2}H or ^{3}H, it became clear that a new acceleration process was involved, since ^{3}He/^{4}He ≈ 5 × 10^{-4} in the solar wind. It also became apparent that there were other abundance enhancements, such as Fe/O that was ~10 times larger than in the solar wind (*e.g.* Gloeckler *et al.* 1975). However, there is still *no* evidence of nuclear-reaction secondaries, ^{2}H, ^{3}H, Li, Be, B, *etc.* in the SEPs; γ-ray and neutron measurements tell us they are produced in flare loops, but they are magnetically trapped in the loops and can not get out into space.

The next generation of measurements of ^{3}He-rich events (Figure 2.5) led to their association with non-relativistic electron events (Reames, von Rosenvinge, and Lin 1985) and with type III radio bursts (Reames and Stone 1986). Thus Lin's (1970) "pure" electron events were actually ^{3}He-rich or "impulsive" SEP events and were associated with the type III-burst electron events discussed by Wild, Smerd, and Weiss (1963). While these events were also Fe-rich, Fe/O was not correlated with ^{3}He/^{4}He (*e.g.* Mason *et al.* 1986), opening the possibility and the need for two different enhancement mechanisms.

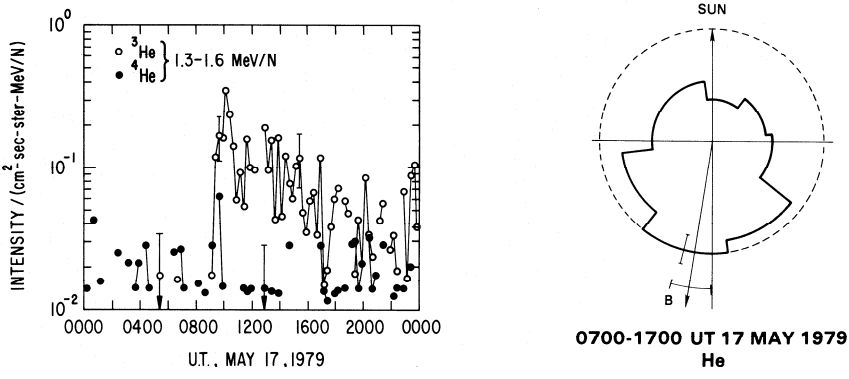

Fig. 2.5 Intensities of ^{3}He and ^{4}He (left) and ^{3}He angular distribution (right) in a small ^{3}He-rich event associated with 2 – 100 keV electrons (Reames, von Rosenvinge, and Lin 1985).

The uniqueness of the ^{3}He enhancement suggested a resonant interaction with plasma waves. For example, Fisk (1978) suggested selective heating of ^{3}He by absorption of electrostatic ion cyclotron waves at the ^{3}He gyrofrequency; this mechanism would require a second process for preferential acceleration of the preheated ions, such as a shock wave.

Temerin and Roth (1992; Roth and Temerin 1997) found that the streaming electrons that produce the type III burst could generate electromagnetic ion cyclotron (EMIC) waves near the gyrofrequency of ^{3}He. Ions mirroring in the converging magnetic field could be accelerated as they continue to absorb the waves, in analogy with the "ion conics" seen in the Earth's aurora. The authors suggested that heavier ions were accelerated through resonance with the second harmonic of their gyrofrequency, but this required specific ionization states and did not produce the extreme and uniform increase in enhancement of the heavy elements that

was commonly found subsequently (*e.g.* Reames 2000; see also Reames, Cliver, and Kahler 2014a, b), as we shall see in Chapter 4.

Ho, Roelof, and Mason (2005) found that there was an upper limit to the fluence of ^{3}He in events so that increasingly large impulsive events had decreasing ^{3}He/^{4}He ratios. This agreed with an estimate by Reames (1999) that an impulsive event can accelerate and deplete most of the ^{3}He in a typical flare (or jet) volume.

^{3}He-rich events were traced to their solar sources by Nitta *et al.* (2006) and by Wang *et al.* (2006) and there was a growing association with narrow CMEs and with solar jets (Kahler, Reames, and Sheeley 2001; see also Reames, Cliver, and Kahler 2014a).

2.4.3. The Seed Population

For a time, it seemed that impulsive and gradual events might be distinguished by their element abundances alone. Impulsive events were ^{3}He-rich, weren't they? Then Mason, Mazur, and Dwyer (1999) found enhancements of ^{3}He in large SEP events that clearly should otherwise be called gradual. In fact, there is even ^{3}He available during relatively quiet times. Earlier evidence of this had been seen by Richardson *et al.* (1990). The mass distribution in Figure 2.6 clearly shows ^{3}He, and although the amount is small, it is 5 times the solar-wind abundance. The authors suggested that the ^{3}He, and also Fe, are suprathermal remnants of previous impulsive SEP events. These *impulsive-suprathermal* ions contribute to the *seed population* for subsequent shock acceleration (see Tylka *et al.* 2001).

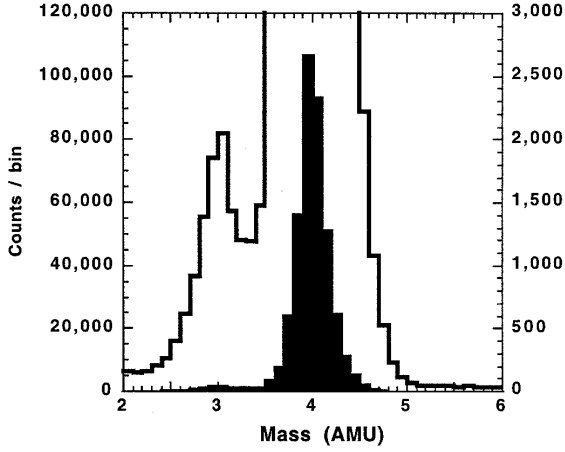

Fig. 2.6. The mass distribution of He is shown directly (solid – left scale) and with an expanded scale (open – right scale) to show ^{3}He at 0.2 – 2.0 MeV amu^{-1} during quiet times (Mason, Mazur, and Dwyer 1999)

Exploring the seed population, Desai *et al.* (2001) found ^{3}He intensity increases at shocks in 25 SEP events with enhancements of 3 to 600 relative to the solar wind and Desai *et al.* (2003) found Fe/O at the shock was correlated with Fe/O upstream. Figure 2.7 shows intensities of ^{3}He, ^{4}He, O, and Fe before and during a strong shock event. The quiet period labeled "upstream" is quite ^{3}He-rich and has Fe/O >1. These strong enhancements do not persist at the shock, but there clearly must be ^{3}He in the seed population, suggesting that it must contain suprathermal

ions from earlier impulsive SEP events. The correlation of Fe/O at the shock with that upstream is consistent with that interpretation. Note, however, that *most* of the ions at the shock peak *do not* come from ^{3}He-rich impulsive suprathermals. We will see that they represent ambient coronal material in most cases, although suprathermal ions from previous gradual SEP events may also contribute.

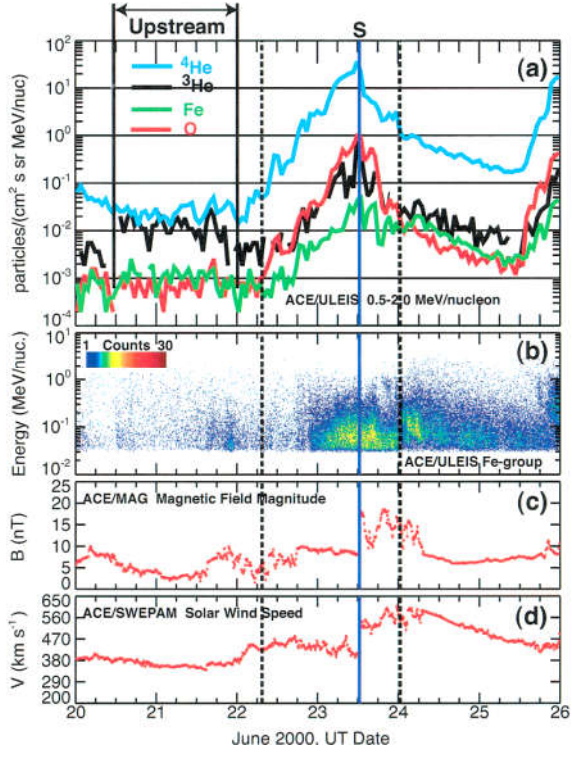

Fig. 2.7. (a) Intensities of 0.5 – 2.0 MeV amu^{-1} ^{3}He, ^{4}He, O and Fe are shown during a large SEP event, with (b) a histogram of Fe arrivals, (c) the magnetic field B, and (d) the solar wind speed. ^{3}He is clearly accelerated, peaking at the shock, S, but is not as strongly enhanced as in the ^{3}He-rich period upstream (Desai *et al.* 2003; see also Bučík *et al.* 2104, 2015; Chen *et al*. 2015)

Tylka *et al.* (2005) found that in two otherwise-similar, large SEP events, the energy dependence of Fe/C above ~10 MeV amu^{-1} suddenly increased in one event and decreased in the other, as shown in the left panel of Figure 2.8. The authors considered the possible selection effect of impulsive suprathermal ions caused by differences in shock geometry. In quasi-perpendicular shock waves, with ***B*** perpendicular to the shock normal, injected ions may need a higher speed to catch up to the shock from behind, so that pre-accelerated impulsive suprathermal ions would be preferentially selected as shown in the right panel of Figure 2.8. Tylka and Lee (2006) calculated the effect different seed populations and shock geometries could have on the energy dependence of Fe/C. The higher-energy effects occur because the location of the high-energy "knee," where the power-law shock spectra roll downward, depends upon Q/A of the ions and sec θ_{Bn}, the angle between ***B*** and the shock normal. Coronal- and impulsive-suprathermal ions have different values of Q and thus contribute differently above the spectral knee.

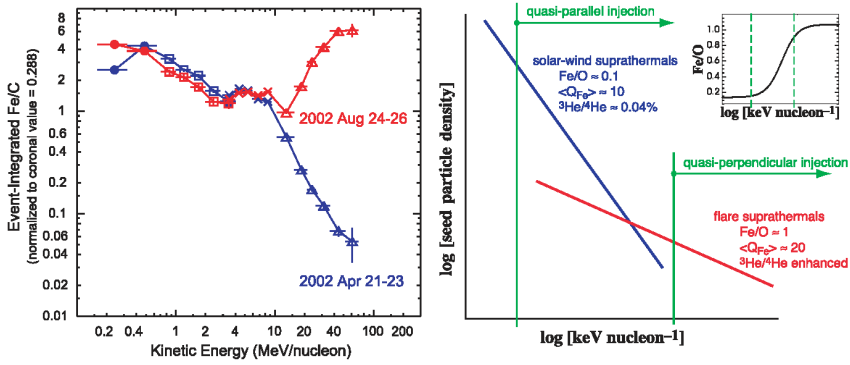

Fig. 2.8 The left panel compares the energy dependence of Fe/C for two gradual events that are otherwise similar in their properties (Tylka *et al.* 2005). The right panel shows hypothetical spectra of two sources of suprathermal ions where different injection thresholds will yield different abundance ratios (Tylka *et al.* 2005). Clearly, it would be unwise to use measurement of Fe/C above ~10 MeV amu^{-1} in an attempt to distinguish impulsive and gradual SEP events.

Tylka and Lee (2006) assumed that the shock spectrum of species i varied as $j_i(E) = k\ E^{-\gamma}\ \exp(-E/E_{0i})$, a form originally suggested by Ellison and Ramaty (1985). Then letting $E_{0i} = E_0 \times (Q_i/A_i) \times (\sec \theta_{Bn})^{2/(2-\gamma)}$, where E_0 is the proton knee energy, a wide variety of energy dependence of Fe/O may be seen as in Figure 2.9.

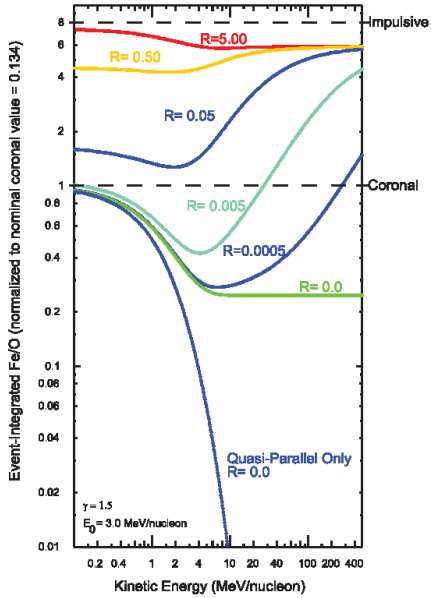

Fig. 2.9. The energy dependence of Fe/O is shown as a function of R which is the ratio, in the seed population, of O in impulsive suprathermal ions to coronal ions. The values of γ and E_0 assumed for this case are shown in the lower left corner of the figure. (Tylka and Lee 2006).

In fact, the seed population for shock acceleration can consist of ambient coronal material as well as residual suprathermal ions from previous impulsive and gradual SEP events. However, Giacalone (2005) noted that high turbulence near

the shock with $\delta B/B \approx 1$ would allow oblique shocks better access to the low-energy seed population and diminish the selective dependence on θ_{Bn}.

2.5 Ionization States

Some of the earliest direct measures of SEP ionization states were the direct measurements at 0.34 – 1.8 MeV amu^{-1} for Fe (Luhn *et al.* 1984, 1987). They found $Q_{Fe} = 14.2 \pm 0.2$ for gradual events, corresponding to a plasma temperature of ~2 MK, but a much higher value of $Q_{Fe} = 20.5 \pm 1.2$ for ^{3}He-rich events. Either the ^{3}He-rich events are much hotter, ~10 MK, or, as we now suspect, the ions may be stripped in transit from the impulsive sources which lie deeper in the corona. Subsequently Leske *et al.* (1995) used geomagnetic cutoffs to find the $Q_{Fe} = 15.2 \pm 0.7$ at 15–70 MeV amu^{-1} in large events and Tylka *et al.* (1995) found $Q_{Fe} = 14.1 \pm 1.4$ at 200–600 MeV amu^{-1}.

More recently, DiFabio *et al.* (2008) found that the ionization states in impulsive SEP events increased with energy, suggesting that the ions had passed through enough material that electron stripping and capture were in equilibrium. The authors suggested that the ions in *impulsive* events were accelerated below 1.5 R_S where densities were higher, beginning at a temperature of 1–3 MK. (We will see in Section 3.1 that acceleration in *gradual* events begins higher, at 2–3 R_S.)

A different approach to determining ionization states was taken by Reames, Meyer, and von Rosenvinge (1994). They noted that in average impulsive SEP events, the elements ^{4}He, C, N, and O showed *no* enhancement relative to reference coronal abundances, Ne, Mg, and Si were enhanced by a factor of ~2.5, and Fe by a factor of ~7. This suggested that, *at the time of acceleration*, C, N, and O were fully ionized like He, and that Ne, Mg, and Si were probably in a stable closed shell configuration with two electrons. This occurs in a temperature range of 3–5 MK. At higher temperatures, Ne would become stripped, have $Q/A = 0.5$ like lighter elements, and could not be enhanced relative to them. At lower temperatures, O could capture electrons and would no longer have $Q/A \approx 0.5$. More recent studies (Reames, Cliver, and Kahler 2014a, b) have lowered this range to 2–4 MK to account for i) more accurate measurements that showed Ne enhancements exceeding those of Mg, and Si, ii) O enhancements causing decreased He/O and C/O, and iii) a power-law fit in A/Q extending to $(Z > 50)$/O (see Section 4.6). These values of 2–4 MK are temperatures of solar active regions where flares and jets occur.

The strong A/Q dependence of the enhancements extending to a factor of ~1000 for $(76 \le Z \le 82)$/O (*e.g.* Reames, Cliver, and Kahler 2014a, b) recently has been theoretically understood as occurring in collapsing islands of magnetic reconnection (*e.g.* Drake *et al.* 2009). Particle-in-cell simulations show that ions are Fermi-accelerated as they are reflected back and forth from the ends of the collapsing islands of magnetic reconnection.

While impulsive SEPs may have passed through the extremely small amount of matter required to attain equilibrium values of Q, they cannot have passed through

enough material to lose significant energy, since the Q^2/A dependence of the energy loss would destroy the strong ~1000-fold enhancement observed for heavy elements such as ($76 \leq Z \leq 82$)/O.

Recent studies of the *A/Q* dependence in *gradual* SEP events (Reames 2016) have found that most of these events (69%) have source-plasma temperatures ≤ 1.6 MK, consistent with shock acceleration of ambient coronal plasma (see Section 5.6). Only 24% of the events have active-region temperatures of 2.5 – 3.2 MK and include large enhancements from impulsive suprathermal ions.

Using the *A/Q*-dependence of abundance enhancements, with *Q vs. T* from atomic physics, these studies provide a new method of determining ionization states at the point of acceleration and early transport. This circumvents the effects of stripping that may be present in the ionization states measured later at 1 AU.

2.6. Shock Theory

Shock acceleration theory had an extensive history in GCR acceleration prior to its application to SEPs and that will not be repeated here. The plasma physics of shocks and shock acceleration has been reviewed by Jones and Ellison (1991; see also Lee 2005, Sandroos and Vainio 2007, Zank, Li, and Verkhoglyadova 2007; Verkhoglyadova, Zank, and Li 2014). Diffusive shock acceleration (DSA) occurs as ions are pitch-angle scattered back and forth across a shock wave, gaining an increment of velocity on each round trip. For an oblique shock wave, particles can gain additional energy in the $\boldsymbol{V}_S \times \boldsymbol{B}$ electric field of the shock (*e.g.* Decker 1983).

As accelerated protons stream away from the shock upstream, they amplify Alfvén waves of wave number $k \approx B/\mu P$, according to quasi-linear theory, where P is the particle rigidity and μ its pitch-angle cosine, that increase the resonant scattering of the ions that follow behind (see Section 5.1.2). Quasi-linear theory assumes that the energy density in wave turbulence is small with respect to the energy density in the field, $\delta B/B << 1$, a condition that may be violated at strong shocks which approach or even exceed the Bohm limit where the proton scattering mean free path equals its gyroradius. Lee (1983) applied equilibrium DSA theory to explain interplanetary shocks and Zank, Rice, and Wu (2000) found that shock acceleration could produce GeV protons near the Sun, assuming that turbulence reaches the Bohm limit at the shock.

Ng, Reames, and Tylka (2003) considered the time-dependent particle transport with amplification of Alfvén waves and Ng and Reames (2008) calculated the time-dependent shock acceleration of protons of >300 MeV.

2.7 Disappearing-Filament Events

A "disappearing" filament occurs when a filament, which may have been visible in the corona for days, is suddenly destabilized and erupts into a CME, disappearing from its former position. An Hα brightening may form a classic double-ribbon pattern along the filament channel with slight heating and soft X-ray emission, but no hard X-ray emission or flaring occurs. Such events can produce a fast CME, a

shock wave, and a substantial gradual SEP event, without the need of a flare or even a solar active region.

An early association of SEPs with filament changes was made by Sanahuja *et al.* (1983) but a clear example was the SEP event of 5 December 1981, shown in Figure 2.10, identified and discussed by Kahler *et al.* (1986). Cane *et al.* (1986) found six other disappearing-filament-associated SEP events with a CME and shock but no impulsive phase or flare, and Gopalswamy *et al.* (2015) have extended this study to recent large gradual SEP events. Flares are simply not required for SEP acceleration. However, these events do not usually produce GLEs, probably because of the weaker magnetic fields involved.

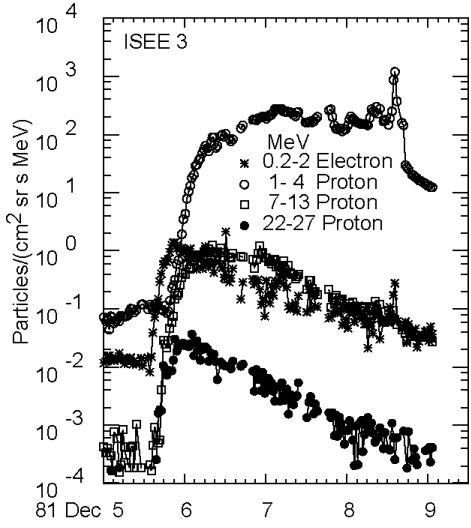

Fig. 2.10. Intensities *vs.* time are shown for the disappearing-filament-associated SEP event of 5 December 1981. The peak in the low energy protons on 8 December occurs at the time of shock passage at 1 AU.

2.8 "The Solar Flare Myth"

By 1993, the idea of impulsive and gradual SEP events was fairly well documented, CMEs and CME-driven shocks had been studied for a decade in relation to SEPs, and ^{3}He-rich events had been studied for two decades. It became increasingly clear that the largest SEP events (and the only ones producing a significant radiation hazards) were related to CMEs and shocks, *not to flares*. The birdcage model (Section 2.3.1) was dead. While reviews of this emerging paradigm were fairly common in invited talks at meetings, it was the publication of the review "The Solar Flare Myth" by Gosling (1993) that drew enormous criticism that surprised the SEP community. This fairly straightforward review was thought to "wage an assault on the last 30 years of solar-flare research" (Zirin 1994). Apparently there was concern that if hazardous SEPs did not come from flares, flare research might be discontinued! The sky was falling! In hindsight, surely the last 23 years have proven such concerns to be unfounded. Unfortunately, however, there is still reluctance to embrace the idea of shock acceleration of SEPs.

The controversy raised by the Gosling (1993) paper led to an invited discussion from three alternative viewpoints in *Eos* where Hudson (1995) argued that the term "flare" should include the CME, shock, and any related physics, Miller (1995) argued that flares, being more numerous, were a better subject for acceleration studies, and Reames (1995) argued for the separate study of the physics of both flare and shock acceleration of SEPs. While the extension of the term "flare" has some philosophical merit, it is important for SEP studies to distinguish a point-source flare from the acceleration source at a broadly extended CME-driven shock, especially when they involve different physical mechanisms.

2.9 Wave Generation and the Streaming Limit

When intensities of particles streaming along $\boldsymbol{B}$ are sufficiently great, they can amplify resonant Alfvén waves that exist or even generate them (Stix 1992; Melrose 1980). These waves increase the scattering and, in the vicinity of shock waves, increase the acceleration. We have mentioned the early study of equilibrium wave growth and shock acceleration (Lee 1983). Here, waves are amplified upstream to compensate for those that are being swept into the shock. In fact, for simplicity, Lee assumed that $\mu = 1$ so that $k \approx B/P$, *i.e.* each wave vector couples to its own single particle rigidity. When we allow $k \approx B/P\mu$, the waves can couple particles of different rigidity, an extremely important factor for many phenomena we observe.

Reames (1990) observed that 3 – 6 MeV proton intensities early in large gradual events never seemed to exceed a plateau value of ~100 – 200 $(\text{cm}^2\ \text{sr}\ \text{s}\ \text{MeV})^{-1}$, subsequently called the "streaming limit," although intensities could rise much higher as the shock approached (see Figure 5.3). Ng and Reames (1994) began by comparing transport with and without wave growth. They found that wave growth throttles the flow of protons, trapping them near the source, limiting their streaming. Ng, Reames, and Tylka (2003) extended these calculations showing how the scattering varied greatly in time and space and affected H, He, O, and Fe differently. The wave generation modifies the "initial" abundances seen early in SEP events (Reames, Ng, and Tylka, 2000). Further observations extended the streaming limit to higher energies (Reames and Ng 1998) and showed how the low-energy spectra can be flattened, but only when sufficient intensities of high energy protons precede them (Reames and Ng 2010). Wave growth and the streaming limit will be considered in more detail in Sections 5.1.2 and 5.1.5.

2.10 SEP – CME Correlation

In his article on "the big-flare syndrome," Kahler (1982) pointed out that the fact that big SEP events are usually accompanied by big flares, does *not* mean that flares *cause* SEP events; rather, in larger events, *all* energetic phenomena are more energetic or intense, including flares, CMEs and SEPs. Flares were once incorrectly thought to cause CMEs. When there is a large rearrangement of the coronal magnetic field, most of the energy released is actually carried out by the CME

(*e.g.* Emslie *et al.* 2004). Flares are not required to produce CMEs or SEP events and are, in fact, a secondary phenomenon (Kahler 1992). When flares do accompany CMEs, the CME can precede the flare. Kahler (1992) asks "how did we form such a fundamentally incorrect view?" Probably, correlations of the other phenomena with highly-visible flares were taken much too seriously.

While correlations do not necessarily imply a causal relationship, they are a starting point, and there is a steep dependence of peak particle intensity in large gradual SEP events on CME speed as shown in Figure 2.11 (Kahler 2001). Two samples of events are shown in the figure i) SEPs measured on *Wind* and CMEs by SOHO/LASCO, both near Earth, and ii) SEPs measured on *Helios*, off the solar limbs, while the *Naval Research Laboratory's Solwind* coronagraph measured CMEs, from near Earth. The latter was an effort to correct for the projection effect in the direction of CME propagation. Of course the "peak intensity" is, in reality, a strong function of longitude, as expected from Figure 2.1 (see also Figure 5.16), as is the speed of the shock driven by the CME; these factors contribute to the spread of the measurement which, as we will see, may be reduced by using the measurements of multiple spacecraft in a single SEP event (see Figure 3.4).

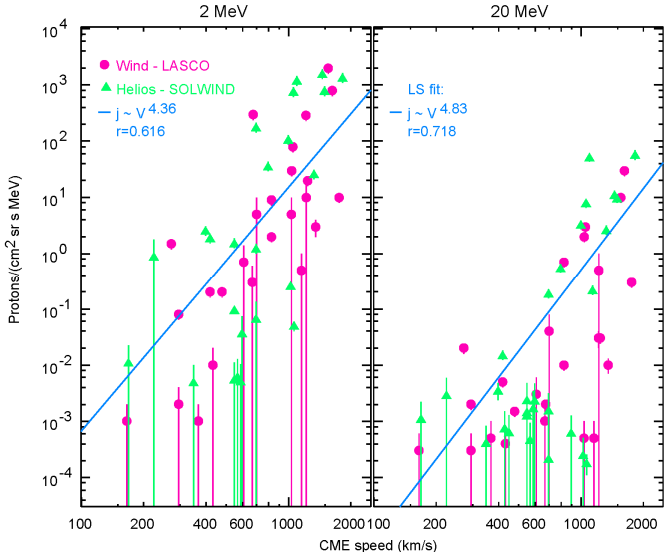

Fig. 2.11. Peak intensity is shown *vs.* CME speed for 2 MeV (left) and 20 MeV (right) protons for two event samples (see text). Power-law least-squares fits and correlation coefficients (r) are shown (see Kahler 2001).

The apparent dependence on CME speed in Figure 2.11 is certainly quite steep, although there is no physical reason that the relationship should be a power law. Fast CMEs are surely required to produce significant SEP events as originally suggested by Kahler *et al.* (1984). However, this type of correlation is only a basis for further study, and must be tested and improved as we will see in Section 3.2. What variables, other than CME speed, contribute to SEP intensities?

References

Bertch, D. L., Fichtel, C. E., Reames, D. V., Relative abundance of iron-group nuclei in solar cosmic rays, Astrophys. J. Lett. **157**, L53 (1969)

Breneman, H.H., Stone, E.C., Solar coronal and photospheric abundances from solar energetic particle measurements, Astrophys. J. Lett. **299**, L57 (1985)

Bučík,,R,. Innes, D.E., Mall, U., Korth, A., Mason, G.M., Gómez-Herrero, R., Multi-spacecraft observations of recurrent ^{3}He-rich solar energetic particles, Astrophys. J. **786**, 71 (2014)

Bučík, R., Innes, D.E., Chen, N.H., Mason, G.M., Gómez-Herrero, R., Wiedenbeck, M.E., Long-lived energetic particle source regions on the Sun, J. Phys. Conf. Ser. **642**, 012002 (2015)

Chen N. H., Bučík R., Innes D. E., Mason G. M., Case studies of multi-day ^{3}He-rich solar energetic particle periods, Astron. Astrophys. **580**, 16 (2015) doi: 10.1051/0004-6361/201525618

Cane, H. V., Kahler, S. W., Sheeley, N. R., Jr., Interplanetary shocks preceded by solar filament eruptions, J. Geophys. Res. **91**, 13321 (1986)

Cane, H. V., Reames, D. V., von Rosenvinge, T. T., The role of interplanetary shocks in the longitude distribution of solar energetic particles, J. Geophys. Res. **93**, 9555 (1988)

Carrington, R.C. Description of a singular appearance seen in the Sun on September, 1859, Mon. Not. Roy. Astron. Soc. **20**, 13 (1860)

Cliver, E. W., The unusual relativistic solar proton events of 1979 august 21 and 1981 may 10, Astrophys. J. **639**, 1206 (2006)

Cliver, E. W., Kahler, S. W., Shea, M. A., & Smart, D. F., Injection onsets of 2 GeV protons, 1 MeV electrons, and 100 keV electrons in solar cosmic ray flares, Astrophys. J, **260**, 362 (1982)

Cook, W. R., Stone, E. C., Vogt, R. E., Elemental composition of solar energetic particles, Astrophys. J. **279**, 827 (1984)

Decker, R. B., Formation of shock-spike events at quasi-perpendicular shocks, J. Geophys. Res., 88, 9959 (1983)

Desai, M. I., Mason, G. M., Dwyer, J. R., Mazur, J. E., Smith, C. W., Skoug, R. M., Acceleration of ^{3}He Nuclei at Interplanetary Shocks", Astrophys. J. Lett., **553**, L89 (2001)

Desai, M. I., Mason, G. M., Dwyer, J. R., Mazur, J. E., Gold, R. E., Krimigis, S. M., Smith, C. W., Skoug, R. M., Evidence for a Suprathermal Seed Population of Heavy Ions Accelerated by Interplanetary Shocks near 1 AU, Astrophys. J., 588, 1149 (2003)

DiFabio, R., Guo, Z., Möbius, E., Klecker, B., Kucharek, H., Mason, G. M., Popecki, M., Energy-dependent charge states and their connection with ion abundances in impulsive solar energetic particle events, Astrophys. J. **687**, 623.(2008)

Drake, J.F., Cassak, P.A., Shay, M.A., Swisdak, M., Quataert, E., A magnetic reconnection mechanism for ion acceleration and abundance enhancements in impulsive flares, Astrophys. J. Lett. **700**, L16 (2009)

Ellison, D., Ramaty, R., Shock acceleration of electrons and ions in solar flares, Astrophys. J. **298**, 400 (1985)

Emslie, A. G., *et al*., Energy partition in two solar flare/CME events, J. Geophys. Res. **109**, A10104 (2004)

Fichtel, C.E., Guss, D. E., Heavy nuclei in solar cosmic rays, Phys. Rev. Lett. **6**, 495 (1961)

Fisk, L. A., ^{3}He-rich flares - a possible explanation, Astrophys. J. **224**, 1048 (1978)

Forbush, S. E., Three unusual cosmic ray increases possibly due to charged particles from the Sun, Phys. Rev. **70**, 771 (1946)

Ganse, U., Kilian, P., Vainio, R., Spanier, F., Emission of type II radio bursts - single-beam versus two-beam scenario, Solar Physics **280**, 551 (2012)

Giacalone, J., Particle acceleration at shocks moving through an irregular magnetic field, Astrophys. J. **624**, 765 (2005)

Gloeckler, G., Hovestadt, D., Vollmer, O., Fan, C. Y., Unusual emission of iron nuclei from the sun, Astrophys, J. Lett. **200**, L45 (1975)

Gopalswamy, N., Xie, H., Yashiro, S., Akiyama, S., Mäkelä, P., Usoskin, I. G., Properties of Ground level enhancement events and the associated solar eruptions during solar cycle 23, Space Sci. Rev. **171**, 23 (2012)

Gopalswamy, N., Mäkelä, P., Akiyama, S., Yashiro, S., Xie, H., Thakur, N., Kahler, S. W., Large solar energetic particle events associated with filament eruptions outside of active regions, Astrophys. J. **806**, 8 (2015)

Gosling, J. T., The solar flare myth, J. Geophys. Res. **98**, 18937 (1993)

Ho, G. C., Roelof, E. C., Mason, G.M., The upper limit on ^{3}He fluence in solar energetic particle events, Atrophys. J. Lett. **621**, L121 (2005)

Hsieh, K. C., Simpson, J. A., The relative abundances and energy spectra of ^{3}He and ^{4}He from solar flares, Astrophys., J. Lett. **162,** L191 (1970)

Hudson, H. S., Solar flares: No "myth", Eos Trans. AGU **76**(41), 405 (1995)

Jokipii, J. R., Parker, E. N., Stochastic aspects of magnetic lines of force with application to cosmic ray propagation, Astrophys J. 155, 777 (1969)

Jones, F. C., Ellison, D. E., The plasma physics of shock acceleration, Space Sci. Rev. **58**, 259 (1991)

Kahler, S. W., The role of the big flare syndrome in correlations of solar energetic proton fluxes and associated microwave burst parameters, J. Geophys. Res. **87**, 3439 (1982)

Kahler, S. W., Solar flares and coronal mass ejections, Annu. Rev. Astron, Astrophys. **30**, 113 (1992).

Kahler, S. W., The correlation between solar energetic particle peak intensities and speeds of coronal mass ejections: Effects of ambient particle intensities and energy spectra, J. Geophys. Res. **106**, 20947 (2001)

Kahler, S. W., Reames, D. V., & Sheeley, Jr., N. R., Coronal mass ejections associated with impulsive solar energetic particle events, Astrophys. J., **562**, 558 (2001)

Kahler, S. W., Sheeley, N. R., Jr., Howard, R. A., Koomen, M. J., Michels, D. J., McGuire R. E., von Rosenvinge, T. T., Reames, D. V., Associations between coronal mass ejections and solar energetic proton events, J. Geophys. Res. **89**, 9683 (1984)

Kahler, S. W., Cliver, E. W., Cane, H. V., McGuire, R. E., Stone, R. G., Sheeley, N. R., Jr., Solar filament eruptions and energetic particle events, Astrophys. J. **302** 594 (1986)

Laming, J. M., A unified picture of the first ionization potential and inverse first ionization potential effects, Astrophys. J. **614**, 1063 (2004)

Laming, J. M., Non-WKB models of the first ionization potential effect: implications for solar coronal heating and the coronal helium and neon abundances, Astrophys. J. **695**, 954 (2009)

Lee, M. A., Coupled hydromagnetic wave excitation and ion acceleration at interplanetary traveling shocks, J. Geophys. Res., **88**, 6109. (1983)

Lee, M. A., Coupled hydromagnetic wave excitation and ion acceleration at an evolving coronal/interplanetary shock, Astrophys. J. Suppl., **158**, 38 (2005)

Leske, R. A., Cummings, J. R., Mewaldt, R. A., Stone, E. C., von Rosenvinge, T. T., Measurements of the ionic charge states of solar energetic particles using the geomagnetic field, Astrophys J. **452**, L149 (1995)

Lin, R. P., The emission and propagation of 40 keV solar flare electrons. I: The relationship of 40 keV electron to energetic proton and relativistic electron emission by the sun, Sol. Phys. 12, 266 (1970)

Lin, R. P., Non-relativistic solar electrons, Space Sci. Rev. **16**, 189 (1974)

Luhn, A., Klecker B., Hovestadt, D., Gloeckler, G., Ipavich, F. M., Scholer, M., Fan, C. Y. Fisk,L. A., Ionic charge states of N, Ne, Mg, Si and S in solar energetic particle events, Adv. Space Res. **4**, 161 (1984)

Luhn, A., Klecker, B., Hovestadt, D., Möbius, E., The mean ionic charge of silicon in He-3-rich solar flares, Astrophys. J. **317**, 951 (1987).

Mason, G. M., Gloeckler, G., Hovestadt, D., Temporal variations of nucleonic abundances in solar flare energetic particle events. II - Evidence for large-scale shock acceleration, Astrophys. J. **280**, 902 (1984)

Mason, G. M., Mazur, J. E., Dwyer, J. R., ^{3}He enhancements in large solar energetic particle events, Astrophys. J. Lett. 525, L133 (1999)

Mason, G. M., Ng, C. K., Klecker, B., Green, G., Impulsive acceleration and scatter-free transport of about 1 MeV per nucleon ions in ^{3}He-rich solar particle events, Astrophys. J. **339**, 529 (1989).

Mason, G. M., Reames, D. V., Klecker, B., Hovestadt, D., von Rosenvinge, T. T., The heavy-ion compositional signature in He-3-rich solar particle events, Astrophys. J. **303**, 849 (1986)

Melrose, D. B., *Plasma Astrophysics*, Vol. 1, (New York: Gordon and Breach) (1980)

Meyer, J. P., The baseline composition of solar energetic particles, Astrophys. J. Suppl. **57**, 151 (1985)

Meyer, P., Parker, E. N., Simpson, J. A., solar cosmic rays of February, 1956 and their propagation through interplanetary space, Phys. Rev. **104**, 768 (1956).

Miller, J. A., Much ado about nothing, Eos Trans. AGU **76**(41), 401 (1995)

Newkirk, G, Jr,, Wenzel, D. G., Rigidity-independent propagation of cosmic rays in the solar corona, J. Geophys. Res. **83,** 2009 (1978)

Ng, C. K., Reames, D. V., Focused interplanetary transport of approximately 1 MeV solar energetic protons through self-generated Alfven waves, Astrophys. J. **424**, 1032 (1994)

Ng, C. K., Reames, D. V., Shock acceleration of solar energetic protons: the first 10 minutes, Astrophys. J. Lett. **686**, L123 (2008)

Ng, C. K., Reames, D. V., Tylka, A. J., Modeling shock-accelerated solar energetic particles coupled to interplanetary Alfvén waves, Astrophys. J. **591**, 461 (2003)

Nitta, N. V., Reames, D. V., DeRosa, M. L., Yashiro, S., Gopalswamy, N., Solar sources of impulsive solar energetic particle events and their magnetic field connection to the earth, Astrophys. J. **650**, 438 (2006)

Reames, D. V., Acceleration of energetic particles by shock waves from large solar flares, Astrophys. J. Lett. **358**, L63 (1990)

Reames, D. V., The dark side of the solar flare myth, Eos Trans. AGU **76**(41), 401 (1995)

Reames, D. V., Particle acceleration at the sun and in the heliosphere, Space Sci. Rev. **90**, 413 (1999)

Reames, D. V., Abundances of trans-iron elements in solar energetic particle events, Astrophys. J. Lett. **540**, L111 (2000)

Reames, D.V., Temperature of the source plasma in gradual solar energetic particle events, Solar Phys., **291** 911 (2016) DOI: 10.1007/s11207-016-0854-9, arXiv: 1509.08948

Reames, D.V., Cliver, E.W., Kahler, S.W., Abundance enhancements in impulsive solar energetic-particle events with associated coronal mass ejections, Solar Phys. **289**, 3817, (2014a) DOI: 10.1007/s11207-014-0547-1

Reames, D.V., Cliver, E.W., Kahler, S.W., Variations in abundance enhancements in impulsive solar energetic-particle events and related CMEs and flares, Solar Phys. **289**, 4675 (2014b) DOI: 10.1007/s11207-014-0589-4

Reames, D. V. Ng, C. K., Streaming-limited intensities of solar energetic particles, Astrophys. J. **504**, 1002 (1998)

Reames, D. V., Ng, C. K., Streaming-limited intensities of solar energetic particles on the intensity plateau, Astrophys. J. **722**, 1286 (2010)

Reames, D. V., Meyer, J. P., von Rosenvinge, T. T., Energetic-particle abundances in impulsive solar flare events, Astrophys. J. Suppl. **90**, 649 (1994)

Reames, D. V., Ng, C. K., Tylka, A. J., Initial time dependence of abundances in solar particle events, Astrophys. J. Lett. **531**, L83 (2000)

Reames, D. V., Stone, R. G., The identification of solar He-3-rich events and the study of particle acceleration at the sun, Astrophys. J., **308**, 902 (1986)

Reames, D. V., von Rosenvinge, T. T., Lin, R. P., Solar He-3-rich events and nonrelativistic electron events - A new association, Astrophys. J. **292**, 716 (1985)

Reid, G. C., A diffusive model for the initial phase of a solar proton event, J. Geophys. Res. **69**, 2659 (1964)

Reinhard, R., Wibberenz, G., Propagation of flare protons in the solar atmosphere, Solar Phys. **36**, 473 (1974)

Richardson, I. G., Reames, D. V., Wenzel, K.-P., Rodriguez-Pacheco, J., Quiet-time properties of low-energy (less than 10 MeV per nucleon) interplanetary ions during solar maximum and solar minimum, Astrophys. J. Lett. **363**, L9 (1990)

Roth, I., Temerin, M., Enrichment of ^{3}He and Heavy Ions in Impulsive Solar Flares, Astrophys. J. **477**, 940 (1997)

Sanahuja, B., Domingo, V., Wenzel, K.-P., Joselyn, J. A., Keppler, E., A large proton event associated with solar filament activity, Solar Phys. **84**, 321 (1983)

Sandroos, A., Vainio, R., Simulation results for heavy ion spectral variability in large gradual solar energetic particle events, Astrophys. J. **662**, L127 (2007)

Serlemitsos, A. T., Balasubrahmanyan, V. K., Solar particle events with anomalously large relative abundance of ^{3}He, Astrophys. J. **198**, 195, (1975)

Stix, T. H., *Waves in Plasmas* (New York: AIP) (1992)

Temerin, M., Roth, I., The production of ^{3}He and heavy ion enrichment in ^{3}He-rich flares by electromagnetic hydrogen cyclotron waves, Astrophys. J. Lett. **391**, L105 (1992).

Thejappa, G., MacDowall, R. J., Bergamo, M., Papadopoulos, K., Evidence for the oscillating two stream instability and spatial collapse of Langmuir waves in a solar type III radio burst, Astrophys. J. Lett. **747**, L1 (2012)

Tylka, A. J., Boberg, P. R., Adams, J. H., Jr., Beahm, L. P., Dietrich, W. F., Kleis, T., The mean ionic charge state of solar energetic Fe ions above 200 MeV per nucleon, Astrophys. J. **444**, L109 (1995)

Tylka, A. J., Cohen, C. M. S., Dietrich, W. F., Lee, M. A., Maclennan, C. G., Mewaldt, R. A., Ng, C. K., Reames, D. V., Shock geometry, seed populations, and the origin of variable elemental composition at high energies in large gradual solar particle events, Astrophys. J. **625**, 474 (2005)

Tylka, A. J., Cohen, C. M. S., Dietrich, W. F., Maclennan, C. G., McGuire, R. E., Ng, C. K., Reames, D. V., Evidence for remnant flare suprathermals in the source population of solar energetic particles in the 2000 bastille day event, Astrophys. J. Lett. **558**, L59 (2001)

Tylka, A. J., Dietrich, W. F., A new and comprehensive analysis of proton spectra in ground-level enhanced (GLE) solar particle events, in *Proc. 31st Int. Cos. Ray Conf* , *Lódz* (2009), http://icrc2009.uni.lodz.pl/proc/pdf/icrc0273.pdf

Tylka, A. J., Lee, M. A., Spectral and compositional characteristics of gradual and impulsive solar energetic particle events, Astrophys. J. **646**, 1319 (2006)

Wang, Y.-M., Pick, M., Mason, G. M., Coronal holes, jets, and the origin of ^{3}He-rich particle events, Astrophys. J. **639**, 495 (2006)

Webber, W. R., Solar and galactic cosmic ray abundances - A comparison and some comments. *Proc. 14th Int. Cos. Ray Conf, Munich*, **5**, 1597 (1975)

Webber, W. R., Roelof, E. C., McDonald, F. B., Teegarden, B. J., Trainor, J., Pioneer 10 measurements of the charge and energy spectrum of solar cosmic rays during 1972 August, Astrophys. J. **199**, 482 (1975)

Wild, J. P., Smerd, S. F., Weiss, A. A., Solar Bursts, Annu. Rev. Astron. Astrophys., **1**, 291 (1963)

Verkhoglyadova, O., Zank, G. P., Li, G., A theoretical perspective on particle acceleration by interplanetary shocks and the Solar Energetic Particle problem, Phys. Reports **557**, 1 (2014)

Zank, G. P., Li, G., Verkhoglyadova, O., Particle Acceleration at Interplanetary Shocks, Space Sci. Rev. **130**, 255 (2007)

Zank, G. P., Rice, W. K. M., Wu, C. C., Particle acceleration and coronal mass ejection driven shocks: A theoretical model, *J*. Geophys. Res., **105**, 25079 (2000)

Zirin, H., Solar storminess, Sky and Telescope, Nov., 9 (1994)

3. Distinguishing the Sources

Abstract Our discussion of history has covered many of the observations that have led to the ideas of acceleration by shock waves or by magnetic reconnection in gradual and impulsive solar energetic particle (SEP) events, respectively. We now present other compelling observations, including onset timing, SEP-shock correlations, injection time profiles, high-energy spectral knees, e/p ratios, and intensity dropouts caused by a compact source, that have helped clarify these acceleration mechanisms and sources. However, some of the strongest evidence now comes from source-plasma temperatures. In this and the next two chapters, we will find that impulsive events come from solar active regions at 2 – 4 MK and, in most gradual events, shock waves accelerate ambient coronal material at <1.6 MK, although some shocks accelerate active-region plasma and reaccelerate residual impulsive suprathermal ions. In addition to helping to define their own origin, SEPs also probe the structure of the interplanetary magnetic field.

The history in Chapter 2 showed how the flow of observations and ideas eventually led to credible evidence of two sites of SEP acceleration and the related physical mechanisms. While some observations have been described, some of the clearest evidence of origin has not yet been presented. In this chapter we continue the story of particle origin, showing where and when SEPs are accelerated, and measurements that allow us to compare impulsive and gradual events. There are many different lines of evidence that must fit together to determine the most probable origin and that evidence continues to grow.

3.1 SEP Onset Times

Even in relatively intense SEP events, it is likely that the earliest detectible particles at each energy will be those that were originally focused in the diverging magnetic field in the inner heliosphere and have scattered least, simply traversing along the magnetic field line from the source with an average pitch-angle cosine, $\langle\mu\rangle \approx 1$. An example of the observed arrival times of particles of different energies is shown in Figure 3.1. The rise of the intensities is clear and sharp and intensities rise by two or three orders of magnitude. If 1% or more of the ions in each energy interval have traveled with $\langle\mu\rangle \approx 1$, we will be able to determine the scatter-free onset time with reasonable accuracy. The accuracy of this scatter-free approximation has been well studied and will be discussed below. The particle transit time $t = L/v$ where L is the path length along the field line and v is the particle velocity. By fitting the measurements we can determine both the path length and the time that the particles left the Sun, the so-called solar particle release (SPR) time.

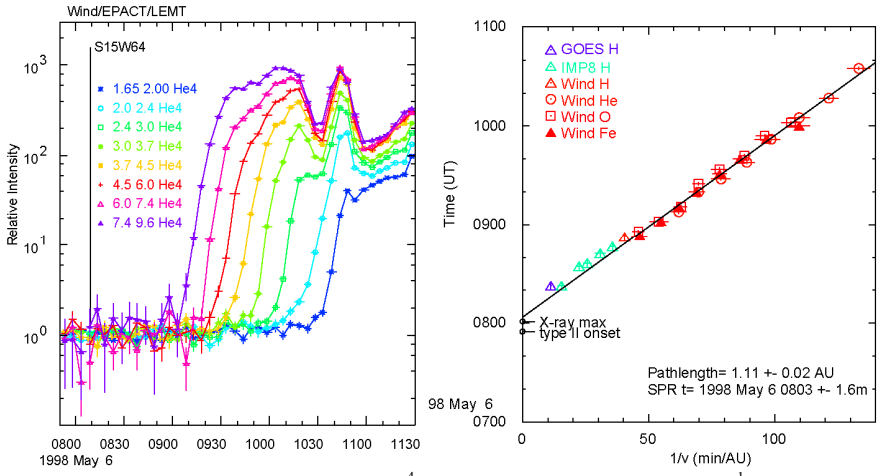

Fig. 3.1. The left panel shows the arrival of ^{4}He ions of the indicated MeV amu^{-1} intervals at the *Wind* spacecraft near Earth. The right panel shows the onset time of these and other intervals *vs.* v^{-1}. For the fitted line, the slope is the pathlength and the intercept is the solar particle release (SPR) time at the Sun (Reames 2009a).

Note that the SPR time is the release time *at the Sun*; to compare with photon observation times at Earth one should add 8.3 min to the SPR time. The path length of 1.11 ± 0.02 AU allows for some curvature of the Parker spiral, typically 1.1 – 1.2 AU. For large gradual events, including the ground level events (GLEs), generally the SPR times occur quite late in the event. Timing in impulsive and gradual events is compared in Figure 3.2.

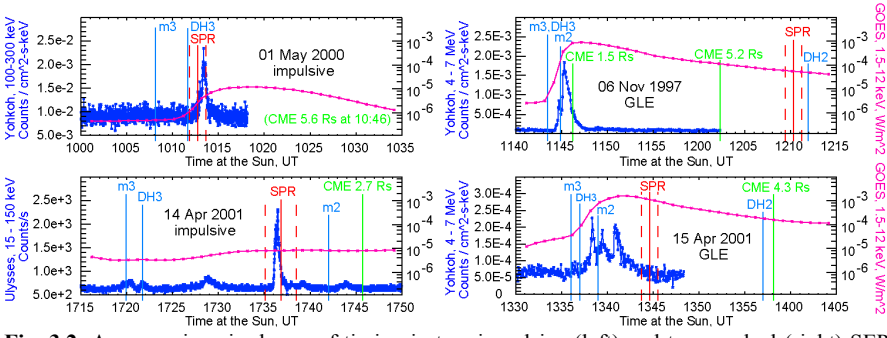

Fig. 3.2. A comparison is shown of timing in two impulsive (left) and two gradual (right) SEP events. Solar particle release (SPR) times of the particles (red with dashed errors) are compared with hard X-ray (dark blue, left), γ-ray (dark blue, right) and GOES soft X-ray (violet) time profiles. Onset times of metric (m) and decametric-hectometric (DH; 1–14 MHz) type II and III radio bursts (light blue) and CME locations (green) are shown (adapted from Tylka *et al.* 2003).

For the impulsive SEP events in Figure 3.2, The SPR times fall rather precisely on the hard-X-ray peak times (there are no measurable γ-rays in these events). For the GLEs, the SPR times often fall well after the γ-rays are over (by up to 30 min), but always after the metric type II onset indicates the formation of a shock wave.

It is interesting to plot the height of the CME leading edge at SPR time as a function of longitude of the observer relative to that of the CME source as shown in the right panel of Figure 3.3. For a multi-spacecraft study of a single event see Reames and Lal (2010).

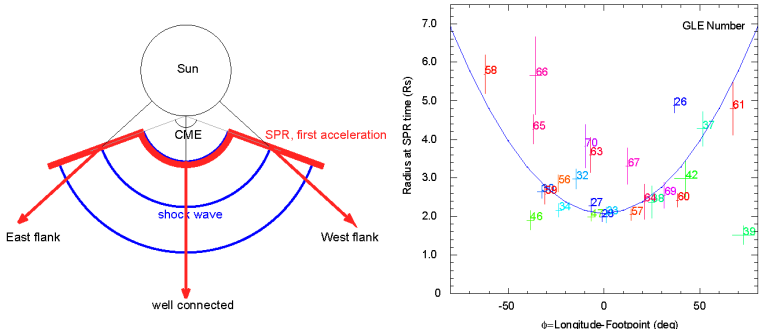

Fig. 3.3. The right panel shows the height of the CME at SPR time *vs*. longitude for numbered GLEs. The cartoon on the left shows the CME and SPR location widening on the flanks (Reames 2009a, b). The height distribution has been fit to a symmetric parabola for comparison; actually a height of 2 – 3 R_S is fairly constant over ~70°. This could be the width of the source shock surface above closed loops that was once incorrectly called the "fast propagation region".

Clearly a correct estimate of the SPR time depends upon the intensities being sufficiently high that a small number of un-scattered ions are detectible. Gopalswamy *et al.* (2012) have simply assumed a path length of 1.2 AU in order to avoid the velocity-dispersion analysis. However, Rouillard *et al.* (2012, see Appendix) have calculated that the error in the SPR time from scattering should be less that 1 – 2 min., comparable with errors from the 5-min-averaged data used. If scattering delayed low energies more, the apparent SPR is too *early*. Note also that the *impulsive* events on the left in Figure 3.2 show *no* evidence of large errors. Tan *et al.* (2013) have found that the SPR times and path lengths of the non-relativistic electrons agree with those of the ions and Rouillard *et al.* (2012) have also shown lateral spreading of the shock wave as imaged by the coronagraphs.

High-energy protons are often strongly beamed along the interplanetary magnetic-field ***B***, so a particular neutron monitor on Earth sees a peak when the asymptotic look direction is aligned with ***B***. As ***B*** varies, neutron monitors often see spiky increases or multiple peaks and valleys of intensity.

Surely there are a few GLEs where the SPR timing alone would permit some kind of (unspecified) acceleration at the time of the associated flare. However, these events may just have faster CMEs or a faster decrease in V_A with radius that would permit earlier ion acceleration by the shock, or earlier arrival of the shock above closed magnetic loops. If the GLEs with late SPR times are clearly shock accelerated, why would we seek a new mechanism for those events with early SPR times which have equally strong shocks? Shock acceleration is able to account for SEP acceleration in all gradual events, including GLEs, especially in GLEs. No other mechanism is required, no other seems capable.

3.2 Realistic Shock-SEP Timing and Correlations

With recent measurements on the STEREO spacecraft, it has been possible to construct three-dimensional distributions of CMEs and shocks and compare them with SEPs, *i.e.* to compare the SEPs and the shock along the same single field line. (Rouillard *et al.* 2011, 2012). Figure 3.4 shows aspects of this comparison.

The left-hand simulation in Figure 3.4 reconstructs the way the CME and shock spread. The actual SPR time depends upon the time an active shock actually strikes the (dashed) field line to an observer. It would be a great improvement on the comparison in Figure 3.3 if we could see the *local* shock as we can here. Some images of the shock are shown in the upper right panels of Figure 3.4.

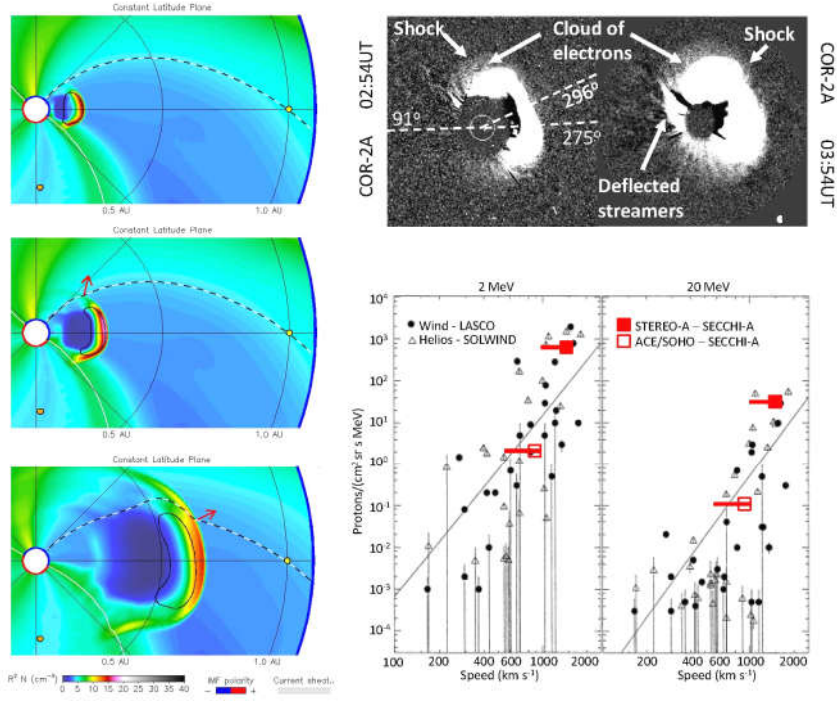

Fig. 3.4. Left-hand panels show a STEREO simulation of the evolution and lateral spread of the CME and shock. Upper-right panels show actual images of the shock. Lower right panels show possible improvement in the intensity – CME-speed correlation (red points) when observed on single field lines at two different longitudes in an event (Rouillard *et al.* 2011, 2012)

The lower-right panels in Figure 3.4 show correlations of peak proton intensities at 2 and 20 MeV with CME speed from the earlier study by Kahler (2001) shown in Figure 2.11. However, no single speed exists for any CME or shock, and there is no single peak proton intensity, since both vary strongly with longitude. The red points in the lower right panel of Figure 3.4 compare intensity and CME speed on single magnetic flux tubes, apparently improving the correlation.

We need this kind of spatial CME – SEP analysis for many events to test the validity of any correlation between shock speed and SEP intensity and to determine its functional shape (*i.e.* non-power-law) and seek dependence on other variables.

More recently, Gopalswamy *et al.* (2013) studied the first GLE of Solar Cycle 24, GLE 71 on 17 May 2012, together with 6 other large, well-connected events with fast CMEs. The evolution of two of the CMEs is compared in Figure 3.5.

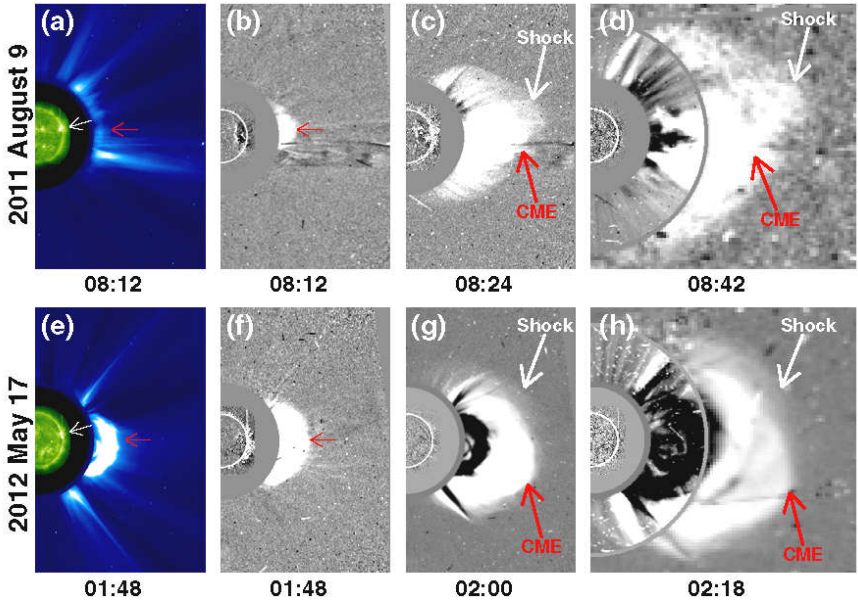

Fig. 3.5. The time evolution of two CMEs, 9 August 2011 and the GLE on 17 May 2012, are shown from their first appearance on SOHO/LASCO. In panels (a) and (e), the SDO/AIA solar image at 195 Å shows the solar sources while the remaining difference images show evolution of the CMEs and shocks. Red arrows point to the CME nose. The shock remains closer to the CME in (h) than in (d), indicating a stronger shock (Gopalswamy *et al.* 2013).

In the GLE, the shock formation height (type II radio burst onset) is at 1.38 R_S and the observed CME height at the time of particle release was directly measured as 2.32 R_S. This is consistent with the findings from extrapolations of GLEs in Cycle 23. The authors concluded that the event of May 2012 was a GLE simply because it was better connected to Earth than the other large SEP events with similar or even faster CMEs.

Thakur *et al.* (2016; see also Tylka and Dietrich 2009) compared the >700 MeV proton channel on GOES as an alternate indicator of GLEs. They found two events that differed, one GLE with no increase at >700 MeV and one >700-MeV increase that was not a GLE. They ascribed the difference to the level of the background. They also found that GLEs were generally observed when the shocks form at 1.2 – 1.93 R_S and when solar particle release (SPR) occurs between 2 – 6 R_S. Note that the electron acceleration that produces the type II burst could

occur while the shock is still propagating within closed magnetic loops, but SPR time must occur when the shock is on open magnetic field lines.

Cliver, Kahler, and Reames (2004) found a strong (~90%) association of decametric-hectometric (DH; 1–14 MHz) type II radio emission produced at ~3 R_S with SEP events with 20 MeV protons. The correlation was only 25% for lower-altitude metric type II's without DH suggesting that shock acceleration is strongest above ~3 R_S.

3.3 Injection Profiles

Relating to SEP increases early in events, Kahler (1994) plotted the intensity of SEPs, not as a function of time, but as a function the height of the CME, using the height-time plot for the CME, as shown in Figure 3.6. Not only are the protons injected late, but their intensities continue to rise until $R > 6$ R_S, even at 21 GeV. A final peak in the Alfvén speed *vs.* height occurs at ~4 R_S and V_A has probably declined to about 600 km s^{-1} at 6 R_S (Mann *et al.* 2003; see also Section 1.4). The Alfvén-Mach number, V_S/V_A remains at ~2 or greater above ~1.2 R_S for these shock waves.

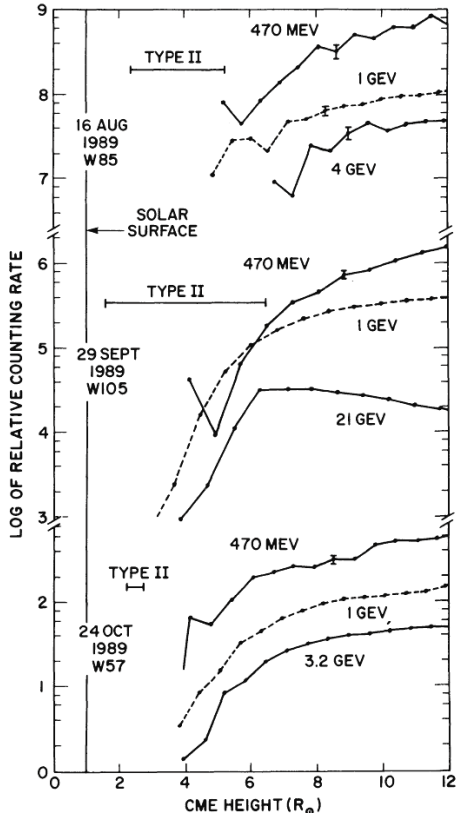

Fig. 3.6. Injection profiles of high-energy protons are shown as a function of CME height for three GLEs in 1989: August 16, September 29, and October 24. The CME speeds for these events are 1377, 1828, and 1453 km s^{-1}, respectively (Kahler 1994).

3.4 High-Energy Spectra and Spectral Knees

Are GLEs fundamentally different from other gradual SEP events? Is it likely that there is some new source of particles that can only be seen at energies above ~0.5 GeV? Much of the evidence connecting gradual SEPs to shock acceleration, especially element abundances and source-plasma temperatures, comes from energies below 100 MeV. Do the high-energy spectra come from the same source? Some spectra are shown in Figure 3.7.

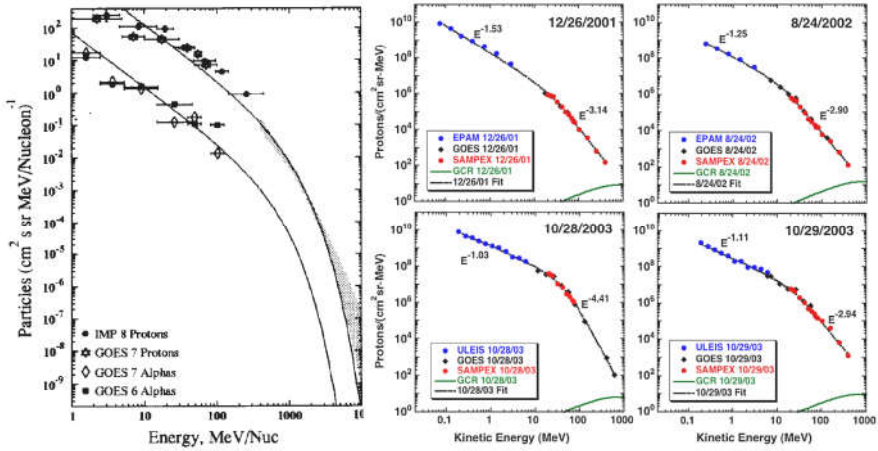

Fig. 3.7. The left panel shows H and He in the large GLE of September 29, 1989 (Lovell, Duldig, and Humble 1998). The shaded region is the spectrum deduced from neutron monitors and the spectra are fit to the shock-spectral shape of Ellison and Ramaty (1985). The four right-hand panels show GLE fluence spectra that are typical of the 16 GLE spectra assembled by Mewaldt et al. (2012) fit to double power-law spectra.

Mewaldt *et al.* (2012) studied spectra and element abundances of 16 GLEs. They found that the empirical double power-law spectral forms give a better fit than the power-law-times-exponential spectrum of Ellison and Ramaty (1985, see also Lee 2005) that models escape of high-energy particles from the shock. In any case, *none* of the 16 GLEs showed evidence of spectral *hardening* that might suggest the existence of a new source that could dominate higher energies.

Tylka and Dietrich (2009) have used the geomagnetic cutoff rigidities at neutron-monitor stations to develop integral rigidity spectra, using data from the world-wide neutron monitor network for 53 GLEs. The proton spectra are fit to double power laws in rigidity, decreasing with a power above 1 GV (430 MeV) in the range of 5 – 7 in 70% of the GLEs (see Section 6.1). None show hardening.

3.5 Intensity Dropouts and Compact Sources

When Mazur *et al.* (2000) plotted the energy of individual ions as a function of their arrival time, as seen in Figure 3.8, they found that the pattern of velocity dispersion that we described in Figure 3.1 was sharply interrupted for time intervals

when the spacecraft was simply not magnetically connected to the particle source. This was seen for impulsive SEP events and would be expected if magnetic flux tubes that were connected to a compact source were interspersed with others that were not. Gaps were not seen in gradual events where a spatially extensive shock wave would be expected to populate all field lines with SEPs.

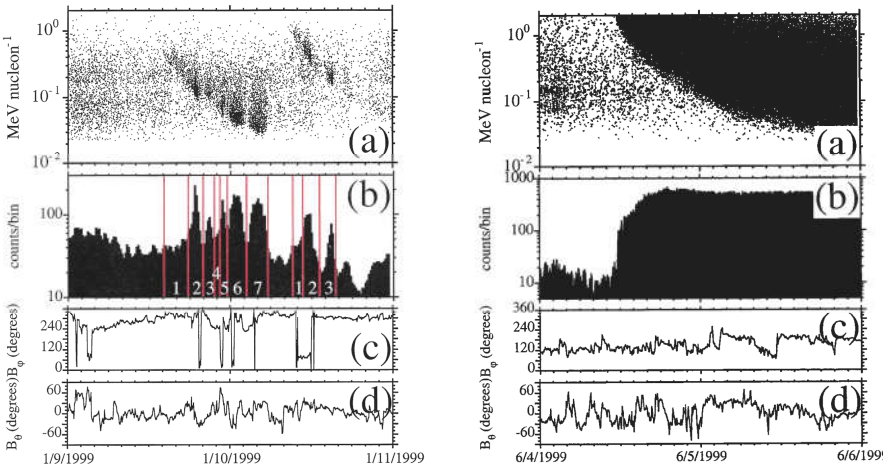

Fig. 3.8. Panels (a) show the energy *vs.* the arrival time of individual ions from an impulsive (left) and a gradual (right) SEP event. Panels (b) show the corresponding ion count rates while (c) and (d) show the magnetic field direction. Particles or gaps occur because some flux tubes connect to the compact source of impulsive SEPs and others do not (Mazur *et al.* 2000).

Subsequent observations (Chollet and Giacalone, 2011) found the boundaries between flux tubes with and without SEPs were extremely sharp. This indicated that there was little or no cross-field transport. The mixing of magnetic flux tubes that do and do not connect to any specific location on the Sun is expected from the random walk of their footpoints prior to the particle event (see Section 2.3.5).

3.6 Abundances

Abundances of elements and isotopes were one of the earliest indications of the two different sources of SEPs:

1. The average abundances of the elements in gradual events, relative to those in the photosphere, measured a FIP pattern related to the abundances in the corona and solar wind (see Sections 1.5.2 and 2.4.1). Since they were associated with fast, wide CMEs driving shock waves, this fit well with the idea of a shock wave sampling ambient coronal abundances.
2. The strong 1000-fold enhancements of ^{3}He/^{4}He, and the associations with streaming electrons, and with the type III radio bursts they produce, were clearly related to an impulsive source at the Sun and soon connected with nar-

row CMEs and solar jets (see Kahler, Reames, and Sheeley 2001; Reames, Cliver, and Kahler 2014a; see also Sections 2.4.2 and 4.7).

In the next chapters (Sections 4.6, 5.6) we will see that the pattern of the power-law dependence of abundance enhancements on A/Q of the ions leads to a determination of Q values and of the associated source-plasma temperature. The results are:

1. Gradual events: ~69% of events < 1.6 MK, 24% of events 2 – 4 MK (Reames 2016)
2. Impulsive SEP events: 2 – 4 MK (Reames, Cliver, and Kahler 2014a, b)

Thus in 69% of gradual events, shocks sweep up material at ambient coronal temperatures. In 24%, shocks traverse active regions and accelerate some residual impulsive suprathermal ions diluted by some ambient active-region plasma. We will develop the techniques for determining source temperatures in Sections 4.6 and 5.6. The temperatures are strong evidence for shock acceleration of large gradual SEP events. *Ambient coronal temperatures of SEPs would seem to be hard to explain for those who would like to accelerate gradual SEPs in hot flares,* or even to *store* SEPs in hot flare loops. Furthermore, GLEs show a similar distribution of source-plasma temperature to non-GLEs. W*e find nothing unique about GLEs*; they just happen to direct a few more high-energy particles toward Earth.

3.7 Electrons

In a review article, Ramaty *et al.* (1980) studied peak intensities of 0.5 – 1.1 MeV electrons *vs.* those of 10 MeV protons. For sufficiently intense protons they found a correlation between the electrons and protons that they ascribed to common acceleration by a shock wave. Cliver and Ling (2007) revisited this study from the perspective of impulsive and gradual SEP events. Their interesting findings are shown in Figure 3.9.

This study makes use of the fact that impulsive events are nearly all magnetically well-connected. The known impulsive events show no evidence of electron-proton intensity correlation. The shock-accelerated events span a much larger region of solar longitude and show electron-proton correlation where the impulsive events are absent, *i.e.* events that are poorly connected or those that have high proton intensities.

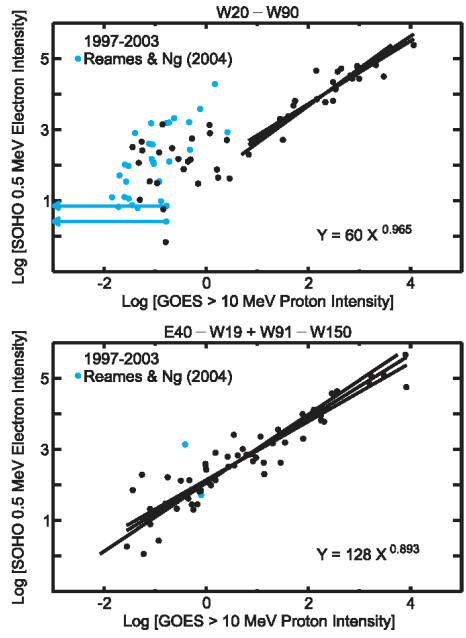

Fig. 3.9. The panels each show peak 0.5 MeV electron intensity *vs.* peak 10 MeV proton intensity. Events in the upper panel are well connected (20W – 90W) while those in the lower panel are poorly connected. The events in blue are impulsive events that are ^{3}He-rich with enhanced heavy elements. A proton-intense subset of well-connected events shows a strong correlation while essentially all of the poorly-connected events are correlated. (Cliver and Ling 2007).

Are the 0.5 MeV electrons accelerated at the same shock as the 10 MeV protons? Apparently so. In general, it is difficult to know how to compare protons and electrons. Unfortunately, low-energy electrons do not resonate with Alfvén waves as low-energy protons do. Should they be compared at the same energy, rigidity, or velocity? Usually the available intervals are used that are neither; yet, despite the lack of an ideal variable for comparison, it is still usually possible to conclude that impulsive SEPs are electron rich, and that shocks accelerate both protons and relativistic electrons.

Recently, an extensive list of over 1000 electron events spanning a solar cycle was prepared by Wang *et al.* (2012). The list includes radio, CME, X-ray, flare, ^{3}He/^{4}He, and 10-MeV proton data.

3.8 SEPs as Probes

As SEPs stream out along the interplanetary field they can map its structure. This was shown early by the radio mapping of the electron population in type III radio bursts. Knowing the direction to the center of the radio signal and the radius from the Sun determined by the frequency and models of the electron density *vs.* radius, the electrons could be followed, as seen in Figure 3.10. Occasionally, trajectories of this kind can be made using triangulation from two or more spacecraft (Reiner *et al.* 1998; see also Li *et al.* 2016). While such electron trajectories generally follow the Parker spiral, it is important to realize that field lines are often distorted by variations in the solar-wind speed and by the passage of CMEs.

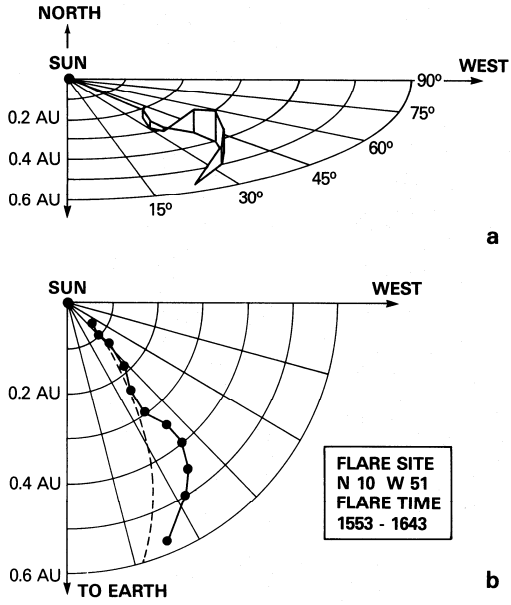

Fig. 3.10 The trajectory of the electron population in the type III radio burst accompanying a ^{3}He-rich SEP event is shown in three dimensions (a) and as a projection on the ecliptic (b) (Reames and Stone 1986)

Low-energy (<100 keV) electrons are often seen passing Earth outbound then returning from a magnetic reflection site beyond Earth (Kahler and Reames 1991; Tan *et al.* 2012, 2013) as shown in the example in Figure 3.11. These electrons are highly scatter-free (Tan *et al.* 2011) and are thus excellent probes of the magnetic topology.

However, electrons are not the only particles affected by their journey, Reames and Ng (2002) found that Fe/O was higher for sunward bound ions than for those that were outward bound in some SEP events. Since Fe scatters less then O, the Fe more rapidly passed Earth and was reflected sunward than was O, so the returning particles were more Fe-rich, *i.e.* they had simply traveled farther from the source.

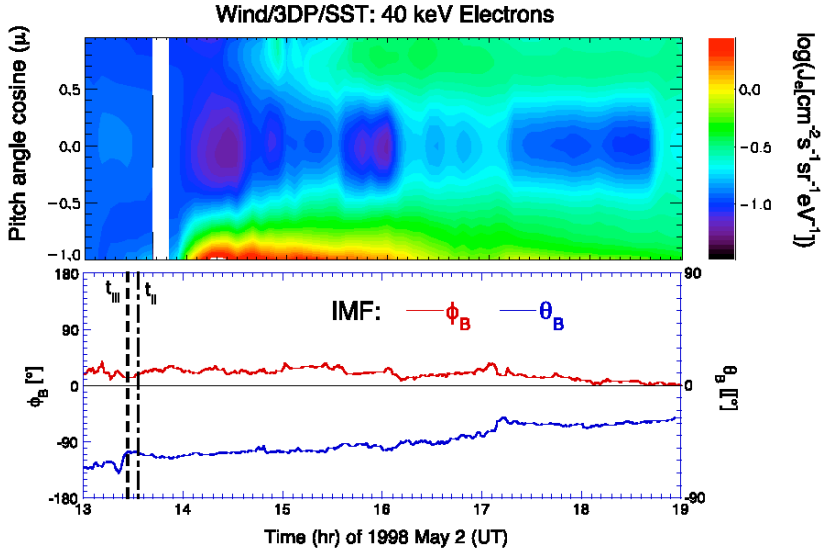

Fig. 3.11. The pitch-angle spectrogram of 40 keV electrons from the 2 May 1998 SEP event is shown in the upper panel. Electrons first appear from the Sun at $\mu \approx -1$ near 1400 UT and reflected electrons appear at $\mu \approx +1$ around 1500 UT. The lower panel shows the field direction (Tan *et al.* 2013).

There should be no surprise that the magnetic fields depart from the simple Parker spiral and become quite complex. Not only is there the random walk of field lines discussed in Section 2.3.5, but there is a constant progression of CMEs that disturb the field as suggested by Figure 3.12.

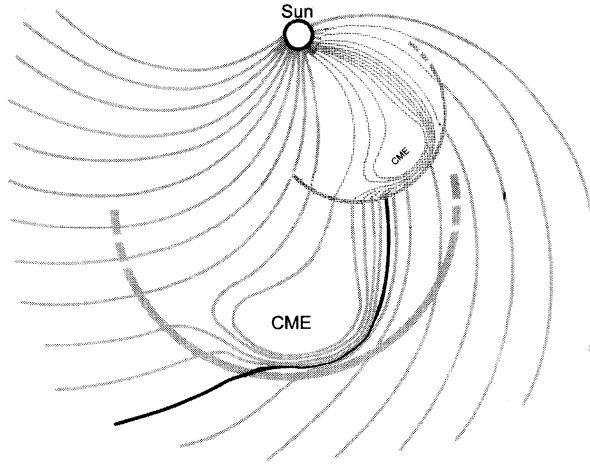

Fig. 3.12 The Sun can emit a progression of CMEs as suggested here. Particles accelerated at a shock preceding the smaller, newer CME can easily be reflected by converging field lines of the outer CME or by turbulence at the shock that precedes it.

The Sun can eject 2.5 CMEs day^{-1} at solar maximum (Webb and Howard 1994). If each CME occupies one steradian and its typical speed is ~400 km s^{-1}, CMEs will be randomly spaced at radial distances of typically ~1 AU apart, one after the other, out into the heliosphere in any direction. While most of them would not generate shocks, they would have low β_P and would carry magnetic flux ropes that contribute to magnetic distortions capable of reflecting particles.

References

Chollet, E. E., Giacalone, J., Evidence of confinement of solar-energetic particles to interplanetary magnetic field lines, Astrophys. J. **688**, 4 (2011)

Cliver, E. W., Kahler, S. W., and Reames, D. V., Coronal shocks and solar energetic proton events, Astrophys. J. **605**, 902 (2004)

Cliver, E. W., Ling, A. G., Electrons and protons in solar energetic particle events, Astrophys. J. **658**, 1349 (2007)

Ellison, D., Ramaty, R., Shock acceleration of electrons and ions in solar flares, Astrophys. J. **298**, 400 (1985)

Gopalswamy, N., Xie, H., Akiyama, S., Yashiro, S., Usoskin, I. G., Davila, J. M, The first ground level enhancement event of Solar Cycle 24: Direct observation of shock formation and particle release heights, Astrophys. J. Lett. **765** L30 (2013)

Gopalswamy, N., Xie, H., Yashiro, S., Akiyama, S., Mäkelä, P., Usoskin, I. G., Properties of Ground level enhancement events and the associated solar eruptions during solar cycle 23, Space Sci. Rev. **171**, 23 (2012)

Kahler, S. W., Injection profiles of solar energetic particles as functions of coronal mass ejection heights, Astrophys. J., **428**, 837 (1994)

Kahler, S. W., The correlation between solar energetic particle peak intensities and speeds of coronal mass ejections: Effects of ambient particle intensities and energy spectra, J. Geophys. Res. **106**, 20947 (2001)

Kahler, S. W., Reames, D. V., Probing the magnetic topologies of magnetic clouds by means of solar energetic particles, J. Geophys. Res. **96**, 9419 (1991)

Kahler, S. W., Reames, D. V., Sheeley, Jr., N. R., Coronal mass ejections associated with impulsive solar energetic particle events, Astrophys. J., **562**, 558 (2001)

Lee, M. A., Coupled hydromagnetic wave excitation and ion acceleration at an evolving coronal/interplanetary shock, Astrophys. J. Suppl., **158**, 38 (2005)

Li, B., Cairns, Iver H., Gosling, J. T., Steward, G., Francis, M., Neudegg, D., Schulte in den Bäumen, H., Player, P. R., Milne, A. R., Mapping magnetic field lines between the Sun and Earth, J. Geophys. Res. **121**, 925 (2016)

Lovell, J. L., Duldig, M. L., Humble, J. E., An extended analysis of the September 1989 cosmic ray ground level enhancement, J. Geophys. Res., **103**, 23,733 (1998)

Mann, G. Klassen, A. Aurass, H., Classen, H.-T., Formation and development of shock waves in the solar corona and the near-Sun interplanetary space, Astron. Astrophys. **400**, 329 (2003)

Mazur, J. E., Mason, G. M., Dwyer, J. R., Giacalone, J., Jokipii, J. R., Stone, E. C., Interplanetary magnetic field line mixing deduced from impulsive solar flare particles, Astrophys. J. **532**, L79 (2000)

Mewaldt, R. A., Looper, M. D., Cohen, C. M. S., Haggerty, D. K., Labrador, A. W., Leske, R. A., Mason, G. M., Mazur, J. E., von Rosenvinge, T. T., Energy spectra, composition, other properties of ground-level events during solar cycle 23, Space Sci. Rev. **171**, 97 (2012)

Ramaty, R., Paizis, C., Colgate, S. A., Dulk, G. A., Hoyng, P., Knight, J. W., Lin, R. P., Melrose, D. B., Orrall, F., Shapiro, P. R., Energetic particles in solar flares, In: *Solar flares: A monograph from Skylab Solar Workshop II.* (A80-37026 15-92) Boulder, Colo., Colorado Associated University Press, p117 (1980)

Reames, D. V., Solar release times of energetic particles in ground-level events, Astrophys. J. **693**, 812 (2009a)

Reames, D. V., Solar energetic-particle release times in historic ground-level events, Astrophys. J. **706**, 844 (2009b)

Reames, D.V., Temperature of the source plasma in gradual solar energetic particle events, Solar Phys., **291**, 911 (2016) DOI: 10.1007/s11207-016-0854-9, arXiv: 1509.08948

Reames, D.V., Cliver, E.W., Kahler, S.W., Abundance enhancements in impulsive solar energetic-particle events with associated coronal mass ejections, Solar Phys. **289**, 3817, (2014a) DOI: 10.1007/s11207-014-0547-1

Reames, D.V., Cliver, E.W., Kahler, S.W., Variations in abundance enhancements in impulsive solar energetic-particle events and related CMEs and flares, Solar Phys. **289**, 4675 (2014b) DOI: 10.1007/s11207-014-0589-4

Reames, D. V., Lal, N., A multi-spacecraft view of solar-energetic-particle onsets in the 1977 November 22 event, Astrophys. J., **723**, 550 (2010)

Reames, D. V., Ng, C. K., Angular distributions of fe/o from wind: new insight into solar energetic particle transport, Astrophys, J. Lett. **575**, L37 (2002)

Reames, D. V., Stone, R. G., The identification of solar He-3-rich events and the study of particle acceleration at the sun, Astrophys. J., **308**, 902 (1986)

Reiner, M. J., Fainberg, J., Kaiser, M. L., Stone, R. G., Type III radio source located by Ulysses/Wind triangulation, J. Geophys. Res. **103**, 1923. (1998)

Rouillard, A.C., Odstrčil, D., Sheeley, N.R. Jr., Tylka, A.J., Vourlidas, A., Mason, G., Wu, C.-C., Savani, N.P., Wood, B.E., Ng, C.K., *et al*., Interpreting the properties of solar energetic particle events by using combined imaging and modeling of interplanetary shocks, Astrophys. J. **735**, 7 (2011)

Rouillard, A., Sheeley, N. R. Jr., Tylka, A., Vourlidas, A., Ng, C. K., Rakowski, C., Cohen, C .M. S., Mewaldt, R. A., Mason, G. M., Reames, D.,*et al*., The longitudinal properties of a solar energetic particle event investigated using modern solar imaging, Astrophys. J. **752**, 44 (2012)

Tan, L. C., Reames, D. V., Ng, C. K., Shao, X., Wang, L., What causes scatter-free transport of non-relativistic solar electrons?, Astrophys J. **728**, 133 (2011)

Tan, L. C., Malandraki, O. E., Reames, D. V., Ng, C. K., Wang, L., Dorrian, G. Use of Incident and Reflected Solar Particle Beams to Trace the Topology of Magnetic Clouds, Astrophys. J. **750**, 146 (2012)

Tan, L. C., Malandraki, O. E., Reames, D. V., Ng, C. K., Wang, L., Patsou, I., Papaioannou, A., Comparison between path lengths traveled by solar electrons and ions in ground-level enhancement events, Astrophys J . **768**, 68 (2013)

Thakur, N., Gopalswamy, N., Mäkelä, P., Akiyama, S., Yashiro, S., Xie, H., Two exceptions in the large SEP events of Solar Cycles 23 and 24, Solar. Phys. **231** 519 (2016)

Tylka, A. J., A. J., Cohen, C.M.S., Dietrich, W.F., Krucker, S., McGuire, R. E., Mewaldt, R.A., Ng, C.K., Reames, D.V, Share, G. H., Onsets and release times in solar particle events, *Proc. 28th Int. Cosmic Ray Conf.,* 3305 (2003)

Tylka, A. J., Dietrich, W. F., A new and comprehensive analysis of proton spectra in ground-level enhanced (GLE) solar particle events, in *Proc. 31st Int. Cos. Ray Conf* , Lódz (2009), http://icrc2009.uni.lodz.pl/proc/pdf/icrc0273.pdf

Wang, L., Lin, R.P., Krucker, S., Mason, G.M., A statistical study of solar electron events over one solar cycle, Astrophys. J. 759, 69 (2012)

Webb, D. F., Howard, R. A., The solar cycle variation of coronal mass ejections and the solar wind mass flux, J. Geophys. Res. 99, 4201 (1994)

4. Impulsive SEP Events

Abstract ^{3}He-rich, Fe-rich, and rich in elements with Z > 50, the abundances of solar energetic particles (SEPs) from the small impulsive SEP events stand out as luminaries of our study. Element abundance enhancements increase 1000-fold as the ~3.6 power of the mass-to-charge ratio *A/Q* from He to Pb, enhanced during acceleration in islands of magnetic reconnection. Their pattern of enhancements suggest a source with C and N fully ionized like He, Ne enhanced more than Mg and Si, and heavy elements following the power-law enhancement *vs. A/Q* with *Q* at a source temperature of 2.5 – 3.2 MK. These temperatures are typical of solar active regions from which these impulsive SEPs come. However, in a few events, the element S is greatly enhanced, apparently by the same resonant-wave mechanism that enhances ^{3}He. Which mechanism will dominate? Impulsive SEP events are associated with slow, *narrow* CMEs, and solar jets where magnetic reconnection on open field lines gives particles direct access to space.

Impulsive SEP events were first identified by their unusual enhancements of ^{3}He/^{4}He, with ~1000-fold increases over the abundance ^{3}He/^{4}He ≈ 5 × 10^{-4} in the solar wind, frequently with ^{3}He/^{4}He > 1, and occasionally with ^{3}He > H. Next we found enhancements of Fe/C or Fe/O of ~10 which were more-stable indicators of impulsive events, since ^{3}He/^{4}He varies widely. Then ~1000-fold increases in elements with (*Z* > 50)/O were added to the unusual picture.

Despite the huge enhancements of ^{3}He, the isotopes ^{2}H and ^{3}H are *not* observed in SEPs (<1% of ^{3}He according to Serlemitsos and Balasubrahmanyan 1975). Observations of γ-ray lines and neutrons show the presence of nuclear reactions in the low corona during flares (*e.g.* Ramaty and Murphy 1987), but isotopes of Li, Be, and B have *never* been observed in SEPs. Limits on Be/O or B/O in large SEP events are < 4 × 10^{-4} (*e.g.* Cook, Stone, and Vogt 1984) Reaction secondaries are trapped on flare loops and cannot escape, and the ^{3}He we see is *not* a nuclear-reaction product, it is accelerated by resonant wave-particle reactions (*e.g.* Temerin and Roth 1992). In fact, it seems that only particles accelerated on *open* field lines, *e.g.* in solar jets (or at shock waves), can ever escape.

4.1 Selecting Impulsive Events

Many years ago, Reames (1988) examined the distribution of all daily abundance averages during 8.5 years with measurable Fe/O ratios, and found a bimodal distribution with peaks near Fe/O ≈ 0.1 and Fe/O ≈ 1.0. The technique was free from bias related to event selection, although long-duration events were certainly more heavily sampled. Periods with Fe/O near 0.1 had unremarkable abundances of other elements, but those near 1.0 also had enhancements in ^{3}He/^{4}He, ^{4}He/H, and

e/p ratios. While the two distributions of Fe/O did have an overlap region, largely because the poor statistics available at that time spread the distributions, the results showed that Fe/O at about 2 MeV amu^{-1} was more reliable for selecting candidate periods for impulsive SEP events than, *e.g.* ^{3}He/^{4}He, which has much larger variations and is difficult for many instruments to measure at low ratios.

A more-recent version of the bimodal abundance study is the two-dimensional histogram shown in Figure 4.1, based upon much more accurate data. Here 8-hr measurements of Ne/O *vs.* Fe/O are binned for a 19-year period, and this time we have the luxury of requiring 20% accuracy to prevent excessive spreading of the distributions. Of course, it is still true that gradual events occupy many more 8-hr periods and impulsive events, with lower intensities, are less likely to achieve 20% accuracy, but the presence of two peaks is clear.

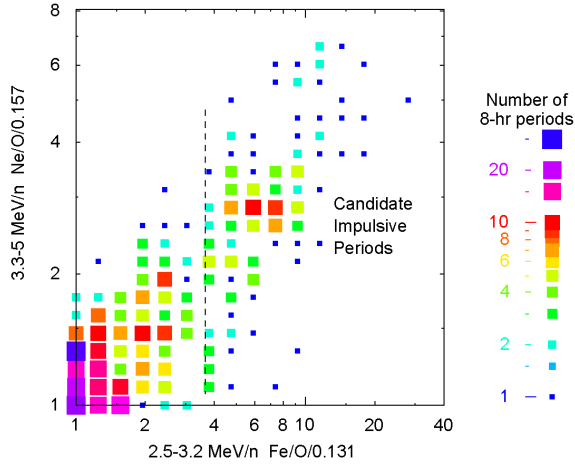

Fig. 4.1. Measured relative enhancements in Ne/O *vs.* Fe/O for 8-hr periods during 19 years are binned for all periods with errors of 20% or less. (Reames, Cliver, and Kahler 2014a)

Periods near coordinates (1, 1) in Figure 4.1, occur during large gradual SEP events for which the normalization was chosen. The peak near (6, 3) in the figure represents impulsive events, but the Ne/O value was not actually used for selection of candidate periods for defining impulsive SEP events.

4.2 Sample Impulsive Events

Figure 4.2 shows intensities of several particle species in a sample of impulsive SEP events with various properties. In events 1, 2, and 5, we have ^{3}He/^{4}He >> 1, and in event 1, ^{3}He > H. In events 1 and 2 the O, which may seem high relative to Fe, is actually background from anomalous cosmic-ray O and is present at almost the same rate before and after the events. In events 5 and 6, O is closer to ^{4}He than in other events, these "He-poor" events have low ^{4}He/O. Events 6 – 13 on the bottom row are an order of magnitude larger in ^{4}He, O, or Fe than those in the first row, and heavy elements begin to appear; these larger events are also not as strongly ^{3}He-rich. Instrument limitations: only groups of elements are resolved above $Z = 34$ and, when ^{3}He/^{4}He < 0.1, ^{3}He is poorly resolved and is not plotted.

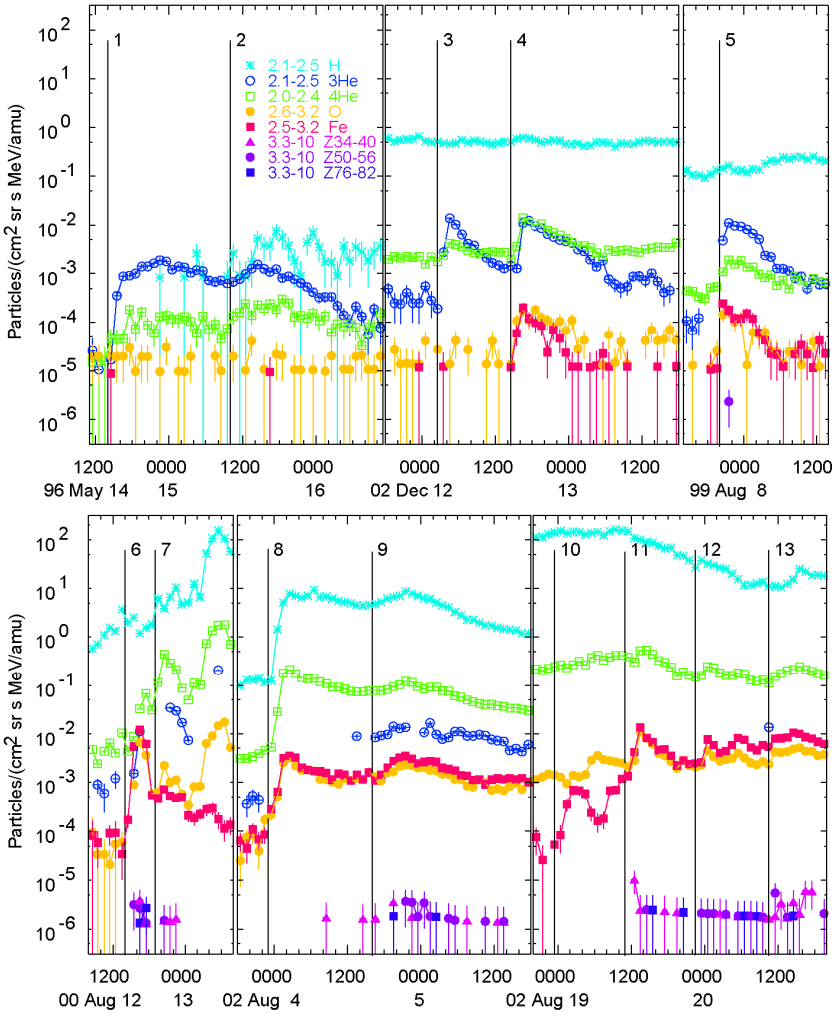

Fig. 4.2. Intensities of H, ^{3}He, ^{4}He, O, Fe, and heavy elements are shown as a function of time during 13 impulsive SEP events (Reames and Ng 2004).

4.3 Energy Dependence

Some sample energy spectra in ^{3}He-rich events are shown in Figure 4.3.

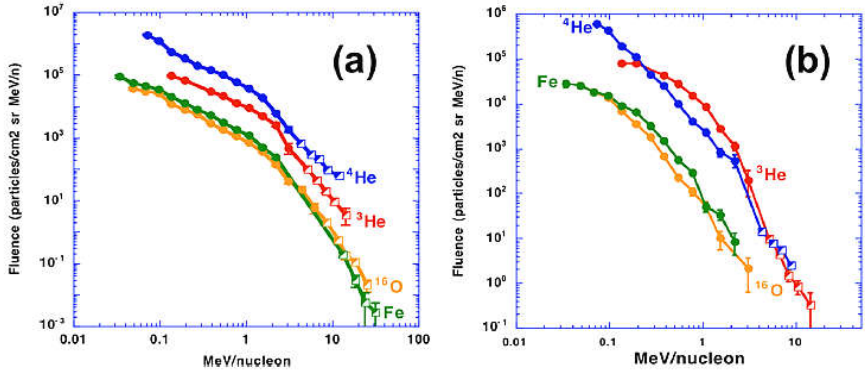

Fig. 4.3. Spectra of ^{3}He, ^{4}He, O and Fe are shown in the (a) 9 September 1998 and the (b) 21 March 1999 events (Mason 2007).

The spectra on the left in Figure 4.3 appear as broken power-law spectra while those on the right are more curved and show large energy variations in ^{3}He/^{4}He as seen in Figure 4.4 below. Abundance ratios of Fe/O show less spectral variation.

Fig. 4.4. Energy dependence is shown for ^{3}He/^{4}He ratios. Red and blue are for events shown in Figure 4.3. (a) and (b), respectively. The green event is 27 September 2000 (Mason 2007).

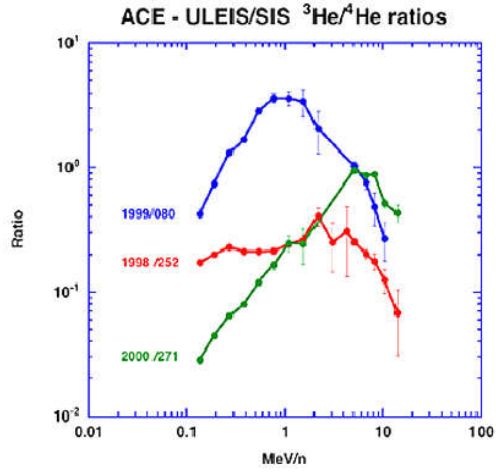

The ^{3}He/^{4}He variations shown in Figure 4.4 make it difficult to characterize an event by this ratio, which seems to peak in the region of 1 – 10 MeV amu^{-1}. Fe/O at a few MeV amu^{-1} is a better alternative for defining impulsive events, as suggested in Figure 4.1.

Liu, Petrosian, and Mason (2006) have been able to fit the complex spectra of ^{3}He and ^{4}He with a model of stochastic acceleration by a power-law spectrum of plasma-wave turbulence, presumably associated with magnetic reconnection. This work follows the tradition of stochastic acceleration involving the general transfer of energy from waves to particles (see reviews: Miller *et al.* 1997; Miller 1998).

These models have difficulty explaining the strong *A/Q*-dependent enhancements extending to heavy elements that we will discuss in Sections 4.5 and 4.6.

4.4 Abundances for Z ≤ 26

Given the spectra and variations of ^{3}He we have seen, it is not surprising that the ^{3}He/^{4}He ratio is uncorrelated with other abundance ratios as seen in Figure 4.5. This was known to Mason *et al.* (1986) and Reames, Meyer, and von Rosenvinge (1994) and is often taken as evidence that the mechanism of ^{3}He enhancement is different from that causing enhancement of Fe/O and heavy elements.

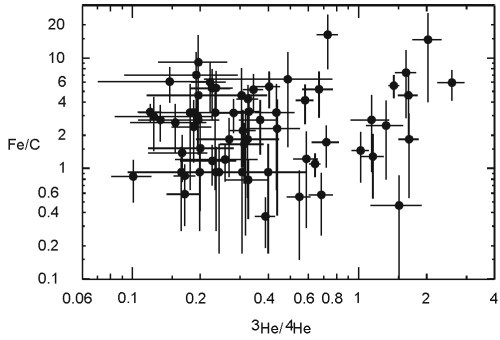

Fig. 4.5. Cross plots of Fe/C *vs.* ^{3}He/^{4}He at 1.3-1.6 MeV amu^{-1} in impulsive SEP events shows little evidence of correlation (Reames 1999; adapted from Reames, Meyer, and von Rosenvinge 1994).

The average enhancements of the elements from ^{4}He through Fe were summarized by Reames (1995, 1999) as seen in Figure 4.6.

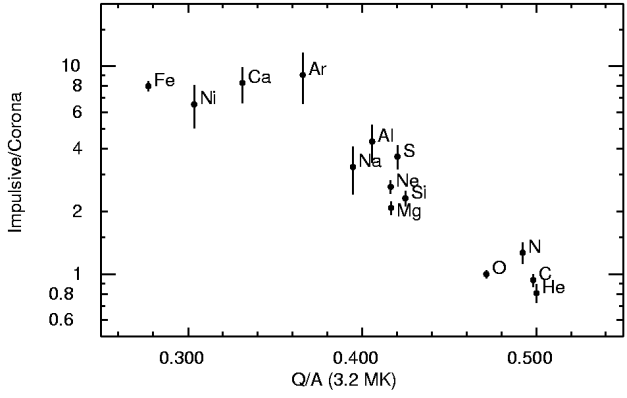

Fig. 4.6. Average abundance enhancements of elements in impulsive SEP events *vs. Q/A* at 3.2 MK as of 1995 as shown by Reames (1999).

It was suggested by Reames, Meyer, and von Rosenvinge (1994) that the grouping of the enhancements of ^{4}He, C, N, and O occurs because C, N, and O, are fully ionized, like ^{4}He, and thus have $Q/A = 0.5$. Ions in the group from Ne – S have closed shells of 2 orbital electrons and $Q/A \approx 0.4$. This occurs at a temperature of about 3 – 5 MK, as we shall see.

4.5 Abundances for 34 ≤ Z ≤ 82

Beginning with the launch of the *Wind* spacecraft late in 1994, abundances of elements in the remainder of the periodic table well above Fe started to become available on a regular basis (Reames 2000). Although resolution of individual elements was not possible, the pattern of enhancement of element groups gave a new perspective to the term "enhancement" as the high-Z elements approached 1000-fold enhancements, comparable with those of ^{3}He. Subsequently, two completely different instrument techniques yielded: i) the abundances *vs.* A at 0.1 – 1.0 MeV amu^{-1} up to A = 200 (Mason *et al.* 2004) and ii) the abundances *vs.* Z at 3.3 – 10 MeV amu^{-1} up to $Z \approx 82$ (Reames and Ng 2004). Both are seen in Figure 4.7.

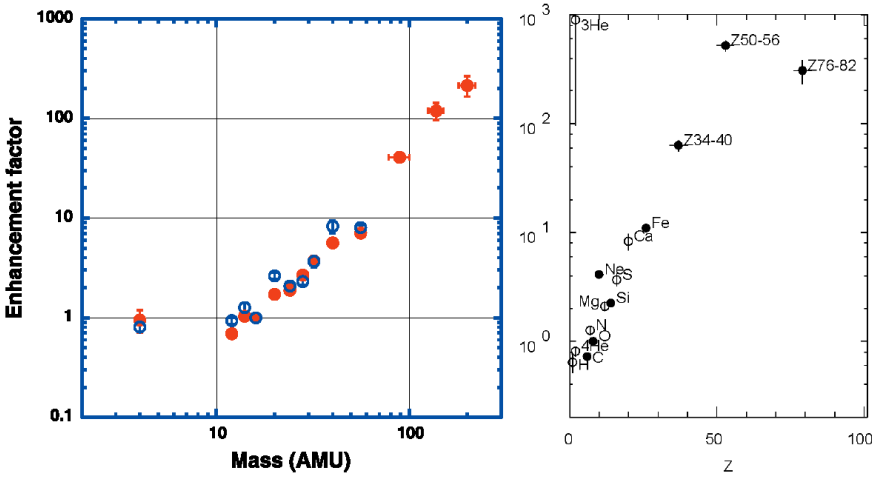

Fig. 4.7. Enhancements relative to solar system and coronal abundances are extended to high masses at 0.1 – 1.0 MeV amu^{-1} in the left panel (red, Mason *et al.* 2004) and to high Z at 3.3 – 10 MeV amu^{-1} in the right (Reames and Ng 2004). Open symbols are from Reames (1995).

Reference abundances used for Figure 4.7 are solar system abundances for the red symbols in the left panel and solar system abundances corrected for FIP to simulate coronal abundances in the right panel.

4.6 Power-Law Enhancements in A/Q: Source-Plasma Temperatures

The atomic physics that describes ionization states as a function of plasma temperature T has been studied for many years. Figure 4.8 shows A/Q *vs.* T, based on Q *vs.* T from atomic physics, which was used by Reames, Cliver, and Kahler (2014a) to determine the appropriate value of T for the power-law fit for impulsive SEP events shown in Figure 4.9. Values of Q *vs.* T below Fe are from Arnaud and Rothenflug (1985), Fe is from Arnaud and Raymond (1992) and elements in the high-Z region from Post et al. (1977).

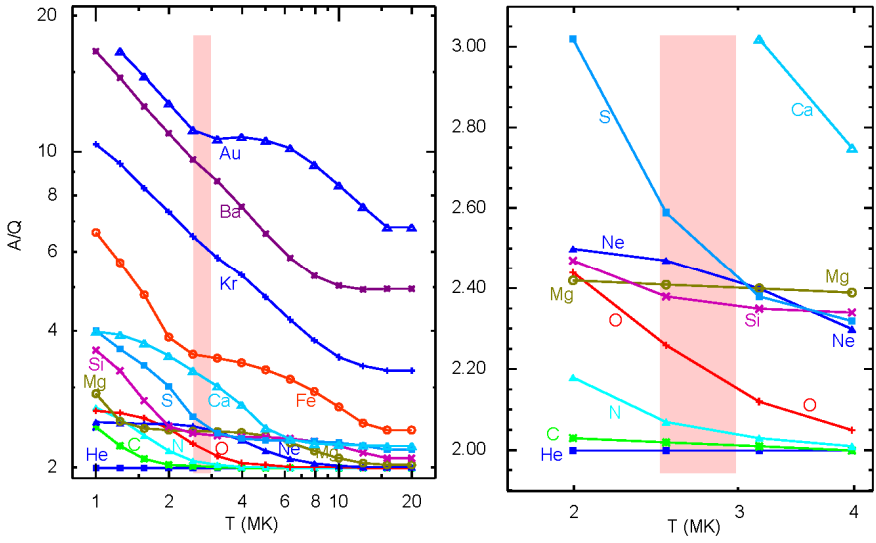

Fig. 4.8. *A/Q* is shown as a function of equilibrium temperature for various elements (left panel) and is enlarged for low *Z* (right panel). Elements below Fe are from Arnaud and Rothenflug (1985), Fe from Arnaud and Raymond (1992) and sample elements in the high-*Z* region from Post et al. (1977). The region used for Fe-rich impulsive SEP events is shaded.

Fig. 4.9. The mean enhancement in the abundances of elements in impulsive SEP events relative to reference gradual events is shown as a function of *A/Q* of the element. For the least-squares fit line shown in the figure the enhancement varies as the 3.64 ± 0.15 power of *A/Q* (Reames, Cliver, and Kahler 2014a).

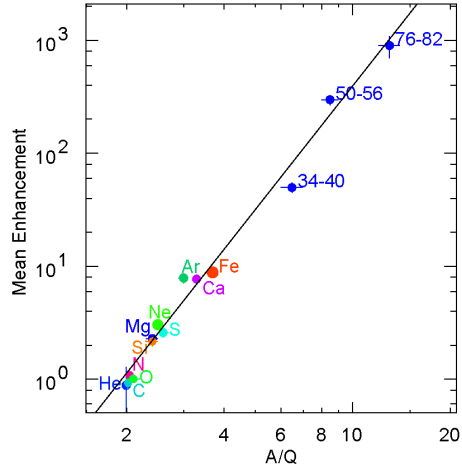

Reames, Cliver, and Kahler (2014a) selected a temperature that was somewhat lower than in earlier work. They noted that *A/Q* for Ne is higher than that for Mg or Si in this region $T \leq 3.0$ MK and would help explain the observation that, in the impulsive event averages, Ne/O > Mg/O > Si/O (see right panel of Figure 4.8). Also, *A/Q* for O was beginning to approach ≈ 2.2 in the region; this would help explain the "He-poor" events observed with low ^{4}He/O. Finally, *A/Q* values in the 2.5 – 3.2-MK region fit the enhancements in the elements with $Z \geq 34$ quite well.

It is also possible to determine a best-fit temperature and a power-law fit for individual impulsive SEP events. Each impulsive event has measured enhancements for the elements and each temperature in a region of interest has its own pattern of *A/Q*. We fit the enhancements *vs. A/Q* for each temperature, note the values of χ^2 for each fit, and then choose the fit, and temperature, with the minimum χ^2. Values of χ^2 *vs. T* are shown for 111 impulsive events in Figure 4.10. The number of events with minima at each temperature is listed along the *T* axis. The right panel shows the spread and magnitude of the enhancements.

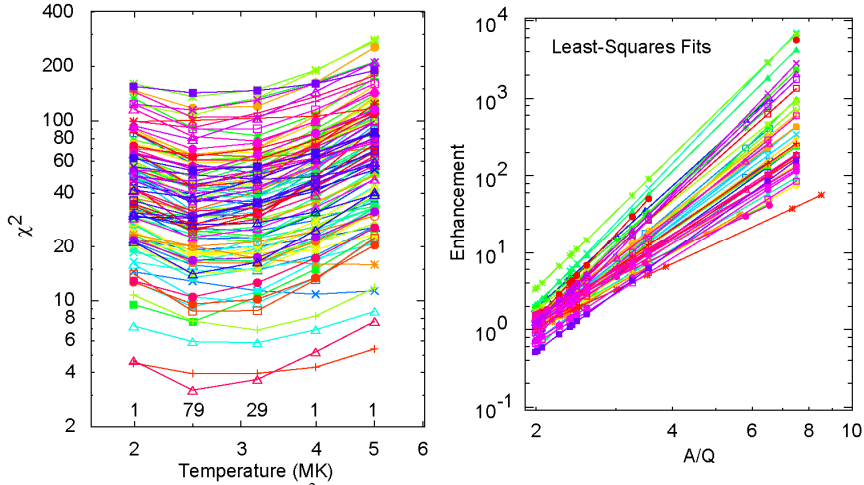

Fig. 4.10. The left panel shows χ^2 *vs. T* for all 111 impulsive SEP events using different colors and symbols for each event. The number of events with χ^2 minima at each temperature is shown along the bottom of the panel. The right panel shows the distribution of the fits (Reames, Cliver, and Kahler 2014b)

Are there any impulsive SEP events outside the region 2 – 4 MK? Reames, Cliver, and Kahler (2015) could find only a few new events outside 2.5 – 3.2 MK by relaxing the requirement for high Fe/O, and none elsewhere. However, Mason, Mazur, and Dwyer (2002) did find a small ^{3}He-rich event with enhanced N that must have had a temperature of < 1.5 MK, but this event was not even visible above 1 MeV amu^{-1} so it must have been a very small event with a very steep energy spectrum. Thus, impulsive SEP events outside solar active regions are rare and very small (but see Section 4.8).

4.7 Associations: CMEs, Flares, and Jets

While gradual SEPs are associated with fast, wide CMEs, impulsive SEP events are associated with smaller, slower, and especially *narrow* CMEs. Are these just extremes on a continuum? Probably not, since narrow CME from solar jets involve plasma motion along ***B*** and usually do not produce shocks, while wide ones are from extensive eruptive events that drive plasma perpendicular to ***B*** and pro-

duce strong shocks (*e.g.* Vršnak and Cliver 2008). Nearly 70% of impulsive Fe-rich SEP events in a recent study have associated CMEs with the properties shown in Figure 4.11.

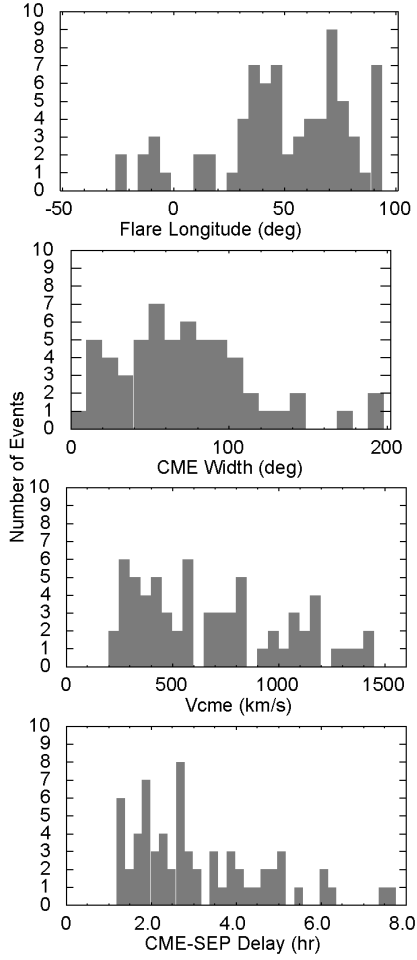

Fig. 4.11. Properties of the impulsive-SEP-associated CMEs and flares are as follows: flare longitude (top), CME width and speed, and the CME-SEP delay (Reames, Cliver, and Kahler 2014a). The median speed is 597 km s^{-1} *vs.* 408 km s^{-1} for all CMEs and 1336 km s^{-1} for gradual SEP events (Yashiro *et al.,* 2004). The average transport delay from CME launch to SEP onset is 2.7 h. From type III onset to SEP onset is 2.3 h, corresponding to a path length of ~1.4 AU, which suggests average pitch cosine, $\langle\mu\rangle \approx 0.8$ or complex paths like that in Figure 3.10.

Any correlation between impulsive SEP abundances and CMEs is difficult to quantify, but Figure 4.12 shows enhancements, relative to He, *vs. Z* for individual events, with measured $Z \geq 50$ ions, where the symbols denote the CME width. The events with the greatest enhancements have small, narrow CMEs or no CME. Yashiro *et al.* (2004) previously examined small ^{3}He-rich SEP events and found associated brightness changes and "coronal anomalies" that were probably small CMEs that were too faint to be cataloged. The evidence in Figure 4.12 suggests that the smaller the CME the greater the enhancements. The smallest events tend to have both suppressed He/O and enhanced ($Z \geq 50$)/O.

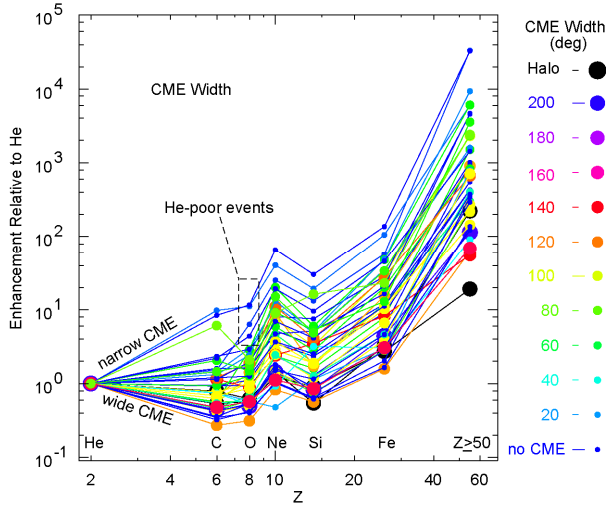

Fig. 4.12. Enhancements relative to He are shown *vs.* *Z* for impulsive SEP events. Symbol sizes indicate the associated CME width (Reames, Cliver, and Kahler 2014a).

When abundance enhancements are displayed as a function of the GOES soft X-ray peak intensity as in Figure 4.13, the smaller B- and C-class events have steeper abundance variations than the brighter M- and X-class X-ray events. The smaller events are also more likely to have large ^{3}He/^{4}He ratios (not shown, see Reames, Cliver, and Kahler, 2014b).

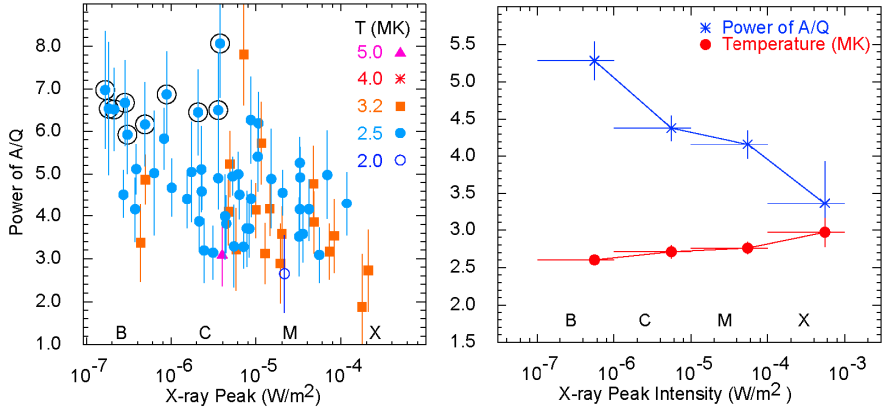

Fig. 4.13. The left panel shows the power of *A/Q vs.* the GOES soft X-ray peak intensity (and "CMX" class) for individual SEP events with temperature as a symbol and color. Circled events are "He-poor" with low ^{4}He/O caused by increased *A/Q* for O. The right panel shows variation of the mean temperature and power of *A/Q* within each soft X-ray class (after Reames, Cliver, and Kahler 2014b).

Flares are produced by magnetic reconnection on *closed* magnetic loops, so the energy and accelerated particles are contained, heating the plasma in the loops (>10 MK) and causing nuclear reactions in their denser footpoints. Jets are reconnection events involving *open* field lines so that plasma and any energetic particles accelerated will be ejected in the diverging field. Thus, it is not at all clear why

there should be *any* correlation of SEP properties with flare heating in the neighboring closed loops of an associated flare as seen in Figure 4.13, which suggests that jets with minimal flaring are more likely to produce stronger abundance enhancements. The cartoon in Figure 4.14 illustrates the basic mechanism behind a jet produced when new magnetic flux emerges, pressing into oppositely directed open magnetic field.

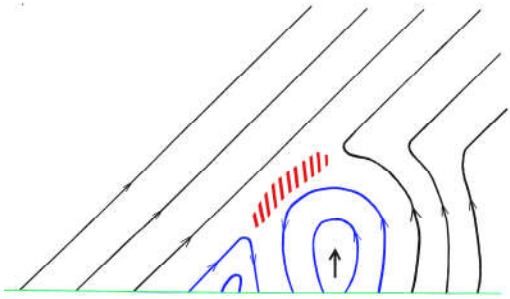

Fig. 4.14. A jet is produced when newly emerging magnetic flux (blue) reconnects with open field lines (black) in the red shaded region. Energetic particles and plasma can escape toward the upper right (Reames 2002).

Jets were identified and described by Shimojo and Shibata (2000) and associated with impulsive SEP events by Kahler, Reames, and Sheeley (2001). X-ray jets were also previously associated with type III radio bursts which provide the streaming electrons that may generate the EMIC waves needed for ^{3}He enhancements (Temerin and Roth 1992; Roth and Temerin 1997). The narrow CMEs associated with two impulsive SEP events are shown in Figure 4.15.

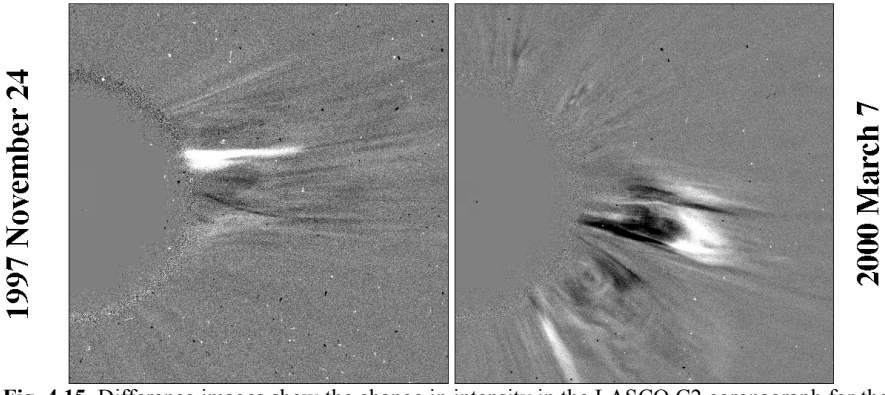

Fig. 4.15. Difference images show the change in intensity in the LASCO C2 coronagraph for the narrow CMEs associated with two impulsive SEP events (Kahler, Reames, and Sheeley 2001)

It has also been possible to trace the magnetic field lines from Earth to the Sun to locate the sources of events (Wang, Pick, and Mason 2006; Nitta *et al.* 2006). Much more sophisticated models of jets have also evolved that show reconnection associated with untwisting of axial field lines and generation of Alfvén waves (Moore *et al.* 2013; Lee, Archontis and Hood 2015). However, such models do

not yet include any related particle acceleration (see recent review of solar jets by Raouafi *et al.* 2016).

The studies of ion acceleration in islands of magnetic reconnection come from particle-in-cell simulations which show Fermi acceleration of ions reflected back and forth from the ends of the collapsing islands of reconnection (Drake *et al.* 2009; Knizhnik, Swizdak, and Drake 2011; Drake and Swizdak 2012). The acceleration produces a strong power-law dependence on A/Q where the power is related to the width distribution of the islands of reconnection. This theory provides the most promising explanation of the element abundance enhancements in impulsive SEP events and is appropriate to involvement of solar jets. However, ^{3}He enhancements seem to require a separate explanation (*e.g.* Temerin and Roth 1992).

4.8. Can We Have it Both Ways?

It seems suspicious to derive ^{3}He enhancements from one mechanism and heavy-element enhancements from another – in the same SEP event. Do both really contribute?

Recently, Mason *et al.* (2016) found 16 ^{3}He-rich events in 16 years with extremely high S/O abundances in the 0.4 – 1.0 MeV amu^{-1} interval. Most of these events are too small to be measured above 1.0 MeV amu^{-1}, the few we can measure show no significant anomalies. Properties of the most extreme event of 16 May 2014 are shown in Figure 4.16.

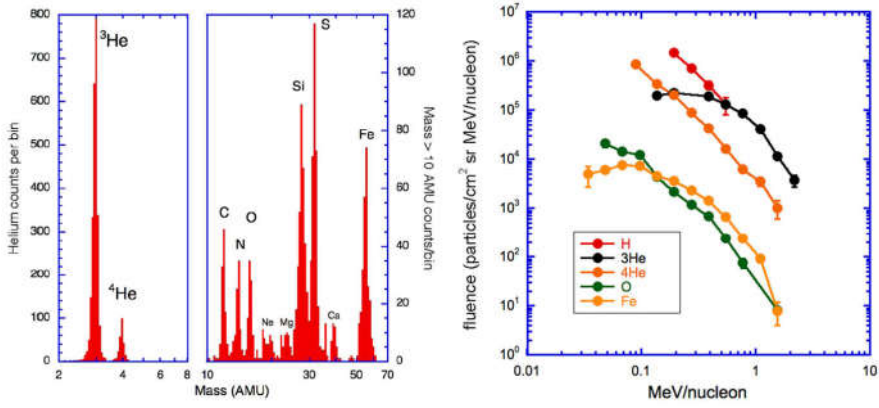

Fig. 4.16. Mass histograms of the 16 May 2014 ^{3}He-rich event are shown in the left two panels and some corresponding energy spectra are shown in the right panel (Mason *et al.* 2016).

This event has ^{3}He/^{4}He = 14.88±1.36 and S/O = 1.14±0.12, although the spectra show that these abundances are not constant but vary with energy. The shapes of the spectra of Si, S, and Fe are similar to that of ^{3}He, strongly suggesting that these elements are all accelerated or modified by the same mechanism.

Mason *et al.* (2016) consider a wide range of plasma temperatures above 0.4 MK. However, most models of resonant wave-particle acceleration (*e.g.* Fisk

1978; Roth and Temerin 1997) suggest that heavy elements might resonate with the same waves as ^{3}He, but through the second harmonic of their gyrofrequency. Since A/Q =1.5 for ^{3}He, naively we might expect Si and S to be accelerated when they have $A/Q \approx 3.0$, if the resonance is broad enough for us to use an average value of A/Q. For S, this average value occurs at 2.0 MK and for Si near 1.5 MK, both reasonable temperatures that might exist near the fringes of active regions (although greatly the enhanced S does not seem to be supported at 2.0 MK by Roth and Temerin 1997). Present theory of ^{3}He involves resonance of ions with electron-beam-generated EMIC waves; direct wave generation in the reconnection region is also a possibility that has not yet been explored.

The enhancements of other elements with less-rounded spectra might result from the power-law in A/Q more-commonly produced at higher energies by magnetic reconnection (*e.g.* Drake *et al.* 2009). It seems possible that the two mechanisms may compete to dominate different species at different energies in different impulsive SEP events, but a clear picture of the physics is still elusive and the degree of enhancement of all species may not be easily accommodated.

The understanding of the relative roles of the reconnection and the resonant wave mechanisms is the largest outstanding problem in the physics of flares, jets, and impulsive SEP events. Nature has tempted us with two huge 1000-fold enhancements, in ^{3}He and in heavy elements. Neither one is subtle. Yet they seem to be unrelated and we are unable to incorporate their explanations into a single physical model that can tell us which will dominate and when.

4.9 Nuclear Reactions: Gamma-ray Lines and Neutrons

It may seem incongruous to discuss γ-ray-line events in a chapter on impulsive SEP events since γ-ray lines are have not been observed in small events or jets. Line emission is observed in large flares from the de-excitation of nuclei produced in nuclear reactions that occur when ions, accelerated on closed coronal loops, are scattered into the loss cone and plunge into the higher-density corona (*e.g.* Ramaty and Murphy 1987). Hard (>20 keV) X-rays, common in flares, are produced by non-relativistic electrons but X-rays tell us nothing about accelerated ions; only γ-ray lines can help here. Protons, undergoing nuclear reactions with C, O, and Fe, for example, produce narrow γ-ray spectral lines in the region of ~0.5 – 7 MeV, whose relative intensities can be used to measure abundances of elements in the corona. Energetic heavier ions in the "beam" interacting with protons in the corona produce Doppler-broadened spectral lines that measure abundances in the accelerated beam, *i.e.* SEPs. These lines suggest that the accelerated ions in large flares are both ^{3}He-rich (Mandzhavidze, Ramaty, and Kozlovsky 1999) and Fe-rich (Murphy *et al.* 1991). Thus it seems that flares and jets might accelerate ions in the same way and γ-ray-line spectroscopy could contribute to our understanding of that process. Unfortunately, the masks used to improve position resolution in modern spectroscopy missions block too many γ-rays to permit γ-ray-line spectroscopy.

Nuclear reactions in the corona also produce ^{2}H, ^{3}H, positrons, π-mesons, and isotopes of Li, Be, and B as inferred from the γ-ray-line spectroscopy. However, as we re-emphasize, *none* of these secondary products (except γ-rays and neutrons) has ever been observed in space. Apparently the secondary ions are magnetically trapped on the loops where they are created, suggesting that the primary ions that produced them were similarly trapped.

Evidence of a spatially extended γ-ray source and long-duration γ-ray events are discussed in Section 5.7.

Neutrons are also produced in nuclear reactions in solar flares and 50 – 300 MeV neutrons have been observed directly in space (Chupp *et al.* 1982; Chupp 1984). Neutrons decay into a proton, electron, and neutrino with a 10-min half life and neutron-decay protons of 5 – 200 MeV have also been measured, allowing a neutron spectrum to be calculated (*e.g.* Evenson *et al.* 1983, 1990). Neutron-decay protons are best measured for eastern solar events where they can be measured on field lines that are much less accessible to protons directly from the shock source, which slowly increase later.

4.10. Open Questions

This section suggests open questions that might be addressed by future research.

1. If most A/Q enhancements come from magnetic reconnection and ^{3}He enhancements come from wave-particle interactions, where and when do these acceleration mechanisms fit into models of solar jets? What parameters control their relative contributions?
2. Why do the impulsive SEP events with the lowest intensities, smallest associated flares and narrowest CMEs have the greatest enhancements of ^{3}He/^{4}He and the heavy-element abundance enhancements with the steepest power of A/Q? Can all these observations be explained by source depletion of the enhanced species? Surely not Fe-enhancements?
3. Measurements by a spacecraft near the Sun could improve SEP onset timing by removing the blurring effect of scattering during transport. What is the duration and time profile of impulsive events at 10 s to 1 min resolution and how does it compare with X-ray, γ-ray, and type-III-burst timing? Note that intensities vary as $\sim r^{-3}$, providing greatly improved statistics nearer the Sun for smaller events. Do the electron and ion sources differ? What is the relative timing of ^{3}He and ^{4}He?
4. For a spacecraft near the Sun, the $\sim r^{-3}$ intensity increase would allow observation of many more small impulsive SEP events from smaller jets. What is the size distribution? Are there nanojets supplying many impulsive suprathermal ions?
5. Discrete ionization states affect the assignment of source-plasma temperatures. $^{12}C^{+5}$ is enhanced but $^{12}C^{+6}$ is not; treating Q as 5.5 is approximate. $A/\langle Q\rangle$ is not the same as $\langle A/Q\rangle$. Then there is ^{13}C which is always enhanced. Can we improve the estimates of T?

References

Arnaud, M., Raymond, J., Iron ionization and recombination rates and ionization equilibrium, Astrophys. J. **398**, 394 (1992)

Arnaud, M., Rothenflug, R., An updated evaluation of recombination and ionization rates, Astron. Astrophys. Suppl. **60**, 425 (1985)

Chupp, E. L., High-energy neutral radiations from the sun, Ann. Revs Astron. Astrophys. **22**, 359 (1984)

Chupp, E. L., Forrest, D. J., Ryan, J. M., Heslin, J., Reppin, C., Pinkau, K., Kanbach, G., Rieger, E., Share, G. H., A direct observation of solar neutrons following the 0118 UT flare on 1980 June 21, Astrophys, J. Lett., **263**, L95 (1982)

Cook, W. R., Stone, E. C., Vogt, R. E., Elemental composition of solar energetic particles, Astrophys. J. **279**, 827 (1984)

Drake, J.F., Cassak, P.A., Shay, M.A., Swisdak, M., Quataert, E., A magnetic reconnection mechanism for ion acceleration and abundance enhancements in impulsive flares, Astrophys. J. Lett. **700**, L16 (2009)

Drake, J.F., Swisdak, M., Ion heating and acceleration during magnetic reconnection relevant to the corona, Space Sci. Rev. **172**, 227 (2012)

Evenson, P. Kroeger, R., Meyer, P., Reames, D., Solar neutron decay proton observations in cycle 21, Astrophys. J. Suppl. **73,** 273 (1990)

Evenson, P., Meyer, P., Pyle, K. R, Protons from the decay of solar flare neutrons, Astrophys. J. **274**, 875 (1983)

Fisk, L. A., ^{3}He-rich flares - a possible explanation, Astrophys. J. **224**, 1048 (1978)

Kahler, S. W., Reames, D. V., & Sheeley, Jr., N. R., Coronal mass ejections associated with impulsive solar energetic particle events, Astrophys. J., **562**, 558 (2001)

Knizhnik, K., Swisdak, M., Drake, J.F., The acceleration of ions in solar flares during magnetic reconnection, Astrophys. J. Lett. **743**, L35 (2011)

Lee, E. J., Archontis, V., Hood, A. W., Helical blowout jets in the sun: untwisting and propagation of waves, Astrophys. J. Lett. **798**, L10 (2015)

Liu, S., Petrosian, V., Mason, G. M., stochastic acceleration of ^{3}He and ^{4}He in solar flares by parallel-propagating plasma waves: general results, Astrophys. J. **636**, 462 (2006)

Mandzhavidze, N., Ramaty, R., Kozlovsky, B., Determination of the abundances of subcoronal ^{4}He and of solar flare-accelerated ^{3}He and ^{4}He from gamma-ray spectroscopy, Astrophys. J. **518**, 918 (1999)

Mason, G. M., ^{3}He-rich solar energetic particle events, Space Sci. Rev. **130**, 231 (2007)

Mason, G.M., Mazur, J.E., Dwyer, J.R., A new heavy ion abundance enrichment pattern in ^{3}He-rich solar particle events, Astrophys. J. Lett. **565**, L51 (2002)

Mason, G. M., Mazur, J. E., Dwyer, J. R., Jokippi, J. R., Gold, R. E., Krimigis, S. M., Abundances of heavy and ultraheavy ions in ^{3}He-rich solar flares, Astrophys. J. **606**, 555 (2004).

Mason, G. M., Nitta, N. V., Wiedenbeck, M. E., Innes, D. E., Evidence for a common acceleration mechanism for enrichments of ^{3}He and heavy ions in impulsive SEP events, Astrophys. J. **823**, 138 (2016)

Mason, G. M., Reames, D. V., Klecker, B., Hovestadt, D., von Rosenvinge, T. T., The heavy-ion compositional signature in He-3-rich solar particle events, Astrophys. J. **303**, 849 (1986)

Miller, J. A., Particle acceleration in impulsive solar flares, Space Sci. Rev. **86**, 79 (1998)

Miller, J. A., Cargill, P. J., Emslie, A. G., Holman, G. D., Dennis, B. R., LaRosa, T. N., Winglee, R. M., Benka, S. G., Tsuneta, S., Critical issues for understanding particle acceleration in impulsive solar flares, J. Geophys. Res. **102**, 14631 (1997)

Murphy, R. J., Ramaty, R., Kozlovsky, B., Reames, D. V., Solar abundances from gamma-ray spectroscopy: Comparisons with energetic particle, photospheric, and coronal abundances, Astrophys. J. **371**, 793 (1991)

Moore, R.L., Sterling, A.C., Falconer, D.A., Robe, D., The cool component and the dichotomy, lateral expansion, and axial rotation of solar X-ray jets, Astrophys. J., **769**, 134 (2013)

Nitta, N.V., Reames, D.V., DeRosa, M.L., Yashiro, S., Gopalswamy, N., Solar sources of impulsive solar energetic particle events and their magnetic field connection to the Earth, Astrophys. J. **650**, 438 (2006)

Post, D.E., Jensen, R.V., Tarter, C.B., Grasberger, W.H., Lokke, W.A., Steady-state radiative cooling rates for low-density, high temperature plasmas, At. Data Nucl. Data Tables **20**, 397 (1977)

Ramaty, R., Murphy, R. J., Nuclear processes and accelerated particles in solar flares, Space Sci. Rev. **45**, 213 (1987)

Raouafi, N. E., Patsourakos, S., Pariat, E., Young, P. R., Sterling, A. C., Savcheva, A., Shimojo, M., Moreno-Insertis, F., DeVore, C. R., Archontis, V, *et al.*, Solar coronal jets: observations, theory, and modeling, Space Sci. Rev. online (2016) DOI: 10.1007/s11214-016-0260-5 (arXiv:1607.02108)

Reames, D. V., Bimodal abundances in the energetic particles of solar and interplanetary origin, Astrophys. J. Lett. **330**, L71 (1988)

Reames, D. V., Coronal Abundances determined from energetic particles, Adv. Space Res. **15** (7), 41 (1995)

Reames, D. V.: Particle acceleration at the Sun and in the Heliosphere, Space Sci. Rev., **90**, 413 (1999)

Reames, D. V., Abundances of trans-iron elements in solar energetic particle events, Astrophys. J. Lett. **540**, L111 (2000)

Reames, D. V., Magnetic topology of impulsive and gradual solar energetic particle events, Astrophys. J. Lett. **571**, L63 (2002)

Reames, D.V., Cliver, E.W., Kahler, S.W., Abundance enhancements in impulsive solar energetic-particle events with associated coronal mass ejections, Solar Phys. **289**, 3817, (2014a) DOI: 10.1007/s11207-014-0547-1

Reames, D.V., Cliver, E.W., Kahler, S.W., Variations in abundance enhancements in impulsive solar energetic-particle events and related CMEs and flares, Solar Phys. **289**, 4675 (2014b) DOI: 10.1007/s11207-014-0589-4

Reames, D.V., Cliver, E.W., Kahler, S.W., Temperature of the source plasma for impulsive solar energetic particles, Solar Phys. 290, 1761 (2015) DOI: 10.1007/s11207-015-0711-2 (arXiv: 1505.02741)

Reames, D. V., Meyer, J. P., von Rosenvinge, T. T., Energetic-particle abundances in impulsive solar flare events, Astrophys. J. Suppl. **90**, 649 (1994)

Reames, D. V., Ng, C. K., Heavy-element abundances in solar energetic particle events, Astrophys. J. **610**, 510 (2004)

Roth, I., Temerin, M., Enrichment of ^{3}He and heavy ions in impulsive solar flares, Astrophys. J. **477**, 940 (1997)

Serlemitsos, A. T., Balasubrahmanyan, V. K., Solar particle events with anomalously large relative abundance of ^{3}He, Astrophys. J. **198**, 195, (1975)

Shimojo, M., Shibata, K., Physical parameters of solar X-ray jets, Astrophys. J. **542**, 1100 (2000)

Temerin, M., Roth, I., The production of ^{3}He and heavy ion enrichment in ^{3}He-rich flares by electromagnetic hydrogen cyclotron waves, Astrophys. J. Lett. **391**, L105 (1992)

Vršnak, B., Cliver, E.W., Origin of Coronal Shock Waves, Solar Phys. **253** 215 (2008) DOI: 10.1007/s11207-008-9241-5

Wang, Y.-M., Pick, M., Mason, G. M., Coronal holes, jets, and the origin of ^{3}He-rich particle events, Astrophys. J., **639**, 495 (2006)

Yashiro, S., Gopalswamy, N., Cliver, E.W., Reames, D.V., Kaiser, M., Howard, R., Association of coronal mass ejections and type III radio bursts with impulsive solar energetic particle event, In: Sakurai, T., Sekii, T. (eds.) *The Solar-B Mission and the Forefront of Solar Physics*, ASP Conf. Ser. 325, 401.

5. Gradual SEP Events

Abstract Gradual solar energetic-particle (SEP) events are the "big proton events" of the past and are usually much more "gradual" in their decay than in their onset. As their intensities increase, particles streaming away from the shock can amplify Alfvén waves that scatter subsequent particles, eventually limiting their flow at the "streaming limit." Waves generated by higher-speed protons running ahead can also throttle the flow of lower-energy ions, flattening spectra and altering abundances in the biggest SEP events. Yet, we find that the *A/Q*-dependent scattering causes abundance patterns, varying in space and time, which determine source-plasma temperatures, since the pattern of *Q* values of the ions depends upon temperature. Different source-plasma temperatures explain much of the variation in element abundances in gradual SEP events. In nearly 70% of gradual events, SEPs are shock-accelerated from ambient coronal plasma of ~0.8 – 1.6 MK, while 24% of the events involve accelerated material from active-region temperatures of 2 – 4 MK and include residual impulsive-suprathermal ions with pre-enhanced abundances. Non-thermal variations of the ions in gradual SEP events from 2 – 4 MK source plasma are greatly reduced, relative to those in impulsive SEPs, from similar plasma, probably because the accelerating shock waves average over impulsive-suprathermal ions from multiple jet sources. Later, SEPs become trapped in a *reservoir* behind the CME in gradual events, where spectra are uniform in space and decrease adiabatically in time as the magnetic bottle containing them slowly expands.

We begin by showing proton intensities in the classic large gradual SEP event of 4 November 2001 in Figure 5.1. This event, from a source longitude of W17 on the Sun, has the typical time profile of a centrally located event (see Section 2.3.3). The figure lists phases of the event along the abscissa which we will study, in approximate time order, although onsets were discussed previously in Section 3.1.

In impulsive SEP events, most particles traveled to us scatter free so we had little need to discuss transport. With increased intensities, particles from gradual SEP events generate or amplify their own spectrum of Alfvén waves for pitch-angle scattering, which complicates their transport more and more as intensities increase. In fact, it is the resonant waves, generated by the out-flowing particles, which scatter subsequent particles back and forth across the shock, incrementally increasing acceleration that drives particles to higher and higher energy.

For recent reviews of gradual SEP events see Desai and Giacalone (2016), and Lee, Mewaldt, and Giacalone (2012). For theoretical background see Parker (1963).

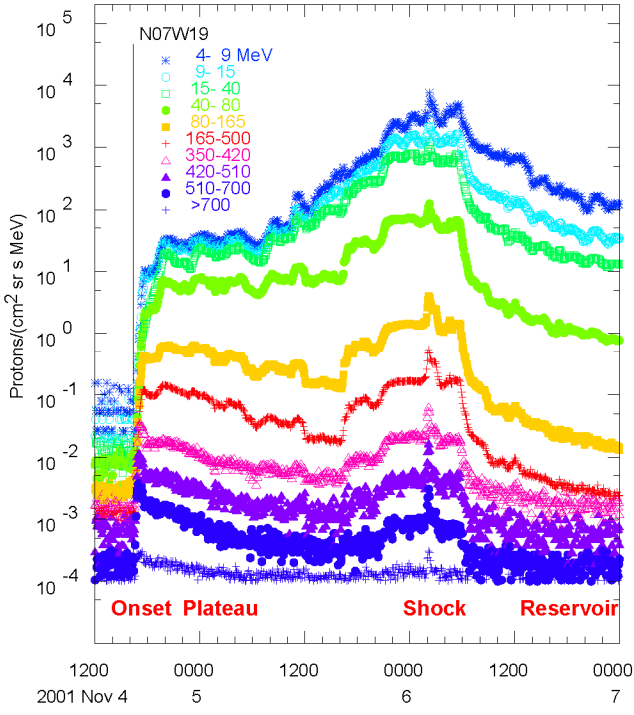

Fig. 5.1. Proton intensities *vs.* time from the NOAA/GOES satellite are shown for the large gradual SEP event of 4 November 2001. Distinctive event phases are listed along the abscissa (Reames 2013).

5.1 Parallel Transport

5.1.1 Diffusive Transport

The diffusion of particles of type X and velocity v by pitch-angle scattering with scattering mean free path λ_X with a power-law dependence on radial position r as $\lambda_0 r^{\beta}$ varies as (Parker 1963; see Equation C1 in Ng, Reames, and Tylka 2003)

$$n_x(r,t) = \frac{1}{4\pi\Gamma(\varepsilon)}\left(\frac{\varepsilon}{3}\right)^{2\varepsilon-1}\left(\frac{3}{\lambda_0 v t}\right)^{\varepsilon}\exp\left[\frac{-3r^{(2-\beta)}}{(2-\beta)^2\lambda_0 v t}\right] \qquad (5.1)$$

where $\varepsilon = 3/(2-\beta)$ and β must be less than 2.

If we examine the ratio of species X and Y, where λ is a power of rigidity and where $L = \lambda_X / \lambda_Y = R^{\alpha} = ((A_X/Q_X) / (A_Y/Q_Y))^{\alpha}$, as a result of the rigidity dependence of λ, and $\tau = 3r^{2-\beta} / [\lambda_Y (2-\beta)^2 v]$, it can easily be shown (*e.g.* Reames 2016a, b) that

$$X/Y = L^{-\varepsilon} \exp\left[(1-1/L)\tau/t\right] \approx L^{\tau/t - \varepsilon} \tag{5.2}$$

The ratio in Equation 5.2 is the enhancement or suppression relative to the ratio at the SEP source and does not include any pre-enhanced impulsive suprathermal ions, although those are also power-law in form. Thus, relative abundances vary approximately as *a power of A/Q*. This will prove to be important in determining source-plasma temperatures (Section 5.6). If the ratio $R > 1$, as for Fe/O, the abundance ratio, X/Y begins at infinity and falls asymptotically to $R^{-\alpha\varepsilon}$. Ratios begin at infinity because diffusion does not account for the particle transit time at the onset. Breneman and Stone (1985) observed that abundance enhancements were power laws in *A/Q*, rising with *A/Q* in some SEP events and falling in others as we saw in Figure 2.4 in Section 2.4.1. In standard diffusion theory, scattering does *not* change with time; thus, the waves affect the particles, but the particles have no affect on the waves (defying energy conservation).

5.1.2 Wave Growth

The amplification of Alfvén waves by streaming protons has been discussed in textbooks on plasma physics for many years (*e.g.* Stix 1962, 1992; Melrose 1980; see also Ng, Reames, and Tylka 2003; Rice, Zank, and Li 2003; Li, Zank, and Rice 2005). In quasi-linear theory, ions, streaming along $\boldsymbol{B}$, resonate with Alfvén waves of wave number k:

$$k = \frac{B}{\mu P} \tag{5.3}$$

in the rest frame of the waves. Here $P=pc/Qe$ is the rigidity of a particle of charge Qe, and momentum p, and μ is the cosine of its pitch angle relative to $\boldsymbol{B}$.

Equation 5.3 results from quasi-linear theory (QLT) where particles are assumed to orbit the unperturbed field and the electric field vector of the circularly-polarized Alfvén wave rotates so as to maintain its phase relative to the direction of rotation of the gyrating particle. This resonance maximizes the transfer of energy between the wave and the particle, seen as pitch-angle scattering in the rest frame of the wave, or wave frame, approximately the plasma rest frame.

The growth rate of the σ polarization mode of Alfvén waves (see Ng, Reames, and Tylka 2003; Stix 1992; Melrose 1980) produced by protons is clearest and simplest in the wave frame, where it is given by

$$\gamma_\sigma(k) = 2\pi^2 g_\sigma e^3 c V_A \iint d\mu dP \frac{P^3}{W^2} R^\sigma_{\mu\mu} \frac{\partial f_H^\pm}{\partial \mu} \tag{5.4}$$

where $g_\sigma = \pm 1$ for outward (inward) wave direction and $f_H^\pm$ is the proton phase-space density in each corresponding wave frame. Here W is the total proton energy, and $R^\sigma_{\mu\mu}$ is the resonance function (see Ng and Reames 1995; Ng, Reames and Tylka 2003) that imposes the resonance condition (Equation 5.3) while allow-

ing for resonance broadening near $\mu \approx 0$. If we can ignore the effects of slow propagation of the waves, then the wave intensity of the σ mode, $I_\sigma(k,r,t)$ obeys the simple equation

$$\frac{\partial I_\sigma(k,r,t)}{\partial t} = \gamma_\sigma(k,r,t) I_\sigma(k,r,t) \tag{5.5}$$

also in the wave frame, where we have explicitly shown the dependence upon space r and time t, which may be quite significant. We will see that the pitch-angle diffusion coefficient for protons depends linearly upon the intensity of resonant waves (Section 5.1.3). Equation 5.5 was used by Ng and Reames (1994) to study time-dependent wave growth during proton transport that was quantitatively consistent with the streaming limit as we will see in Section 5.1.5.

Thus, streaming protons grow the waves, and then the waves scatter the subsequent protons to reduce the streaming and the wave growth. This causes the scattering mean free paths to vary in both time and space (Ng, Reames, and Tylka 2003). While the wave growth caused by heavier ions is negligible, they respond to the waves in ways that are not always obvious, *a priori*. Waves, grown by protons at a particular value of μP, connect to other energies and other species with the same value of μP, as shown in Equation 5.3.

Wave growth is commonly combined with quasi-parallel shock acceleration, where scattering is especially important. However, wave growth is entirely a transport phenomenon, its dependence upon the particles is only through $\partial f_H^{\pm}/\partial\mu$; it is otherwise completely independent of the nature of the proton source. Wave growth will also be important near quasi-perpendicular shocks when streaming intensities of protons become large. This point is sometimes overlooked by students.

Working in the wave frame is illustrative but inconvenient when both inward and outward waves are present and when the Alfvén speed V_A decreases as r^{-1} with distance. Transforming to the plasma frame introduces terms of order $(V_{SW}+g_\sigma V_A)/v$ (see *e.g.* Ng, Reames, and Tylka 2003)

5.1.3 Particle Transport

The equation of particle transport may be simplified in the fixed inertial frame where f is the phase space density of a given particle species averaged over gyrophase (Roelof 1969; Ng and Reames 1994; Ng, Reames, and Tylka 1999)

$$\frac{\partial f}{\partial t} + \mu v \frac{\partial f}{\partial r} + \frac{1-\mu^2}{r} v \frac{\partial f}{\partial \mu} - \frac{\partial}{\partial \mu}\left(D_{\mu\mu} \frac{\partial f}{\partial \mu} \right) = G \tag{5.6}$$

The third term in Equation 5.6 represents focusing of the particles in the diverging magnetic field while the fourth term represents pitch-angle scattering with the diffusion coefficient $D_{\mu\mu}$. Here v is the particle speed, μ is its pitch angle, and the term G on the right-hand side of the equation represents particle sources, for ex-

ample, it might be a power-law energy spectrum times a delta-function at the radial location of a shock wave.

The diffusion coefficient $D_{\mu\mu}$ is given by

$$D_{\mu\mu} = \frac{v^2}{4P^2} \sum_{\sigma} \int dk I_{\sigma} R^{\sigma}_{\mu\mu} \tag{5.7}$$

where P is the particle rigidity and σ runs over wave modes. The wave intensity I_σ and the resonance function $R^{\sigma}_{\mu\mu}$ were discussed in the previous section.

The set of Equations 5.4 – 5.7 completely describe the evolution of both particles and waves and their coupling together. Equation 5.4 shows that the growth of waves is controlled by the streaming particles and Equation 5.7 relates the particle scattering to the intensity of waves. Scattering causes wave growth as a direct consequence of energy conservation (Ng, Reames, and Tylka 2003, Appendix B)

5.1.4 Initial Abundance Ratios

We noted above that in diffusion theory, when λ has a power-law dependence on rigidity, hence upon A/Q, ratios like Fe/O or He/H begin with large enhancements that decrease with time. While this occurs for small gradual SEP events, Figure 5.2 shows that He/H can reverse in large SEP events where wave growth becomes important. This is an example of a case where the arrival of protons depends upon their own velocity, but their affect on He, for example, depends upon protons of a higher velocity, and their common value of μP.

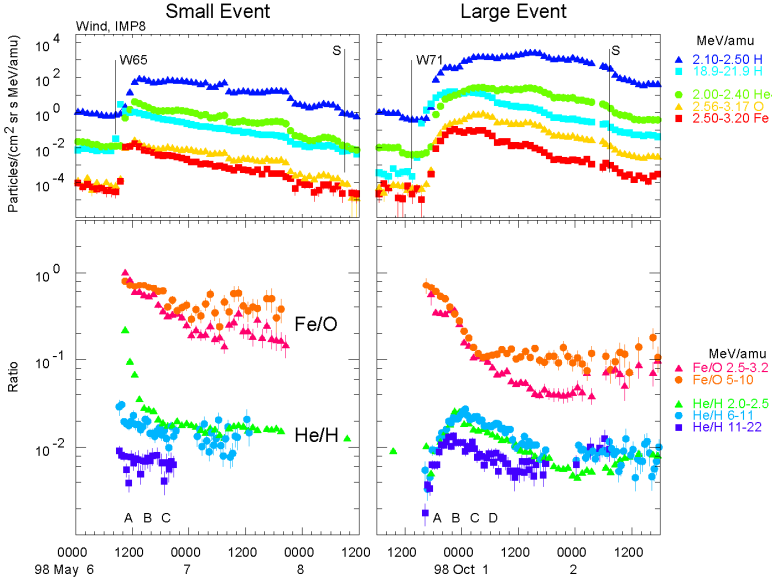

Fig. 5.2. Particle intensities and abundance ratios are shown for small (left) and large (right) gradual SEP events (Reames, Ng, and Tylka 2000). Proton spectra at A, B, C, and D, shown in the reference, are much more intense in the October event.

Why does the initial behavior reverse for He/H in the large event? The early ions stream out into space from the event with $\mu \approx 1$ with few resonant Alfvén waves and little scattering. The H at 2 MeV, for example, suffers little scattering and is only beginning to make its own resonant waves. The He at 2 MeV amu^{-1}, however, is scattered by waves that were amplified by 8-MeV protons (same rigidity) that came out much earlier. If the intensity of 8-MeV protons is high (*i.e.* a big event), they arrive earlier and generate waves so the 2-MeV amu $^{-1}$ He will be scattered much more than the 2-MeV H. Similar logic applies to He/H at higher energies. This effect does not occur for Fe/O since both species are scattered by earlier proton-generated waves. Also, waves that scatter Fe are coupled to protons of quite high energy, which are less intense, so they actually increase Fe/O initially. The progression of enhancements is modeled by Ng, Reames, and Tylka (2003).

5.1.5 The Streaming Limit

In a study of large SEP events observed at the *Helios* spacecraft in solar orbit, Reames (1990) noticed that there was an early plateau period (see Figure 5.1) during large SEP events near 1 AU, where the proton intensities seemed to have an upper limit of intensities as shown in Figure 5.3.

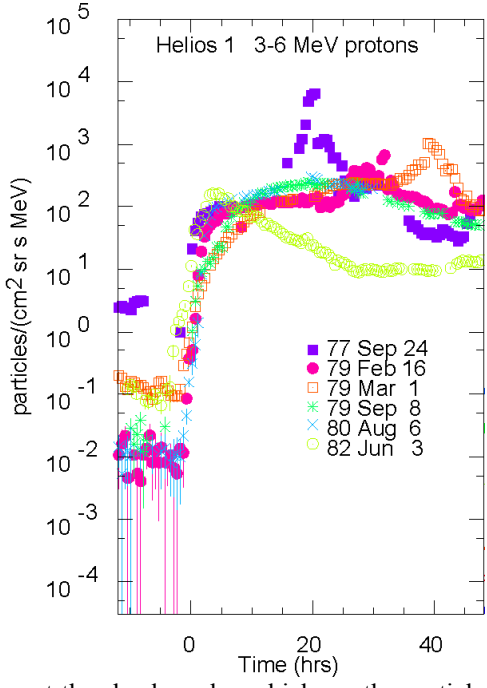

Fig. 5.3. Initial intensities of 3 – 6 MeV protons are shown overlapped for six large SEP events, all near 1 AU. Intensities do not seem to exceed ~200 (cm^2 sr s MeV)$^{-1}$ early in the events, but can become much higher later when shock peaks arrive (Reames 1990).

The intensities can rise much higher at the shock peaks, which are the particle source, because particles at the shock have no net streaming. The streaming limit is a transport phenomenon.

Imagine an experiment that slowly increases the SEP injection intensity at a source near the Sun. At first, the intensity at 1 AU would increase proportionally. Then, at higher source intensities, wave growth would begin to scatter and trap the particles, with most wave growth near the source where intensities are highest. Eventually, further increasing flow from the source would increase the wave growth and scattering so much that the intensity at 1 AU would no longer increase. This is the "streaming limit" that also emerges from theoretical transport models that include wave growth (*e.g.* Lee, 1983, 2005; Ng and Reames 1994; Ng, Reames, and Tylka 2003, 2012). The intensity behavior at 1 AU *vs.* that at the source near the Sun is shown in the left panel of Figure 5.4 while the right panel shows the spatial dependence caused by increasing injection levels at the source.

Note that the wave growth depends upon the *absolute* value of the streaming intensity and the parameters shown in Equation 5.4; there are *no arbitrarily adjustable parameters*. The peak intensity in the left panel of Figure 5.4 is just over 200 $(cm^2\ sr\ s\ MeV)^{-1}$, similar to the value observed in Figure 5.3.

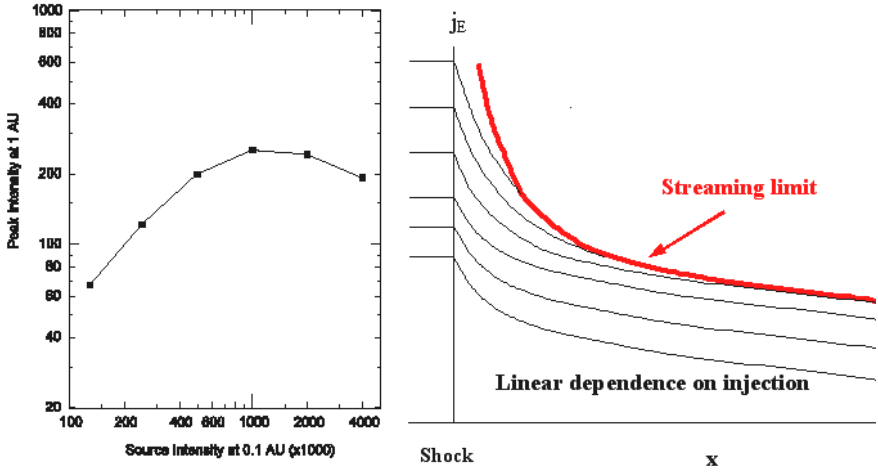

Fig. 5.4. The left panel shows intensity at 1 AU *vs.* that at 0.1 AU. The right panel shows the spatial variation as the source intensity level is increased with linear behavior at low intensities (see Ng and Reames 1994; Ng, Reames, and Tylka 2003, 2012).

However, the plateau intensities in the largest gradual SEP events can involve more than just waves that are self-generated by particles of a single energy. They can involve waves generated by higher-energy protons that contribute to the scattering of lower-energy ions by coupling through the μ dependence of Equation 5.3. These waves preferentially retard the low-energy particles and flatten the power-law source spectra on the plateau as seen in the left panel of Figure 5.5. Intense protons of 10 – 100 MeV stream out early, generating waves as they scatter toward smaller μ. Waves generated at high P and low μ resonate with ions of low P and $\mu \approx 1$ which are coming behind more slowly. Thus, waves amplified by pro-

tons of 10 MeV at $\mu \approx 0.5$ will scatter ions at 2.5 MeV amu^{-1} and $\mu \approx 1$, retarding their flow and thus flattening their spectrum at 1 AU.

Some proof of this mechanism in given by its absence in the 2 May 1998 SEP event; its plateau proton spectrum is shown in the right panel of Figure 5.5. The spectrum in this event remains a power law since the intensity of 10 MeV protons is two orders of magnitude smaller than that in 28 October 2003. The low intensities of 10 – 100 MeV protons do not generate enough waves to suppress the low-energy spectrum in the May event. The theoretical fits to these spectra, shown in Figure 5.5, support this explanation. Wave growth can control spectral shape.

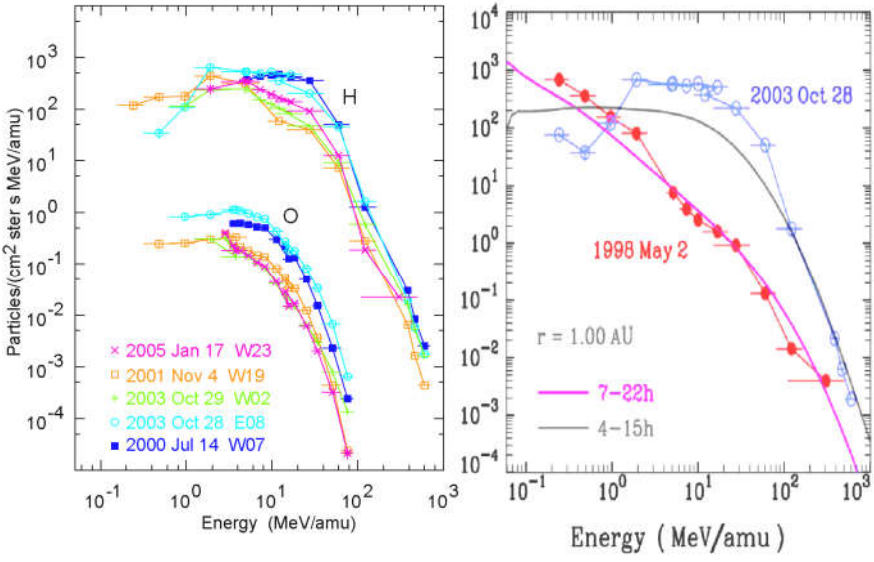

Fig. 5.5. The left panel shows energy spectra of H and O in five large gradual SEP events (all GLEs) that are flattened at low energies (Reames and Ng 2010). The right panel shows that the small event of 2 May 1998, with greatly reduced H intensities at 10 – 100 MeV, cannot generate enough waves to suppress lower energies. Model fits to the spectra are shown in grey and purple (Ng, Reames, and Tylka 2012).

5.1.6 Electron Transport

Non-relativistic electrons cannot resonate with Alfvén waves, so they do not participate in much of the physics we have just described. Low-energy electrons usually propagate scatter free with highly-anisotropic angular distributions mainly because of absorption by the solar wind of 0.1 – 1 Hz frequencies that would resonate with the electrons. Electron spectra often show a break in the ~100-keV energy region. Above the break the spectrum steepens and the width of the angular distribution broadens as scattering becomes much more important (see Tan *et al.* 2011). It is sometimes erroneously concluded that 1 MeV electrons are accelerated much later than those at 20 – 50 keV in SEP events; this apparent delay could result from transport rather than acceleration.

5.2 Angular Distributions

Angular distributions also show the effects of increased scattering when high proton intensities amplify waves. This is seen in the angular distributions of H and He ions in large and small SEP events as shown in Figure 5.6. The particle intensities remain clustered along the field direction around 180° for more than a day in the angular distributions in the small event on the left in Figure 5.6 but, in the more intense event on the right, the angular distributions begin to spread in only a few hours.

Of course, the scattering and the wave growth depend upon the initial wave intensity. However, small impulsive and gradual events usually remain scatter-free and angular distributions rapidly isotropize in more-intense gradual events and especially in GLEs (see Reames, Ng, and Berdichevsky 2001). Most SEP events begin nearly scatter free at energies above a few MeV amu^{-1}, but not at low energies where μ-coupling shown in Figure 5.5 applies and traps ions with energies below a few MeV amu^{-1} near their source.

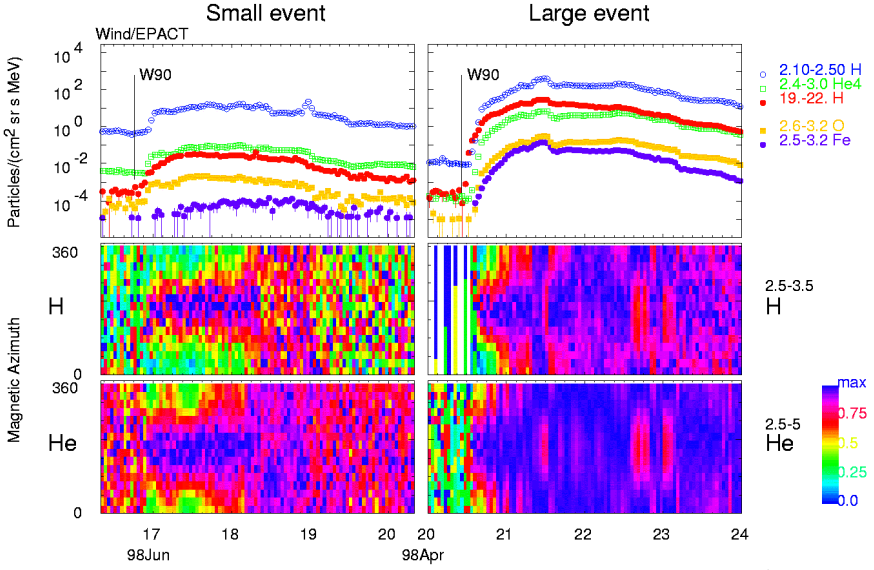

Fig 5.6. Intensities (top) and angular distributions, relative to ***B***, for H (middle) and ^{4}He (bottom) are shown for large (left) and small (right) gradual SEP events. Note the much higher intensity of the (red) 19 – 22 MeV protons in the upper right panel.

5.3 Models and Shock Acceleration

General information about shock formation and acceleration may be found in comprehensive review articles (Jones and Ellison 1991; Lee, Mewaldt, and Giacalone 2012). However, there is such compelling experimental evidence of wave growth in the larger gradual SEPs events that we focus on models that include it.

The earliest time-equilibrium model of shock acceleration with self-consistent treatment of particles and waves was the work of Bell (1978a, b) on GCRs, which was subsequently adapted to interplanetary shocks by Lee (1983). Shock models were applied to acceleration of GeV protons in the corona by Zank, Rice and Wu (2000, see also Lee 2005, Sandroos and Vainio 2007, Zank, Li, and Verkhoglyadova 2007; Afanasiev, Batterbee, and Vainio, 2016).

The time-dependent self-consistent model of particle transport with wave amplification (Ng, Reames, and Tylka 2003) was applied to shock acceleration by Ng and Reames (2008) resulting in modeling of the time-evolution of the proton spectra at the shock shown in Figure 5.7 along with the evolution of the radial dependence of the intensity upstream of the shock for a given energy proton. A streaming limit soon forms within 0.1 R_S of the shock as seen in the right panel.

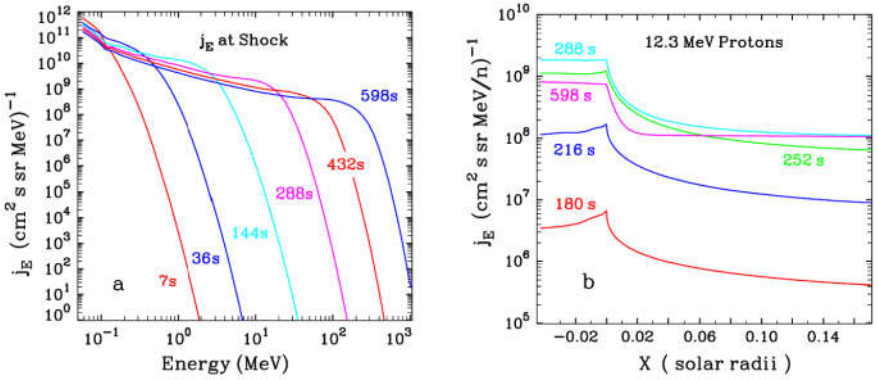

Fig. 5.7. The left panel shows the time evolution of the proton energy spectrum at the shock for the first ~10 min. The right panel shows the time evolution of the spatial distribution of 12.3 MeV protons upstream of the shock. Once accelerated at ~3 min, 12.3 MeV proton intensities increase to form a streaming limit within 0.1 R_S of the shock at ~4.2 min (Ng and Reames 2008).

An interesting feature of the time-dependent numerical acceleration calculations is the growth of waves as the proton spectrum grows to higher energy. With the growth of waves that resonate with particles of the highest energy E_1 and rigidity P_1, some protons will begin to be accelerated to still-higher energy E_2 and rigidity P_2. Initially, the only waves that can trap ions at E_2 are those that resonate with protons with $\mu_2 < P_1/P_2$, *i.e.* only at small μ_2 can ions at the new energy find resonant waves generated by lower-energy protons. Thus at each new energy the particles begin with a pancake distribution at small μ (Ng and Reames 2008).

The Ng and Reames (2008) model prevents the scattering from approaching the Bohm limit by requiring that the scattering mean free path be more than three times the particle gyroradius, so that the quasi-linear approximation remains valid. This makes the maximum energy lower and the acceleration rate slower than that in the calculation of Zank, Rice, and Wu (2000), who assumed the more-likely Bohm limit where scattering mean free path equals the particle gyroradius, *i.e* $\delta B/B \approx 1$, as has been observed in strong shocks (Lario and Decker 2002;

Terasawa *et al.* 2006). It is also true that an oblique shock, where ions gain energy in the $\boldsymbol{V_S} \times \boldsymbol{B}$ electric field, can affect the acceleration time and maximum energy by increasing the particle energy gained on each traversal of the shock. We would speculate that a fast shock traversing a sufficiently dense seed population should have no trouble accelerating GeV protons in a few minutes or even less.

It can not escape our attention that it is much easier for theoreticians to work in a universe where particle scattering in constant in time, and waves never grow. Quasi-perpendicular shocks need no change in scattering to increase acceleration, only a small change in θ_{Bn}. Such approximations are often useful in making tractable solutions to explore specific functional dependences. However, observations show that wave growth dominates the largest SEP events. Further realistic studies that include it could help advance our understanding of these important events.

5.4 Shock Acceleration *In Situ*

Traveling interplanetary shock waves near Earth are the local continuation of the CME-driven shock waves that produce gradual SEP events. These shocks provide an opportunity to directly measure, *in situ*, the properties of accelerated particles together with the characteristics of the shock and its driver under an extremely wide variety of shock conditions (see *e.g.* Berdichevsky *et al.* 2000). Desai *et al.* (2003) showed that low-energy ion abundances near the shock peak were much more closely related to ambient abundances of those ions upstream of the shock than to the abundances of the corresponding elements in the solar wind, as might be expected from our discussion of the seed population in Section 2.4.3. Desai *et al.* (2004) found that energy spectra at the shocks were better correlated with the spectra upstream than with those expected from the shock compression ratio. Especially for low-energy ions, shock acceleration persists far out from the Sun and tends to reaccelerate ions from the same population that was accelerated earlier.

The choice of a location to measure the ambient, background, or reference abundances and spectra upstream of the shock is difficult. If it is chosen prior to the time that shock leaves the Sun, perhaps ~2 – 3 days before the shock arrival, then solar rotation insures that background is sampled at a longitude of 26-40 degrees to the west of the longitude sampled at the shock peak. If it is chosen hours prior to the shock arrival, background will be dominated by particles accelerated earlier by the same shock. Neither choice is ideal.

In effect, the re-acceleration of ions from the seed population found in the reservoir of an earlier event evokes the classical two-shock problem considered, for example, in the review by Axford (1981) and more recently by Melrose and Pope (1993). Here, the integral equilibrium distribution function $f(p)$ of momentum p of accelerated particles from a shock with compression ratio s is

$$f_a(p) = ap^{-a} \int_0^p dq\ q^{a-1} \phi(q) \tag{5.8}$$

where $a=3s/(s\text{-}1)$ and $\phi(p)$ is the injected distribution. If we take $\phi(p)$ as a delta function at p_0 we find a power-law spectrum $f_a(p) \sim (p/p_0)^{-a}$ after the first shock. If we reapply Equation 5.8, injecting $f_a(p)$ into a shock with compression ratio s' and let $b=3s'/(s'\text{-}1)$, we find that integrating the power law gives

$$f_{a,b}(p) = \frac{kab}{p_0(b-a)}\left[\left(\frac{p}{p_0}\right)^{-a} - \left(\frac{p}{p_0}\right)^{-b}\right] \quad \text{for } a \neq b. \qquad (5.9)$$

The corresponding intensity is $j(E)=p^2f(p)$.

Note that Equation 5.9 is symmetric in the powers a and b, and will be dominated by the shape of the hardest, flattest spectrum, either the background (*i.e.* a) or the new shock, b. Thus, it is no surprise that one finds local-shock spectra that are dominated by the shape of the upstream background spectrum (Desai *et al.* 2004; Reames 2012) produced earlier when the shock was stronger. A further complication occurs when we include a spectral knee with a factor like exp $(-E/E_0)$ (*e.g.* Ellison and Ramaty 1985; see also Mewaldt *et al.* 2012) to allow for the finite acceleration time. At energies above the knee, observers will find spectra that are much steeper than either the background or the expected equilibrium spectra.

These possibilities for spectral shapes were considered in the observations of Reames (2012), who studied ^{4}He spectra of ~1 – 10 MeV amu^{-1} in 258 *in situ* interplanetary shocks observed by the *Wind* spacecraft. The purpose of this study was to determine which shock parameters were important to produce measurable particle acceleration and which were not. Figure 5.8 shows a well-defined shock event, shock number 83.

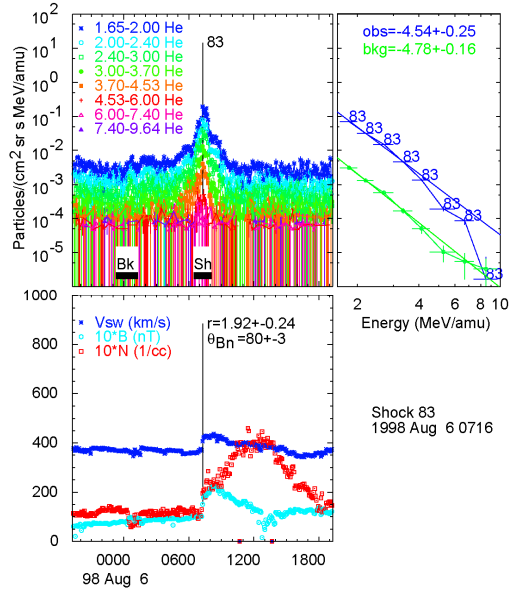

Fig. 5.8. Particle intensities are shown *vs.* time in the upper left panel with plasma parameters below for shock number 83. Spectra of the shock and background are shown to the right with spectral slopes indicated.

Particle intensities in Figure 5.8 are shown in the upper left panel, the plasma parameters: solar-wind speed V_{SW}, magnetic field B, and density N, in the lower left panel, and the shock and background spectra in the upper right panel. The times over which the two spectra are taken are shown in the upper left panel (Bk and Sh). This is a quasi-perpendicular shock with the angle between B and the shock normal, $\theta_{Bn} = 80^o \pm 3^o$

Figure 5.9 compares properties of the shocks in this study. The left panel shows a histogram of the shock speed distribution for all of the shocks and for the subset that showed measurable particle acceleration. High shock speed was the strongest determinant for measurable acceleration, followed by high shock compression ratio, and large θ_{Bn}. High background intensity was also important; more input produced more output. Measurable acceleration was more than twice as likely for shocks with $\theta_{Bn}>60^o$ as for those with $\theta_{Bn}<60^o$. Quasi-parallel shocks, *i.e.* small θ_{Bn}, may have been more likely to have knee energies below the energy of observation. Recently, Zank *et al.* (2006) have suggested that "higher proton energies are achieved at quasi-parallel rather than highly perpendicular interplanetary shocks within 1 AU." The *in situ* observations (Reames 2012) show the opposite; quasi-perpendicular shocks are favored; this difference may occur because ample pre-accelerated seed populations were available for the real shocks.

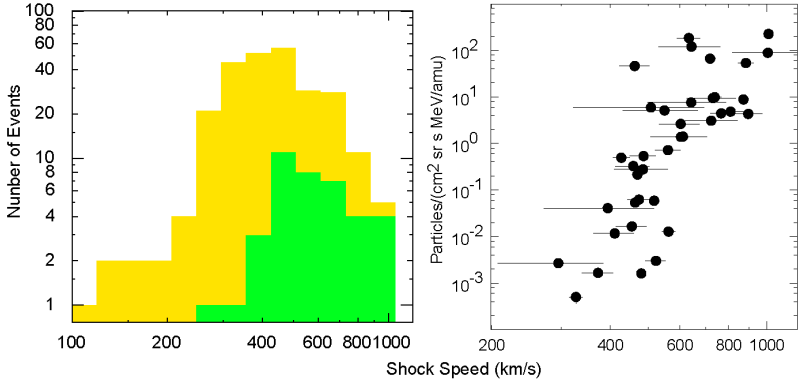

Fig. 5.9. The left panel shows the distribution of shock waves at 1 AU with measurable acceleration of >1 MeV amu^{-1} ^{4}He *vs.* shock speed (green) within the distribution of all 258 shock waves *vs.* shock speed (yellow and green) observed by the *Wind* spacecraft. The right panel shows the background-corrected peak intensity of 1.6 – 2.0 MeV amu^{-1} ^{4}He *vs.* shock speed for the shocks *in situ*. Shock speed is the strongest determinant of accelerated intensity for local shocks; this mirrors the correlated behavior of peak intensity *vs.* CME speed in Figure 2.11 (adapted from Reames 2012, 2013).

The right panel in Figure 5.9 shows the background-corrected peak shock intensity of 1.6 – 2.0 MeV amu^{-1} ^{4}He as a function of shock speed. The shock speed has a correlation coefficient of 0.80 with intensity. This correlation for *in situ* shocks mirrors the correlation of peak proton intensity with CME speed in Figure 2.11 as modified by Rouillard *et al.* (2012) and shown in the lower right-hand panel of Figure 3.4.

Particle intensities peak at the time of shock passage in nearly all of the events in the Reames (2012) study. However, sometimes intensities peak before or after shock passage when a spacecraft encounters magnetic flux tubes that connect it to a stronger part of the shock nearby, perhaps even one with a different value of θ_{Bn}.

Absolute intensities of accelerated particles are not directly predicted by acceleration theories that omit wave growth. The rate of injection of seed particles is treated as an adjustable parameter – more input results in more output, and this is the case for *in situ* events. However, streaming protons and increasing wave intensities can trap particles near the source. At a few powerful shock waves, such as 20 October 1989, it has been observed that the energy in energetic particles exceeds that in the plasma and magnetic field (Lario and Decker 2002). Those authors suggested that the peak intensities of particles up to 500 MeV are simply trapped in a region of low density and low magnetic field near a shock. Maybe, but, how did they get there? Surely they were accelerated there. Perhaps the wave-trapped particles are in the process of destroying (*i.e.* pushing apart B at) the shock that accelerated them. Another shock where the particle energy exceeds the magnetic energy is that of 6 November 2001, in Figure 5.1 (C. K. Ng, private communication), where the sharp proton peak up to 700 MeV shows a shock that is still clearly intact. This is the issue of "cosmic-ray-mediated" shocks discussed by Terasawa *et al.* (2006) for two additional interplanetary shocks. This is a fascinating process that can be observed, *in situ*, at some interplanetary shocks.

5.5 Abundances and FIP

We began by discussing the reference abundances in Chapter 1 and comparing them with the solar photospheric abundances as a function of first ionization potential (FIP) in Figure 1.6. The reference abundances are obtained by averaging over many gradual SEP events. Since the transport of particles varies as a power of A/Q (see Equation 5.2), different species such as Fe and O will be distributed differently in space and time, but these particles are conserved. If we can successfully average over time or space we will recover the source abundances. If this assumption is correct and our averaging is representative, the reference abundances will approach the coronal abundances. Evidence for the space-time distribution is shown in Figure 5.10.

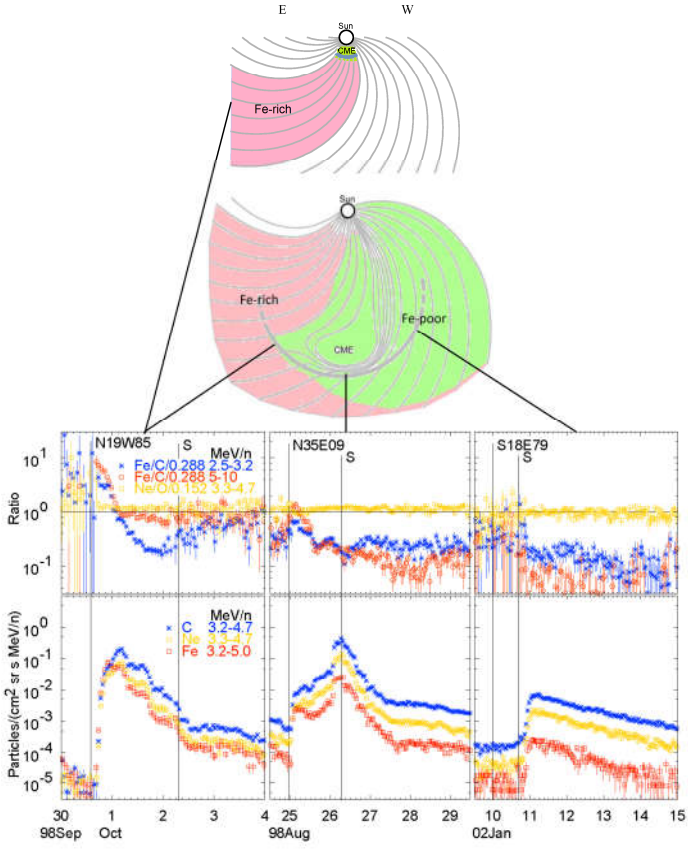

Fig. 5.10. Intensities of C, Ne, and Fe are shown for three gradual SEP events at different solar longitudes in the lower panels, relative abundances in the middle panels, and the location and evolution of a CME above (after Reames 2014).

The SEP event on the East flank of the CME (W85 source, on the left in Figure 5.10), shows enhancement of Fe/O early then suppression later, since Fe, with higher A/Q, scatters less than O. Ne/O, involving similar values of A/Q, varies little. Solar rotation and the Parker spiral translates this time variation into a spatial one and the events toward the West flank of the CME show mainly depleted Fe/O.

5.6 Source-Plasma Temperatures

Since particle transport in gradual SEPs varies as a power of A/Q, and Q varies with T, we can use this power law to find the source-plasma temperature T that gives the best-fit pattern of A/Q, just as we did for impulsive events. Figure 5.11 (similar to Figure 4.8) shows A/Q *vs.* T with Q derived from the atomic physics.

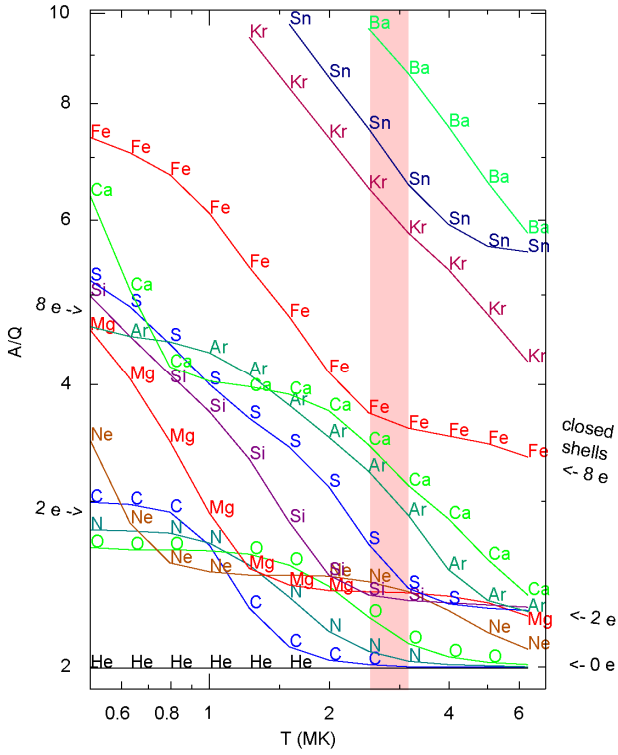

Fig. 5.11. *A/Q* is plotted as a function of the theoretical equilibrium temperature for the elements named along each curve. Points are spaced 0.1 units of $\log_{10} T$ from 5.7 to 6.8. Bands produced by closed electron shells with 0, 2, and 8 orbital electrons are indicated, He having no electrons at this *T*. Elements tend to move from one closed-shell group to another as the temperature changes. (Data for $Z \leq 28$ from Mazzotta *et al.* 1998, for $Z > 28$ from Post *et al.* 1977)

The red shaded region in Figure 5.11 is 2.5 – 3.2 MK, corresponding to active region temperatures that we found for the impulsive SEP events (see Section 4.6). As we decrease *T* below this region, O, then N, then C move from the 0-electron to the 2-electron closed shells. Meanwhile, Ca, then Ar, then S, then Si, then Mg move from the 2-electron to the 8-electron shells. Thus, we can tell the temperature by the pattern of abundance enhancements. We need only notice which elements are in which group; which elements have no enhancement like He; which elements are in the group with Ne; which are in the group with Ar.

Figure 5.12 compares the observed pattern of enhancements early in a large gradual SEP event (on the left) with the pattern of *A/Q* (on the right). The patterns match best near $T \approx 0.6$ MK, an unusually low temperature for SEP events. Note that C, N, and O have moved well above He to the 2-electron shell with Ne, while Mg, Si, and S have moved up to the 8-electron shell close to Ar and Ca. Patterns of enhancement in other SEP events are shown in Reames (2016a).

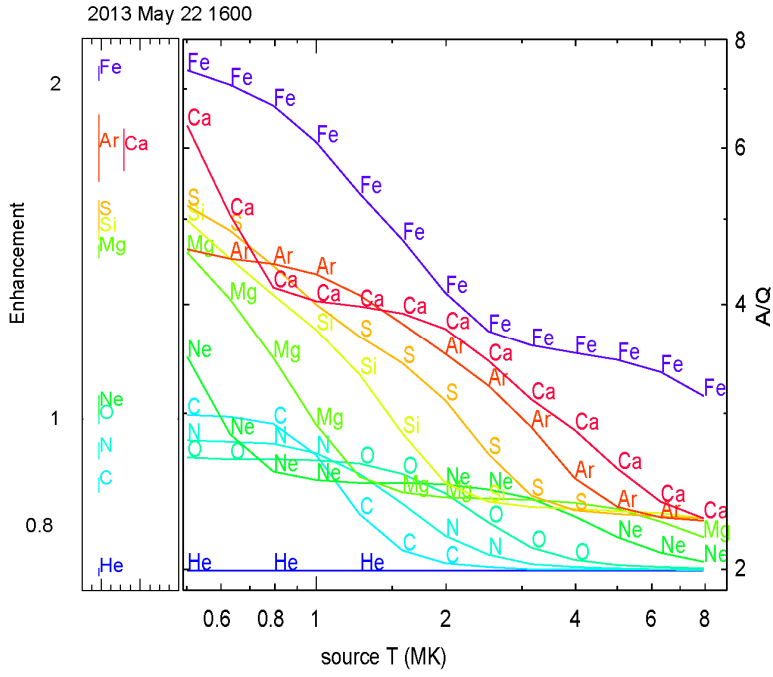

Fig. 5.12. The left panel shows the abundance enhancements at ~3 – 5 MeV amu^{-1} observed early in the 22 May 2013 SEP event. The right panel compares a section of the *A/Q vs. T* plot from Figure 5.11. The patterns match at about 0.6 MK (Reames 2016a)

For the LEMT telescope on the *Wind* spacecraft, 8-hr intervals during a large SEP event will provide adequate statistics for the rarer elements to determine enhancement patterns. For each 8-hr period we can calculate least-squares fits of enhancement *vs. A/Q(T)* for all values of T in the range of interest and plot χ^2 of the fit *vs. T* (upper-right panel in Figure 5.13). The minimum value of χ^2 gives the best-fit temperature and power of *A/Q* for that time. This process gives the source-plasma temperature as a function of time during an event, as shown in the upper-left panel of Figure 5.13 for the event of 8 November 2000. For this event we find temperatures near 1 MK for all time periods with either abundance enhancements or suppressions. For two of the time periods, the best fits to enhancement *vs. A/Q* are shown in the lower-right panel of Figure 5.13. However, for time periods when enhancements in the abundances are flat, neither enhanced nor suppressed, we cannot measure T, since any *A/Q* values will fit and χ^2 has no minimum. Larger enhancement or suppression of the abundances produces clearer minima in χ^2 and smaller errors in T.

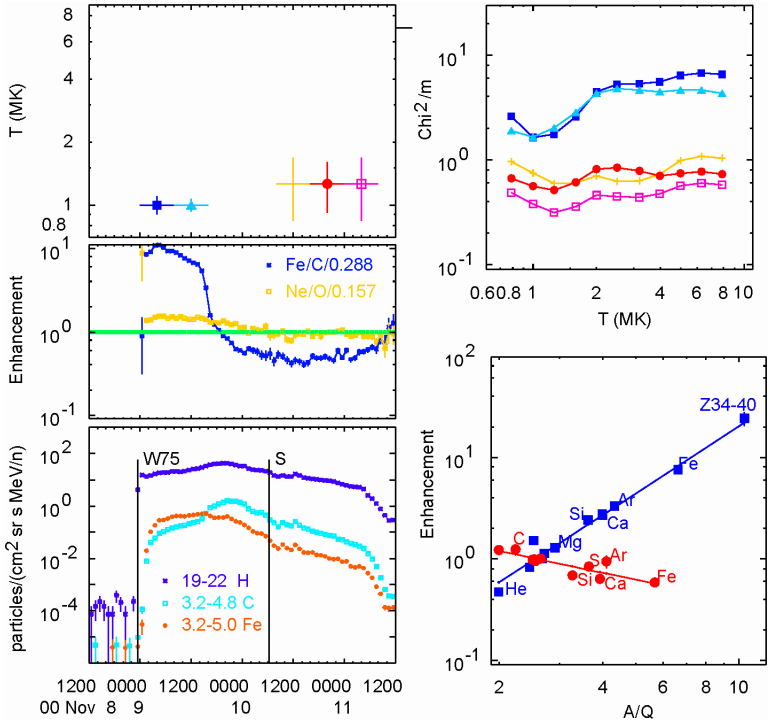

Fig. 5.13. Clockwise from the lower-left panel are the intensities of H, C, and Fe during the 8 November 2000 SEP event, the enhancements in Fe and Ne during the event, the best-fit temperatures in color-coded 8-hr intervals, values of χ^2/m *vs. T* for each time interval (where *m* is the number of degrees of freedom), and two sample fits of enhancements, relative to O, *vs. A/Q* (Reames 2016a).

For 45 gradual SEP events that had reasonably well-defined temperatures, Reames (2016a) found:

- 69% (31 events) showed ambient coronal temperatures $T \leq 1.6$ MK
- 24% (11 events) had $2.5 \leq T \leq 3.2$ MK active region temperatures, like impulsive SEP events.

Some (11) of the events with ambient coronal temperatures showed a second minimum at the upper limit of *T* in χ^2 *vs. T*. These probably represent a component of ions that have been stripped by passing residual impulsive suprathermal ions through a small amount of material before reacceleration by the shock.

While the gradual event temperatures and fit parameters are not strongly correlated with any particular properties of the accelerating CME or shock, Figure 5.14 shows *T vs.* CME speed. The un-weighted correlation coefficient is -0.49 for these events. Events that happen to be GLEs are identified in the figure; their temperature distribution and other properties are similar to those of the other gradual SEP events.

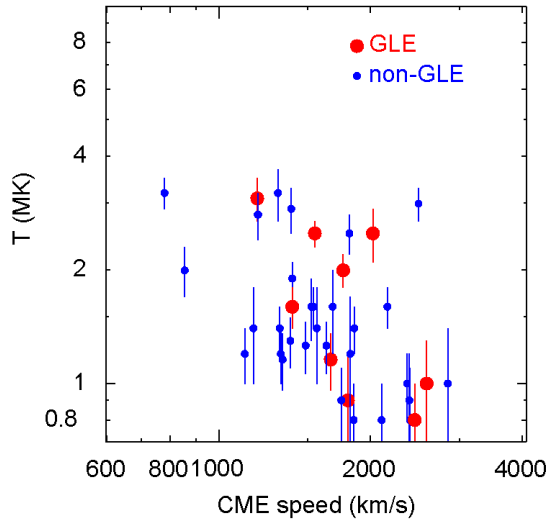

Fig 5.14. Source-plasma temperature is shown as a function of associated CME speed for gradual SEP events with GLE events identified (data from Reames 2016a).

We now realize that attempts to study abundance cross-correlations in gradual SEP events were ineffective because most variations were caused by temperature differences that previously were not known. For example the average value of Fe/O is a factor of ~10 higher in gradual events with T = 3.2 MK than in those with T = 1.5 MK. This is shown in Figure 5.15 which plots normalized Fe/O *vs.* C/He, for intervals during the gradual SEP events, in both panels, with T as symbols in the lower panel and power of A/Q as symbols in the upper.

The area of abundances showing active-region temperatures $T \geq 2$ MK is immediately distinguishable, clustering in the upper left of the lower panel of Figure 5.15. These events are distinguished as open circles in the upper panel as well. Points during events accelerated from specific temperatures of ambient coronal plasma stretch from upper right, with steep A/Q enhancements early in the events, toward the lower center, where the A/Q slopes are reduced or negative, late in the events.

One might well ask: why do we use theoretical values of Q *vs.* T when there are actually some measurements of Q (*e.g.* DiFabio *et al.* 2008)? Mainly, Q_{Fe} for example, measured at 1 AU, is observed to increase with energy at low energies, suggesting that the ions have traversed enough material after acceleration to strip them to equilibrium charges that depend upon their velocity, especially in these impulsive events. The theoretical charges are more likely to be appropriate earlier, *i.e.* at the time of acceleration. In addition, the theoretical charges from atomic physics are available for essentially all elements we measure.

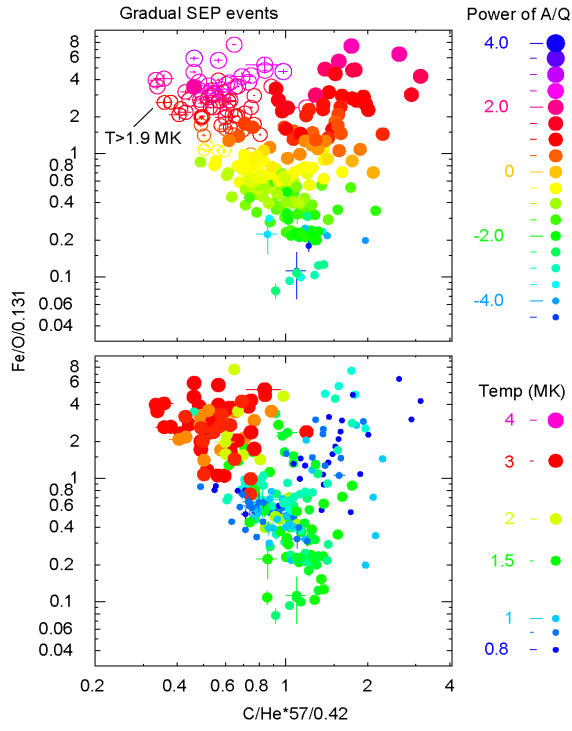

Fig. 5.15. Normalized abundance ratios Fe/O *vs.* He/C is plotted in both panels with symbol size and color representing *T* (lower panel) and power of *A/Q* (upper panel). (Reames 2016b)

5.7 Spatial Distributions and the Reservoir

As spacecraft began to probe more-distant areas of the heliosphere, it became possible to view spatial distributions of SEPs, and their time variations, within a single SEP event. While spatial gradients were expected, it was rather surprising that equal intensities of ~20 MeV protons were found over long distances of solar longitude of ~180° on the *Pioneer* spacecraft by McKibben (1972). Twenty years later equal intensities were found late in large events over 2.5 AU between *Ulysses* and IMP 8 near Earth by Roelof *et al.* (1992) who named the regions "reservoirs." Reservoirs extend to *Ulysses* at heliolatitudes up to >70°, N and S (Lario 2010), and they are also seen in other electron observations (Daibog *et al*. 2003).

The *Helios* mission provided another opportunity to measure the evolution of SEP events at different longitudes confirming that the longitude distribution of Figure 2.1 was appropriate for each individual event. Figure 5.16 shows that, at widely separated spacecraft, the intensities merge with that at *Helios 1* as each spacecraft joins it in the reservoir. Spectra are identical throughout the reservoir but decrease adiabatically with time as the volume of this "magnetic bottle" expands. (The drawing in the lower panel of Figure 5.16 shows the spacecraft pene-

trating the CME; in reality, of course, the spacecraft are nearly stationary as the CME expands past them, but that version would be much more difficult to draw.)

If there were significant leakage from the reservoir, one would expect the highest-energy protons to leak first, since they are faster, scatter less, and encounter the boundary most often, but this would steepen the spectrum with time and is *not* observed. Thus the leakage is minimal.

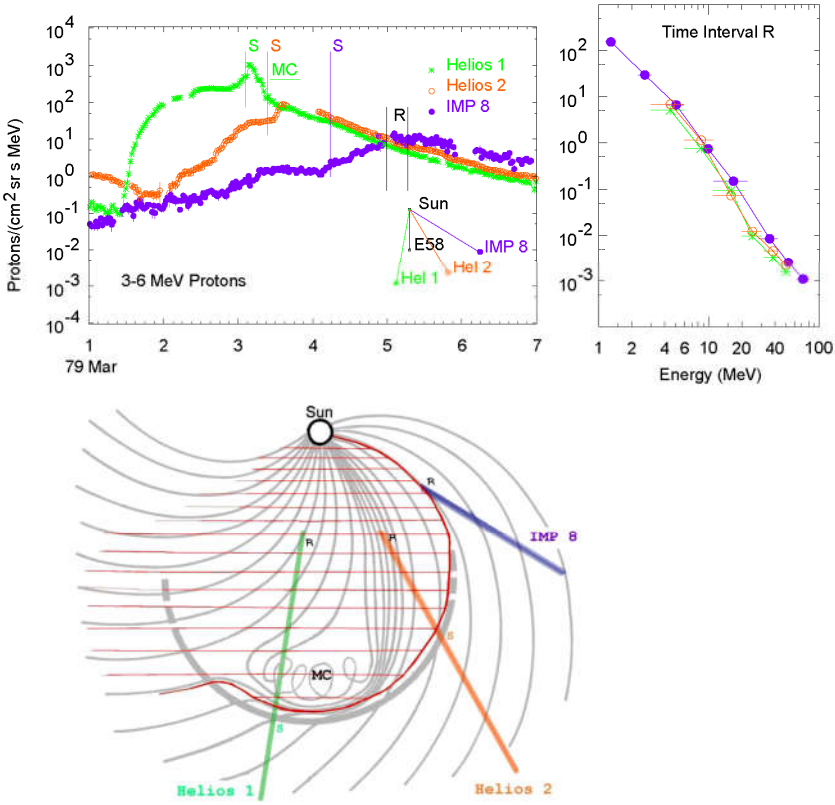

Fig. 5.16. The upper left panel shows the intensities of 3 – 6 MeV protons at three spacecraft *vs.* time. The paths of the spacecraft into the expanding CME are shown below as they penetrate into the reservoir region (red hashing) behind the shock and CME where all intensities and spectra (upper right) are equal spatially, though they decrease with time as the trapping volume expands (Reames 2013; after Reames, Kahler, and Ng 1997b).

One common, but rather poor, way of comparing spatial variations is to plot peak intensity at, say three, spacecraft *vs.* longitude and fit the three points with a parabola. Does this measure particle spread in longitude? Suppose we made such a plot with the data shown in Figure 5.16. The intensity at *Helios 1* peaks at the time of shock passage. The intensity at *Helios 2* peaks when it enters the reservoir, where it has the same intensity as *Helios 1*. The intensity at IMP 8 peaks when it enters the reservoir later, where *all three intensities are equal*. What does

the parabola defined by these three peak intensities measure? Is it the spread of the particles or the spread in the trapping volume behind the CME with time? The peaks all occur at different times and that *essential* timing information is lost when plotting only peak intensities *vs.* longitude. Isn't it more important to note that all intensities are equal when the intensity at IMP 8 peaks? It seems more productive to try to *distinguish* spatial and temporal effects rather than combining them.

For a single spacecraft, one way to show that spectra do not change their shape in time is to normalize the intensity-*vs.*-time plots at one point in time. If they stay normalized subsequently, then the spectral shapes are invariant. This is shown for two gradual SEP events in Figure 5.17. This technique demonstrates invariance even when the spectra do not have power-law form. Multiple spacecraft at different locations can be included or abundance variations can be compared similarly. Note that the reservoir can extend upstream of the CME and shock on the East flank, as seen in the left panel of Figure 5.17; here the particles may be contained by self-amplified waves from earlier streaming.

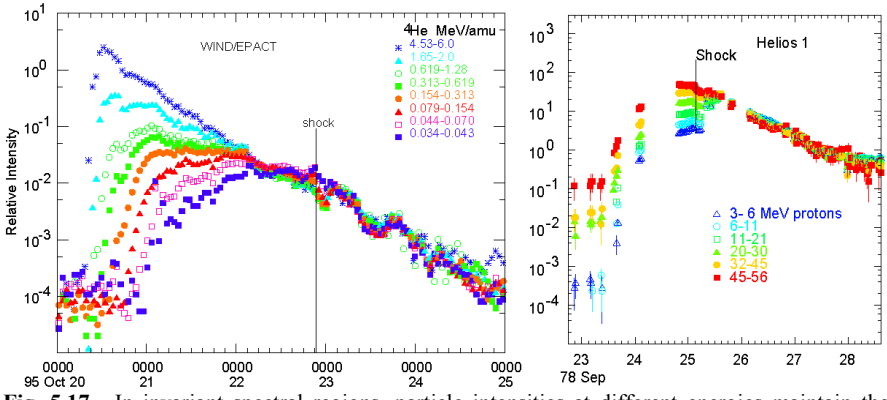

Fig. 5.17. In invariant spectral regions, particle intensities at different energies maintain the same relative normalization as a function of time, as shown for different species in two different events (Reames 2013; after Reames *et al*. 1997a and Reames, Kahler, and Ng 1997b).

The realization that the slow decline in a gradual SEP event results from expansion of a reservoir is most important because it displaces the previous idea that slow particle diffusion explained the decay phase of events. Actually, reservoirs are scatter free, as shown by the striking example from Mason *et al.* (1989) shown as Figure 2.2 in Section 2.3.4. A whole literature of fitting SEP events to diffusion theory had emerged, leading to the "Palmer (1982) consensus" that "$\lambda_\parallel$ = 0.08-0.3 AU over a wide range of rigidity." This is yet another example of the misapplication of diffusion theory; the intensity decline comes from the expansion of a magnetic bottle in time, not inefficient transport through space. There are no significant spatial gradients within reservoirs.

It is important to recognize that reservoirs trap energetic ions in an expanding volume above the solar surface for a long period of time. While this population of particles tends to be mirrored in the converging magnetic fields above the corona,

some undoubtedly scatter into the loss cone and plunge into the corona to produce γ-rays (just as the particles in flaring loops must do). Vestrand and Forrest (1993) observed γ-ray production spanning over ≈30° of the Sun's surface in the large GLE of 29 September 1989. Also, Ryan (2000) discussed long-duration γ-ray events lasting an hour or more while the flare-associated X-rays died away rapidly. See, also, the recent long-duration γ-ray observations by Ackermann *et al.* (2014) and Ajello *et al.* (2014). Reservoirs provide an invariant spectrum of shock-accelerated ions that can bombard a large area of the solar corona with slowly decreasing SEP intensities for hours or days.

5.8 Non-thermal Variations: Impulsive *vs.* Gradual SEPs

Knowing the source-plasma temperatures allows us to compare impulsive and gradual SEP events from the same temperature source – *e.g.* from active regions. Figure 5.18 compares the normalized abundances of O/C *vs.* C/He for impulsive and gradual SEP events plotted at the same scale. The impulsive events have been limited to those with modest <20% statistical errors in the ratios and the gradual events come from active region plasma at $T \geq 2$ MK.

Especially at a temperature of 3.2 MK (red symbols in Figure 5.18) the elements He and C are likely to be fully ionized and O is nearly so (as seen in Figure 5.11). Thus the ratios should be unaltered source abundances for both populations. However the dashed line also shows that the normalization is wrong for C/He since the central mean should be at 1.0. This suggests that the reference abundance He/O should be 91 rather than 57. This would bring He in somewhat better alignment with other high-FIP elements on a FIP plot (Figure 1.6) and is shown as a red open circle on that figure.

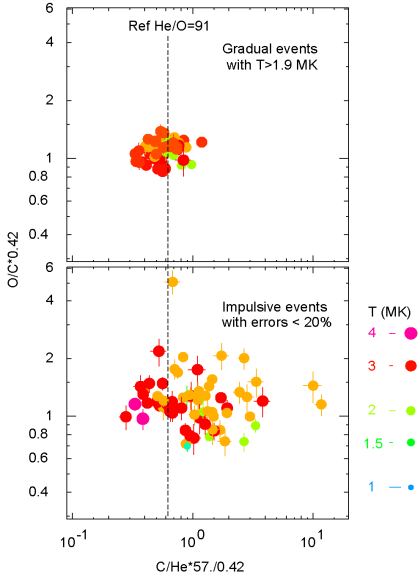

Fig. 5.18. Enhancements of O/C *vs.* C/He are compared, for gradual events with $T \geq 2.0$ MK (upper panel) and impulsive events with < 20% errors (lower panel). Both panels are plotted at the same scale and T is indicated by the size and color of the symbols. (1) The distribution is much smaller for the gradual events. (2) The median of the distribution of C/He for the gradual events, shown as a dashed line, implies a reference value for He/O of 91 rather than 57 (Reames 2016b)

More significantly, the spread in the distribution of gradual events is much smaller than that of impulsive events in Figure 5.18. The spread in the impulsive events must come from non-thermal abundance variations in the local plasma where reconnection is occurring. However, neither wave-particle interactions nor magnetic reconnection can alter C/He when both elements have $A/Q = 2.0$. If the shock of a gradual SEP event were accelerating only suprathermal ions from a single impulsive source, we would expect the same non-thermal distribution for gradual events that we see for impulsive events. This is *not* the case.

As the shock in a gradual event passes over an active region, it must average contributions (i) from impulsive suprathermal ions, which have enhancements in Fe/O and ^{3}He/^{4}He, for example, and (ii) from ions in the ambient ~3 MK plasma, which have no such enhancements. Ko *et al.* (2013) found that Fe-rich gradual SEP events were commonly connected to active regions. The result of the two contributions is to reduce the enhancements, as observed, and somewhat reduced distributions in the spread of abundance ratios, more like those in the upper panel of Figure 5.18.

However, if we really want to reduce the spread of the distributions as seen in gradual events, we need to average over *several* small jets producing impulsive SEP events rather than only one; n events will reduce the spread by a factor of $\sqrt{n}$. It is likely that the number of small impulsive SEP events in an active region increases as the event size decreases, contributing a fairly steady flow of impulsive suprathermal ions; each temporarily contributes to the potential seed population before it diminishes. Based on the increasing number of flares with decreasing size, Parker (1988) proposed that a large number of small nanoflares could actually heat the corona. We need only a small increase in the number of jets producing impulsive SEP events that are too small to resolve as separate events, yet adequate to contribute to the seed population of impulsive suprathermal ions above a solar active region which may be subsequently sampled and averaged by a shock wave. Thus, no single impulsive event determines the seed population for acceleration by the shock wave in a subsequent gradual SEP event.

Many small jets (*i.e.* nanojets?) could also contribute to the periods of persistent ^{3}He seen by Wiedenbeck *et al.* (2008), of long-lived and recurrent sources (Bučík *et al.* 2014, 2015; Chen *et al.* 2015) and, of course, to the substantial persistent ^{3}He abundances below 1 MeV amu^{-1} in the seed population directly observed at 1 AU upstream (see figure 2.7) of the shock wave (*e.g.* Desai *et al.* 2003).

Source-plasma temperatures provide a powerful new tool for the comparative study of SEP events.

5.9 Open Questions

This section suggests open questions that might be addressed in future research.

1. What can cause the large non-thermal spread of abundances such as C/He in impulsive SEP events when both He and C should be fully ionized? Does source depth in the corona matter?
2. How well do SEP-derived temperatures correlate with directly observed temperatures near the observer's magnetic footpoint early in a gradual SEP event?
3. How do reservoirs contain particles of all energies with such apparently equal efficiency? How do they attain uniformity of intensities with longitude when the particles upstream of the shock do not? Is diffusion along the turbulent shock a factor?
4. In principle, a shock could accelerate 1-MK plasma at one longitude and 3-MK plasma at another longitude. Is this seen? Is there enough lateral transport in and behind the shock to mix SEPs from these sources late in events?
5. What happens when the energy in SEPs exceeds the energy in B at a shock, especially a quasi-perpendicular shock? Does acceleration cease?
6. Some gradual events show evidence of a component of stripped ions (Reames 2016a). Can we distinguish those that do and those that do not have stripped ions by radius and density of their seed population sources? Is there other evidence of deeper and shallower sources of impulsive suprathermal ions?
7. Spectral knees at shocks have been studied theoretically, but is there a theoretical understanding how the spectrum, *at the shock*, could become a double power-law extending to high energies, rather than an exponential? What parameters control the energy and the change in spectral slope? (There are models that would explain the double power law with diffusive transport.)
8. Measurements by a spacecraft nearer the Sun could improve SEP onset timing by removing the blurring effect of scattering during transport. How does the SEP onset time at 10-second or less resolution compare with X-ray and γ-ray-line onsets, type II burst timing, and local shock measurement? Note that intensities may vary as $\sim r^{-3}$, causing extremely high rates in instruments. To what extent do electron and ion sources differ in gradual SEP events?
9. Discrete ionization states affect the assignment of source-plasma temperatures. $^{12}C^{+5}$ is enhanced but $^{12}C^{+6}$ is not; treating Q as 5.5 is approximate. $A/\langle Q\rangle$ is not the same as $\langle A/Q\rangle$. Then there is ^{13}C which is always enhanced. Can we improve the estimates of T?

References

Ackermann, M., *et al.*, High-energy gamma-ray emission from solar flares: summary of Fermi large area telescope detections and analysis of two M-class flares, Astrophys. J. **787**, 15 (2014)

Ajello, M., *et al.*, Impulsive and long duration high-energy gamma-ray emission from the very bright 2012 March 7 solar flares, Astrophys. J. **789**, 20 (2014)

Afanasiev, A., Battarbee, M., Vainio, R., Self-consistent Monte Carlo simulations of proton acceleration in coronal shocks: Effect of anisotropic pitch-angle scattering of particles, Astron. and Astrophys. **584**, 81 (2016)

Axford, W. I., Acceleration of cosmic rays by shock waves, *Proc. 17th Int. Cosmic Ray Conf. (Paris)* **12**, 155 (1981)

Bell, A. R., The acceleration of cosmic rays in shock fronts. I, Monthly Notices Roy. Astron. Soc. **182**, 147 (1978a)

Bell, A. R., The acceleration of cosmic rays in shock fronts. II, Monthly Notices Roy. Astron. Soc. **182**, 443 (1978b)

Berdichevsky, D. B., Szabo, A., Lepping, R. P., Viñas, A. F., Mariana, F., Interplanetary fast shocks and associated drivers observed through the 23rd solar minimum by Wind over its first 2.5 years, J. Geophys. Res. **105**, 27289 (2000)

Breneman, H.H., Stone, E.C., Solar coronal and photospheric abundances from solar energetic particle measurements, Astrophys. J. Lett. **299**, L57 (1985)

Bučík,,R,. Innes, D.E., Mall, U., Korth, A., Mason, G.M., Gómez-Herrero, R., Multi-spacecraft observations of recurrent ^{3}He-rich solar energetic particles, Astrophys. J. **786**, 71 (2014)

Bučík, R., Innes, D.E., Chen, N.H., Mason, G.M., Gómez-Herrero, R., Wiedenbeck, M.E., Long-lived energetic particle source regions on the Sun, J. Phys. Conf. Ser. **642**, 012002 (2015)

Chen N. H., Bučík R., Innes D. E., Mason G. M., Case studies of multi-day ^{3}He-rich solar energetic particle periods, Astron. Astrophys. **580**, 16 (2015) doi: 10.1051/0004-6361/201525618

Daibog, E. I., Stolpovskii, V. G., Kahler, S. W., Invariance of charged particle time profiles at late stages of scr events from the data of multisatellite observations, Cosmic Research **41**, 128 (2003)

Desai, M. I., Giacalone, J., Large gradual solar energetic particle events, Living Reviews of Solar Physics, doi: 10.1007/s41116-016-0002-5 (2016)

Desai, M. I., Mason, G. M., Dwyer, J. R., Mazur, J. E., Gold, R. E., Krimigis, S. M., Smith, C. W., Skoug, R. M., Evidence for a suprathermal seed population of heavy ions accelerated by interplanetary shocks near 1 AU, Astrophys. J., **588**, 1149 (2003)

Desai, M. I., Mason, G. M., Wiedenbeck, M. E., Cohen, C. M. S., Mazur, J. E., Dwyer, J. R., Gold, R. E., Krimigis, S. M., Hu, Q., Smith, C. W., Skoug, R. M., Spectral properties of heavy ions associated with the passage of interplanetary shocks at 1 AU, Astrophys. J., **661**, 1156 (2004)

DiFabio, R., Guo, Z., Möbius, E., Klecker, B., Kucharek, H., Mason, G.M., Popecki, M., Energy-dependent charge states and their connection with ion abundances in impulsive solar energetic particle events, Astrophys. J. **687**, 623 (2008)

Ellison, D., Ramaty, R., Shock acceleration of electrons and ions in solar flares, Astrophys. J. **298**, 400 (1985)

Jones, F. C., Ellison, D. E., The plasma physics of shock acceleration, Space Sci. Rev. **58**, 259 (1991)

Ko Y,-K., Tylka, A. J., Ng C. K., Wang Y.-M., Dietrich W. F., Source regions of the interplanetary magnetic field and variability in heavy-ion elemental composition in gradual solar energetic particle events, Astrophys. J. **776**, 92 (2013)

Lario, D., Heliospheric energetic particle reservoirs: Ulysses and ACE 175-315 keV electron observations, *Proc. 12th Solar Wind Conf.*, AIP Conf. Proc. **1216**, 625 (2010)

Lario, D., Decker, R. B., The energetic storm particle event of October 20, 1989, Geophys. Res. Lett. **29** 1393 (2002)

Lee, M. A., Coupled hydromagnetic wave excitation and ion acceleration at interplanetary traveling shocks, J. Geophys. Res., **88**, 6109. (1983)

Lee, M. A., Coupled hydromagnetic wave excitation and ion acceleration at an evolving coronal/interplanetary shock, Astrophys. J. Suppl., **158**, 38 (2005)

Lee, M. A., Mewaldt, R. A., Giacalone, J., Shock acceleration of ions in the heliosphere, Space Sci. Rev. **173** 247 (2012)

Li, G., Zank, G. P., Rice, W. K. M., Acceleration and transport of heavy ions at coronal mass ejection-driven shocks, J. Geophys. Res. **110** 6104 (2005)

Mason, G. M., Ng, C. K., Klecker, B., Green, G., Impulsive acceleration and scatter-free transport of about 1 MeV per nucleon ions in ^{3}He-rich solar particle events, Astrophys. J. **339**, 529 (1989).

Mazzotta, P., Mazzitelli, G., Colafrancesco, S, Vittorio, N., Ionization balance for optically thin plasmas: Rate coefficients for all atoms and ions of the elements H to Ni, Astron. Astrophys Suppl. 133, 403 (1998).

McKibben, R. B., Azimuthal propagation of low-energy solar-flare protons as observed from spacecraft very widely separated in solar azimuth, J. Geophys. Res. **77**, 3957 (1972)

Melrose, D. B.: 1980, *Plasma Astrophysics* (New York: Gordon and Breach).

Melrose, D. B., Pope, M. H., Diffusive shock acceleration by multiple shocks, Proc. Astron. Soc. Au. **10**, 222 (1993)

Mewaldt, R. A., Looper, M. D., Cohen, C. M. S., Haggerty, D. K., Labrador, A. W., Leske, R. A., Mason, G. M., Mazur, J. E., von Rosenvinge, T. T., Energy spectra, composition, other properties of ground-level events during solar cycle 23, Space Sci. Rev. **171**, 97 (2012)

Ng, C. K., Reames, D. V., Focused interplanetary transport of approximately 1 MeV solar energetic protons through self-generated Alfven waves, Astrophys. J. **424**, 1032 (1994)

Ng, C. K., Reames, D. V., Pitch angle diffusion coefficient in an extended quasi-linear theory, Astrophys J. **453**, 890 (1995)

Ng, C. K., Reames, D. V., Shock acceleration of solar energetic protons: the first 10 minutes, Astrophys. J. Lett. **686**, L123 (2008)

Ng, C. K., Reames, D. V., Tylka, A. J., Effect of proton-amplified waves on the evolution of solar energetic particle composition in gradual events, Geophys. Res. Lett. **26**, 2145 (1999)

Ng, C. K., Reames, D. V., Tylka, A. J., Modeling shock-accelerated solar energetic particles coupled to interplanetary Alfvén waves, Astrophys. J. **591**, 461 (2003)

Ng, C.K., Reames, D.V., Tylka, A.J., Solar energetic particles: shock acceleration and transport through self-amplified waves, AIP Conf. Proc. **1436**, 212 (2012)

Palmer, I. D., Transport coefficients of low-energy cosmic rays in interplanetary space, Rev. Geophys. Space Phys. **20**, 335 (1982)

Parker, E.N.: *Interplanetary Dynamical Processes,* Interscience, New York (1963)

Parker E. N., Nanoflares and the solar X-ray corona, Astrophys J. **330** 474 (1988)

Post, D.E., Jensen, R.V., Tarter, C.B., Grasberger, W.H., Lokke, W.A., Steady-state radiative cooling rates for low-density, high temperature plasmas, At. Data Nucl. Data Tables **20**, 397 (1977)

Reames, D. V., Acceleration of energetic particles by shock waves from large solar flares, Astrophys. J. Lett. **358**, L63 (1990)

Reames, D. V., Particle energy spectra at traveling interplanetary shock waves, Astrophys. J. **757,** 93 (2012)

Reames, D.V.: The two sources of solar energetic particles, Space Sci. Rev. **175**, 53 (2013)

Reames, D.V., Element abundances in solar energetic particles and the solar corona, Solar Phys., **289**, 977 (2014)

Reames, D.V., Temperature of the source plasma in gradual solar energetic particle events, Solar Phys., **291** 911 (2016a) DOI: 10.1007/s11207-016-0854-9, arXiv: 1509.08948

Reames, D. V., The origin of element abundance variations in solar energetic particles, Solar Phys, **291** 2099 (2016b) DOI: 10.1007/s11207-016-0942-x, arXiv: 1603.06233

Reames, D. V., Barbier, L. M., von Rosenvinge, T. T., Mason, G. M., Mazur, J. E., Dwyer, J. R., Energy spectra of ions accelerated in impulsive and gradual solar events, Astrophys. J. **483**, 515 (1997a)

Reames, D. V., Ng, C. K., Berdichevsky, D., Angular Distributions of Solar Energetic Particles , Atrophys. J. **550** 1064 (2001)

Reames, D. V., Ng, C. K., Streaming-limited intensities of solar energetic particles on the intensity plateau, Astrophys. J. **722**, 1286 (2010)

Reames, D. V., Kahler, S. W., Ng, C. K., Spatial and temporal invariance in the spectra of energetic particles in gradual solar events, Astrophys. J. **491**, 414 (1997b)

Reames, D. V., Ng, C. K., Tylka, A. J., Initial time dependence of abundances in solar particle events, Astrophys. J. Lett. **531**, L83 (2000)

Rice, W. K. M., Zank, G.P., Li, G., Particle acceleration and coronal mass ejection driven shocks: Shocks of arbitrary strength, J. Geophys, Res. **108** 1369 (2003)

Roelof, E. C., Propagation of solar cosmic rays in the interplanetary magnetic field, *Lectures in High-Energy Astrophysics*, ed. H. Ögelman and J. R. Wayland, Washington, D. C. NASA SP-199 (1969)

Roelof, E. C., Gold, R. E., Simnett, G. M., Tappin, S. J., Armstrong, T. P., Lanzerotti, L. J., Low-energy solar electrons and ions observed at ULYSSES February-April, 1991 - The inner heliosphere as a particle reservoir, Geophys. Res. Lett. **19**, 1247 (1992)

Rouillard, A., Sheeley, N. R. Jr., Tylka, A., Vourlidas, A., Ng, C. K., Rakowski, C., Cohen, C .M. S., Mewaldt, R. A., Mason, G. M., Reames, D.,*et al*., The longitudinal properties of a solar energetic particle event investigated using modern solar imaging, Astrophys. J. **752**, 44 (2012)

Ryan, J. M., Long-duration solar gamma-ray flares, Space Sci. Rev. **93**, 581 (2000)

Sandroos, A., Vainio, R., Simulation results for heavy ion spectral variability in large gradual solar energetic particle events, Astrophys. J. **662**, L127 (2007)

Stix, T. H.: 1962, *The Theory of Plasma Waves* (New York: McGraw-Hill)

Stix, T. H.: 1992, *Waves in Plasmas* (New York: AIP).

Tan, L. C., Reames, D. V., Ng, C. K., Shao, X., Wang, L., What causes scatter-free transport of non-relativistic solar electrons?, *Astrophys J* **728**, 133 (2011)

Terasawa, T., Oka, M., Nakata, K., Keika, K., Nosé, M., McEntire, R. W., Saito, Y., Mukai, T., 'Cosmic-ray-mediated' interplanetary shocks in 1994 and 2003, Adv. Space. Res. **37**, 1408 (2006)

Vestrand, W. T., Forrest, D. J., Evidence for a spatially extended component of gamma rays from solar flares, Astrophys. J. Lett. **409**, L69 (1993)

Wiedenbeck, M.E, Cohen, C.M.S., Cummings, A.C., de Nolfo, G.A., Leske, R.A., Mewaldt, R.A., Stone, E.C., von Rosenvinge, T.T., Persistent energetic ^{3}He in the inner heliosphere, *Proc. 30th Int. Cosmic Ray Conf.* (Mérida) 1, 91 (2008)

Zank, G. P., Li, G., Florinski, V., Hu,, Q., Lario,, D., Smith, C. W., Particle acceleration at perpendicular shock waves: Model and observations, J. Geophys. Res., **111**, A6108 (2006)

Zank, G. P., Li, G., Verkhoglyadova, O., Particle Acceleration at Interplanetary Shocks, Space Sci. Rev. **130**, 255 (2007)

Zank, G. P., Rice, W. K. M., Wu, C. C., Particle acceleration and coronal mass ejection driven shocks: A theoretical model, *J*. Geophys. Res., **105**, 25079 (2000)

6. High Energies and Radiation Effects

Abstract In this chapter we characterize the high-energy proton spectra that can penetrate shielding and determine the radiation dose to humans and equipment in space. High-energy spectral breaks or "knees", seen in all large SEP events, determine the contribution of highly penetrating protons. The streaming limit, discussed earlier, places an upper bound on particle fluences early in events and the radial variation of intensities is important for near-solar and deep-space missions. The streaming limit is a strong function of radial distance from the Sun. We also briefly consider a mission to Mars and radiation-induced chemistry of the upper atmosphere of Earth.

We must recognize that solar energetic particles (SEPs) are of more than scientific interest. They can be a serious radiation hazard to astronauts and equipment in space beyond the protection of Earth's atmosphere and magnetic field. Protons of ~150 MeV can penetrate 20 gm cm ^{2} (7.4 cm) of Al or 15.5 cm of water (or human flesh). Such protons are considered to be "hard" radiation, in that they are very difficult to shield, and they are orders of magnitude more intense than the GeV protons that define a ground-level event (GLE). Most of the other radiation risk to humans in space from SEP events comes from protons in the energy region above about 50 MeV, or "soft" radiation. This is where protons begin to penetrate spacesuits and the skin of spacecraft. Studies of radiation dosage and engineering design and tradeoff are beyond the scope of this book (see Barth *et al*. 2003; Xapsos *et al*. 2007; Cucinotta *et al*. 2010; Carnell *et al.* 2016), as is SEP forcasting (*e.g.* Kahler and Ling 2015; Laurenza *et al.* 2009). However, it is certainly relevant to characterize the high-energy SEP spectra and their limits and spatial variations that affect radiation doses (*e.g.* Reames and Ng 1998; Reames 1999, 2013).

6.1 High-Energy Spectra

The single most important factor, in the dose of penetrating protons, may be the location of the high-energy spectral break or knee. A comparison of spectra in two events is shown in Figure 6.1 where the contributions of "hard" and "soft" radiation boundaries are shown. The spectra in the two events are similar in the 10 – 100 MeV region, partly controlled by the streaming limit (see Sections 5.1.5 and 6.2). The spectrum of the April 1998 event (green) contributes mostly soft radiation in the region shaded yellow. The *additional* dose from the September 1989 SEP event is shaded red. Even behind 10 g cm^{-2} of material, astronauts would receive a dose of 40 mSv hr^{-1} (~4 rem hr^{-1}) at the intensities in the September 1989 event. The *annual* dose limit for a radiation worker in the United States is 50 mSv (see review Cucinotta *et al.* 2010).

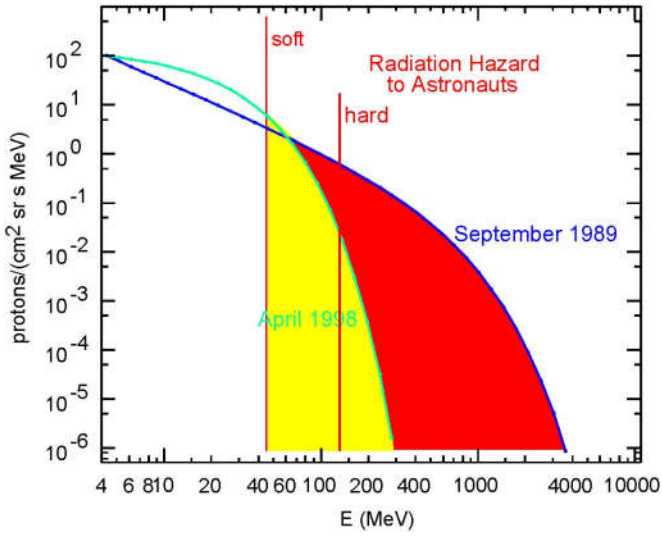

Fig. 6.1. Proton spectra in the SEP events of 20 April 1998 (green; based on Tylka *et al.* 2000) and 29 September 1989 (blue; based on Lovell, Duldig, and Humble 1998) are compared. Typical energies of "soft" and "hard" radiation are shown. The hazardous portion of the spectrum of the April event is shaded yellow and the *additional* hazardous radiation from the September event is shaded red. (Reames 2013).

In Figure 6.1, the proton knee for the April 1998 event is about 40 MeV while that for the September 1989 event is nearer 400 MeV. This spectral shape makes an important difference.

An extensive recent study of high-energy spectra in ground-level events (GLEs) has been conducted by Tylka and Dietrich (2009) which merged neutron-monitor data with satellite-based data. Two of these spectra are shown in Figure 6.2. The authors construct *integral* rigidity spectra using the magnetic cutoff rigidity of the stations. They then correct for the fact that higher-energy protons produce increasingly more secondary neutrons, and they compare with satellite measurements. The spectra are then fit to the empirical double power-law (Band *et al.* 1993) spectra above 0.137 GV (10 MeV), for which the parameters are stated, and to a single power law in the neutron-monitor region. Note that the Cherenkov-radiation-based GOES/HEPAD instrument and the IMP/GSFC instrument overlap the neutron-monitor measurements extremely well up to rigidities just above 1 GV.

Much of the neutron-monitor data have lain idle for 50 years. Tylka and Dietrich have performed a great service to finally find a way to analyze the data, compute spectra, and organize all of these data in a form that is useful for comparing and studying high-energy SEP events. Those responsible for determining the risk of radiation hazards to astronauts should certainly take advantage of this thorough study.

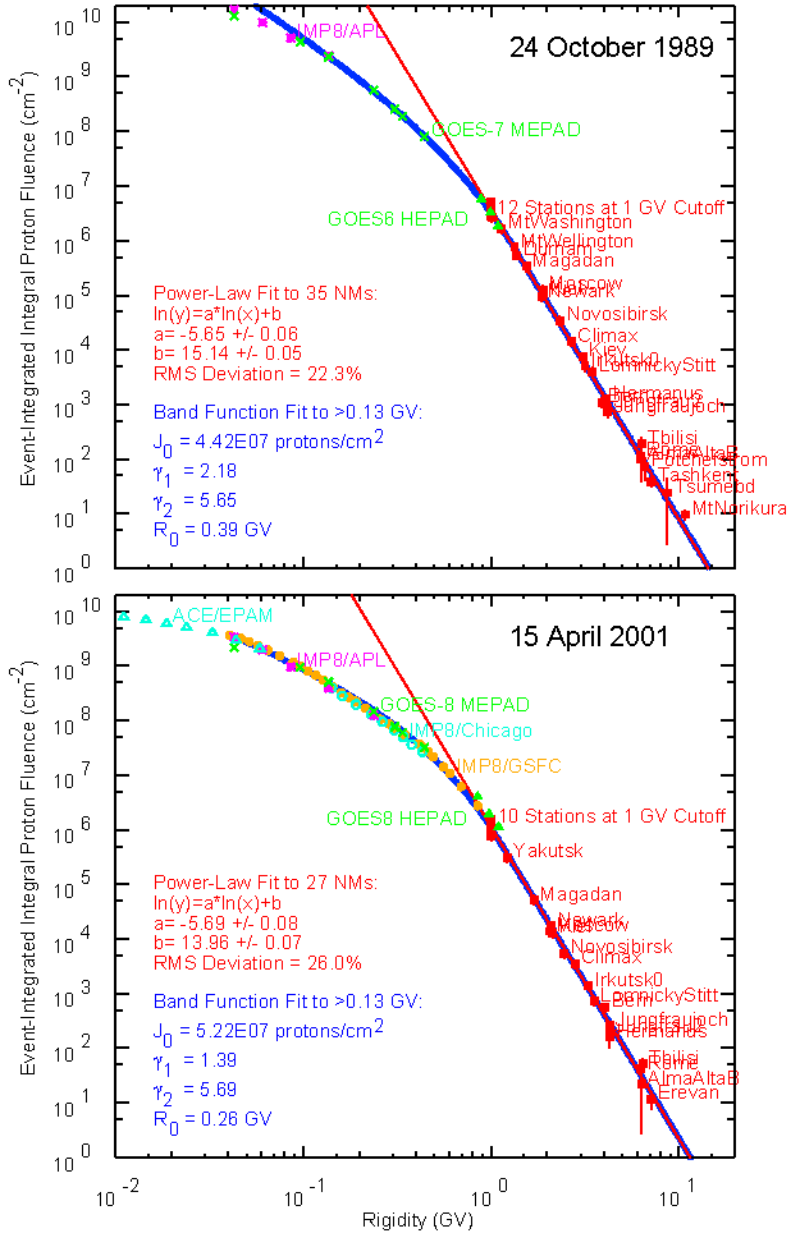

Fig 6.2. Integral rigidity spectra are shown for two large GLEs. Cutoff rigidities for individual neutron-monitor stations (listed) are used; the spectra are corrected for neutron production *vs.* proton energy, and compared with the named satellite measurements. Fits to double power-law (Band) spectra are shown (Tylka and Dietrich 2009)

The fluence and the power-law fit above 1 GV (430 MeV) for the GLEs from Tylka and Dietrich (2009) are shown in Figure 6.3. The largest fluence is 4×10^6 protons cm^{-2} sr^{-1} for the 23 February 1956 event, but the flattest spectra in the high-energy region are for the events of 7 May 1978 and 29 September 1979 (seen also in Figures 6.1 and 6.5) events with rigidity spectral indices near 4.0. Most of the GLEs have spectral indices between 5 and 7.

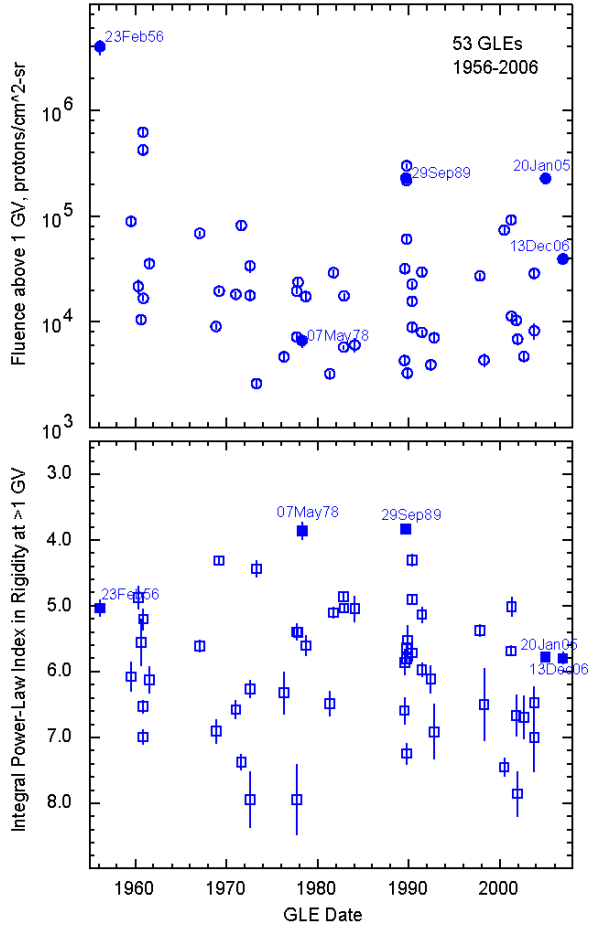

Fig 6.3. The upper panel shows the proton fluence above 1 GV (430 MeV) *vs.* time for each GLE. The lower panel shows the integral rigidity power-law spectral index also above 1 GV (Tylka and Dietrich 2009)

6.2 The Streaming Limit

Protons streaming out early in an SEP event generate waves that throttle the flow of subsequent particles, trapping them near the source. The streaming limit (see Section 5.1.5) is a transport phenomenon placing an upper bound on equilibrium intensities early in events once the waves become established (Reames and Ng 1998, 2010). If we plot the probability of attaining a given intensity, *i.e.* the num-

ber of hours a given intensity is observed in ~11 years, as in Figure 6.4, we see a sudden drop above the streaming limit. Intensities near shock peaks are not limited by this mechanism since no net streaming is involved. However, shock peaks occur late, when shocks have weakened and particles have spread spatially.

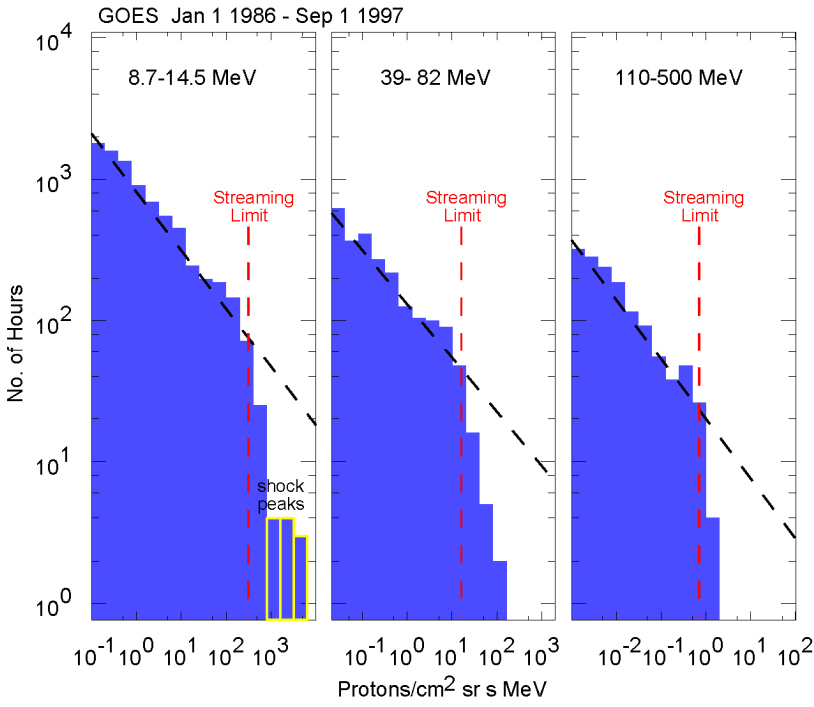

Fig. 6.4. The number of hours a given intensity is observed in ~11 years is shown for three different proton energy bins. Only intensities near the rarer shock peaks are seen above the streaming limit (Reames 2013).

The black dashed lines in Figure 6.4 are power-law fits below the streaming limit that decrease as the ~0.4 power of the intensity. This is often expressed as the slope, *i.e.* the rate of change in the number for a given change in the intensity, which decreases as the 1.4 power of the intensity in this case. Cliver *et al.* (2012) have recently compared different size measures of SEP events and of hard and soft solar X-ray events.

The streaming limit is not conveniently low so as to prevent excessive radiation exposure, but at least it does offer a limit which is in force for a day or so before intensities begin to ramp up as the shock approaches. This allows astronauts time to reenter their vehicles and seek shelter, for example. The intensity level applied as the limits in Figure 6.4 are shown during several large GLEs in Figure 6.5. At the lower energies, up to ~80 MeV, the peak at the shock exceeds the streaming limit by an order of magnitude or more.

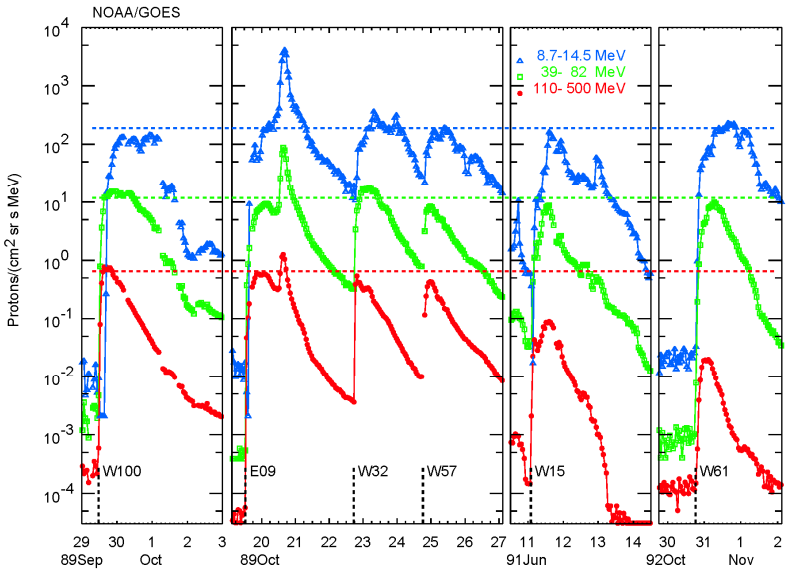

Fig. 6.5. Intensity levels are shown in six large SEP events with the corresponding streaming limit (Reames and Ng 1998)

The rate of rise of the proton intensity can also be a factor in the *establishment* of equilibrium of the streaming limit as shown in Figure 6.6. The fast rise of high-energy protons in the SEP event of 20 January 2005 allows the intensity to exceed the equilibrium limit until there has been enough wave growth to establish the equilibrium. Most events have slower evolution and do not overshoot the limit. Finally, Lario, Aran, and Decker (2009) have pointed out that trapping might also allow intensities to exceed the streaming limit.

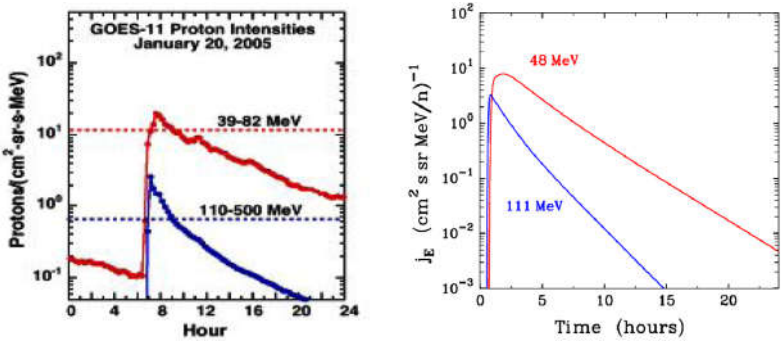

Fig. 6.6. The left panel shows that intensities in the event of January 20, 2005 briefly exceed the expected streaming limits from Figure 6.5 (Mewaldt *et al.* 2007). The right panel shows that time-dependent calculations described by Ng, Reames, and Tylka (2012) also exceed these limits because there has not yet been enough proton flow to establish wave equilibrium at the highest energies. The fluence above 1 GV for this event is compared with other events in Figure 6.3.

6.3 Radial Dependence

Radial dependence of SEP intensities can be complex, but is often important for radiation assessment, especially on missions that approach the Sun. There is a wide variation in behavior. We might expect an impulsive injection to diverge like r^{-3} while we have seen that reservoirs have no radial variation at all. Theoretically the dependence on space and time in a large gradual SEP event is shown in the example in Figure 6.7.

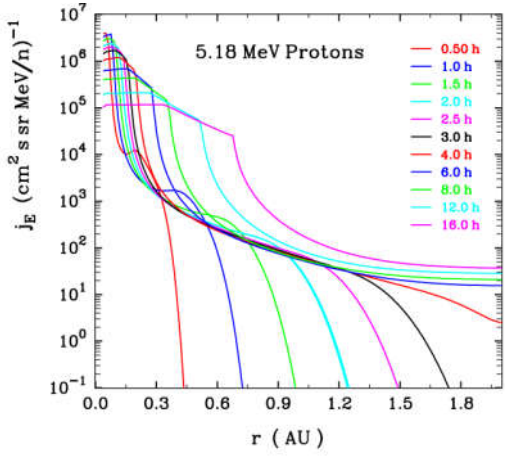

Fig. 6.7. Theoretical intensity of 5.18 MeV protons *vs.* radius is shown as it varies with time during a large SEP event. Soon after arrival at a given radius, intensities rise to the streaming limit at that radius. At 1 AU, intensities are bounded near ~100 (cm^2 s sr MeV)$^{-1}$ until the shock reaches ~0.7 AU (Ng, Reames, and Tylka 2003, 2012).

Notice that the streaming limit is itself a strong function of radius and that the peak intensity at the shock follows a different radial track; both are the same at the shock when it is near the Sun. There can be a severe radiation hazard to equipment on a spacecraft that approaches the Sun. However, the probability may be small for occurrence of a large gradual SEP event during a brief passage of spacecraft perihelion.

A model for calculating the radial dependences has been described by Verkhoglyadova *et al.* (2012).

6.4 A Mission to Mars

A mission to Mars beginning 26 November 2011 carried instruments that led to an estimate that the radiation dose during a ~1-yr round-trip mission would be 660±12 mSv (Zeitlin *et al.* 2013). Of course, this mission occurred during the notoriously weak Solar Cycle 24 that did not contain an SEP event like that of 23 February 1956 (see Figure 6.3). Fortunately those events are very rare.

For the timing of a manned mission to Mars, one can go during solar maximum when SEP events are more probable and GCR intensities are reduced, or during solar minimum when SEPs are reduced and GCRs are at maximum (see Figure 1.8). The continuous radiation of GCRs causes cancer risk in astronauts, while the SEPs pose a small risk of radiation sickness or even a fatal exposure. Most plan-

ning assumes a trip to Mars during solar maximum to reduce the cancer risk. It is assumed that SEP risk can be reduced somewhat by a safe-haven shelter with shielding of 30 – 40 g cm^{-2}, combined with an adequate warning system. GCR radiation is not reduced by shielding; it is actually increased by production of secondaries (Carnell *et al.* 2016).

Little effort is presently expended on studying the hazard from SEP events, assessing their risk, and ensuring an appropriate structure is in place to provide adequate warning. In addition, there is little planning for contingencies in case of an extreme event. The probability of an extremely hazardous event occurring during a specific mission, even a one-year mission, is relatively small, perhaps less than a few percent. The problem actually comes when there is a continuous human presence outside the Earth's magnetosphere; then it is not a question of if, but when.

6.5 The Upper Atmosphere of Earth

Ionization of the upper atmosphere during large SEP events can have significant long-term effects on the chemistry of the Earth's polar atmosphere. SEP ionization produces HO_x and NO_y in the mesosphere and stratosphere and the lifetime of the NO_y allows it to affect ozone for months to years. Mesospheric ozone depletions of 50% can last for hours or days. Significant ozone depletions of >10% can last a few months after SEP events. However, interference with the Cl- and Br-loss cycles actually caused an increase in total ozone, for example in 1992 – 1994, a few years after the October 1989 series of SEP events shown in Figure 6.5 (Jackman, Fleming, and Vitt, 2000; Jackman *et al.* 2006). Recent events from January and March 2012 have also produced effects (von Clarmann *et al.* 2013).

References

Band, D., Matteson, J., Ford, L., Schaefer, B., Palmer, D., Teegarden, B., Cline, T., Briggs, M., Paciesas, W., Pendleton, G., *et al*., SE observations of gamma-ray burst spectra. I - Spectral diversity, Astrophys. J., **413**, 281 (1993)

Barth, J. L., Dyer, C. S., Stassinopoulos, E. G., Space, atmospheric, and terrestrial radiation environments, IEEE Trans. Nucl. Sci. **50**, 466. (2003)

Carnell, L., S. Blattnig, S, Hu, J. Huff, M. H. Kim, R. Norman, Z. Patel, L. Simonsen, and H. Wu., *NASA 1 evidence report: Risk of Acute Radiation Syndromes Due to Solar Particle Events* (2016) https://humanresearchroadmap.nasa.gov/evidence/reports/Acute.pdf?rnd=0.543557888150009

Cliver, E. W., Ling, A. G., Belov, A., Yashiro, S., Size distributions of solar flares and solar energetic particle events, Astrophys. J. Lett. **756,** L29 (2012)

Cucinotta, F. A., Hu, S., Schwadron, N. A., Kozarev, K., Townsend, L. W., Kim, M.-H. Y., Space radiation risk limits and Earth-Moon-Mars environmental models, Space Weather **8** S00E09 (2010)

Jackman, C. H., Deland, M. T., Labow, G. J., Fleming, E. L., López-Puertas, M., Satellite measurements of middle atmospheric impacts by solar proton events in Solar Cycle 23, Space Sci. Rev. **125**, 381 (2006)

Jackman, C. H., Fleming, E. L., Vitt, F. M., Influence of extremely large solar proton events in a changing stratosphere, J. Geophys. Res. **105** 11659 (2000)

Kahler, S. W., Ling, A. Dynamic SEP event probability forecasts, Space Weather **13**, 665 (2015)

Lario, D., Aran, A., Decker, R. B., Major solar energetic particle events of solar cycles 22 and 23: Intensities close to the streaming limit, Solar Phys. **260**, 407 (2009)

Laurenza, M., E. W. Cliver, J. Hewitt, M. Storini, A. G. Ling, C. C. Balch, M. L. Kaiser, A technique for short-term warning of solar energetic particle events based on flare location, flare size, and evidence of particle escape, Space Weather, **7** S04008 (2009) DOI: 10.1029/2007SW000379

Lovell, J. L., Duldig, M. L., Humble, J. E., An extended analysis of the September 1989 cosmic ray ground-level enhancement, J. Geophys. Res., **103**, 23,733 (1998)

Mewaldt, R. A., Cohen, C. M. S., Haggerty, D. K., Mason, G. M., Looper, M. L., von Rosenvinge, T. T.. Wiedenbeck, M. E., Radiation risks from large solar energetic particle events, AIP Conf. Proc. **932**, 277 (2007)

Ng, C. K., Reames, D. V., Tylka, A. J., Modeling shock-accelerated solar energetic particles coupled to interplanetary Alfvén waves, Astrophys. J. **591**, 461 (2003)

Ng, C.K., Reames, D.V., Tylka, A.J., Solar energetic particles: shock acceleration and transport through self-amplified waves, AIP Conf. Proc. **1436**, 212 (2012)

Reames, D. V., Solar energetic particles: Is there time to hide? Radiation Measurements **30**/3, 297 (1999)

Reames, D.V.: The two sources of solar energetic particles, Space Sci. Rev. **175**, 53 (2013)

Reames, D. V. Ng, C. K., Streaming-limited intensities of solar energetic particles, Astrophys. J. **504**, 1002 (1998)

Reames, D. V., Ng, C. K., Streaming-limited intensities of solar energetic particles on the intensity plateau, Astrophys. J. **722**, 1286 (2010)

Tylka, A. J., Boberg, P. R., McGuire, R. E., Ng, C. K., Reames, D. V., Variation in solar energetic particle elemental composition observed by ACE and Wind, in AIP Conf. Proc. **528**, *Acceleration and Transport of Energetic Particles Observed in the Heliosphere*, ed. R. A. Mewaldt, J. R. Jokipii, M. A. Lee, E. Möbius, T. H. Zurbuchen (Melville: AIP), 147 (2000)

Tylka, A. J., Dietrich, W. F., A new and comprehensive analysis of proton spectra in ground-level enhanced (GLE) solar particle events, in *Proc. 31st Int. Cos. Ray Conf* , Lódz (2009), http://icrc2009.uni.lodz.pl/proc/pdf/icrc0273.pdf

Verkhoglyadova, O. P., Li, G., Ao, X., Zank, G. P., Radial Dependence of Peak Proton and Iron Ion Fluxes in Solar Energetic Particle Events: Application of the PATH Code, Astrophys. J. **757**, 75 (2012)

von Clarmann, T., Funke, B., López-Puertas, M., Kellmann, S., Linden, A., Stiller, G. P., Jackman, C. H., Harvey, V. L., The solar proton events in 2012 as observed by MIPAS, Geophy. Res. Lett. **40** 2339 (2013)

Xapsos, M. A., Stauffer, C., Jordan, T., Barth, J. L., Mewaldt, R. A., Model for cumulative solar heavy ion energy and linear energy transfer spectra, IEEE Trans. Nucl. Sci. **54**, 1985 (2007)

Zeitlin, C, Hassler, D. M., Cucinotta, F. A., Ehresmann, B., Wimmer-Schweingruber, R. F., Brinza, D. E., *et al*., 2013, Measurements of energetic particle radiation in transit to Mars on the Mars Science Laboratory, Science **340**, 1080 (2013)

7. Measurements of SEPs

Abstract Those who study solar energetic particles (SEPs) should be aware of the basic types of experiments that have contributed most of the observations studied in this book, and especially the tradeoff of their strengths and weaknesses, and how they fail. However, this is *not* a comprehensive review, only an introduction. We focus on generic dE/dx *vs.* E instruments that are the workhorses of SEP studies, and also study time-of-flight *vs.* E instruments that dominate precision measurements below 1 MeV amu^{-1}. Single-detector instruments and high-energy techniques are discussed briefly.

Nearly every experimenter who builds instruments thinks he has made the best tradeoff within the triple constraints of weight, power, and expense, to maximize the scientific return. Many instruments are designed to extend coverage to a previously unmeasured region: energy coverage, isotope resolution, heavy elements. Others hitchhike on spacecraft going to a new and interesting region of space.

The rate of energy loss of an ion in a detector material is approximately

$$\frac{dE}{dx} \approx \frac{4\pi e^2 n_e}{mc^2\beta^2}\left(\frac{Q^2}{A}\right)\left[\ln\left(\frac{2mc^2\beta^2\gamma^2}{I}\right) - \beta^2\right] \tag{7.1}$$

where m and e are the mass and charge of an electron, n_e is the electron density, I is the "mean ionization potential" of the stopping material, and β and γ are the relativistic velocity and Lorentz factor of the ion as defined in Section 1.5.4. Here we have again used $E = \mathcal{E}/A = M_u(\gamma - 1) \approx \frac{1}{2} M_u \beta^2$, a function of velocity alone, to show that the only dependence on the stopping ion is Q^2/A and its velocity β. $M_u = m_u c^2 = 931.494$ MeV.

Equation 7.1 is derived from the electron-ion scattering cross section (Rutherford scattering) where we view incoming electrons of the stopping material being scattered by the electric field of the ion. Energy transfers to the electrons are integrated from a minimum of I to a maximum of $2mc^2\beta^2\gamma^2$, which is approximately the maximum energy that can be transferred to a scattered electron. Note that, when $Q \approx Z$, the dominant energy dependence of dE/dx is $\sim\beta^{-2}$, or nonrelativistically, $\sim E^{-1}$, sometimes a useful approximation.

At relativistic energies, dE/dx reaches a broad minimum at ~2.5 GeV amu^{-1} then rises slightly from density effects not included here. At low energies, dE/dx actually peaks, because Q decreases, but $Q \to Z$ at moderate energies. A simple approximation sometimes used for this is $Q \approx Z\,[1 - \exp(-\beta/\beta_0)]$. For capture into the K orbital, $\beta_0 \approx Z/137$; for the Fermi-Thomas model $\beta_0 \approx Z^{2/3}/137$. Modern em-

pirical tables use more complex expressions and tabulate both stopping power and range (Hubert, Bimbo, and Gauvin 1990). The particle range $R = \int dE\ (dE/dx)^{-1}$. For energies down to 1 keV amu^{-1}, the tables of Paul and Schinner (2003) are available.

7.1 Single-Element Detectors

Conceptually, the simplest detector is that with a single sensitive element. Modern "solid-state" detectors are a Si wafer biased as a capacitor that collects the electron-hole pairs produced when an ionizing particle penetrates, loses energy, or stops within its volume. The charge collected, proportional to the energy loss, is measured as a pulse height by analog-to-digital converters. Single-element detectors are generally shielded to define the access geometry for low-energy particles.

Measuring the energy of each arriving particle works at low energies, but penetrating particles contribute as if they had a much lower energy (Figure 7.1). When the SEPs have a steep energy spectrum, the contribution of high-energy particles may be small, but early in SEP events nearly all particles are penetrating and single-detector instruments falsely appear to show low-energy particles arriving much earlier than they possibly could. This effect is sometimes called "punch-through," it occurs in *every* SEP event, and can cause serious misconceptions. These detectors also confuse heavier ions similarly, even though they deposit an increasing amount of energy. Single-element telescopes should never be used for SEP onset timing. They are more appropriate for the study of energetic particle spectra at interplanetary shock waves.

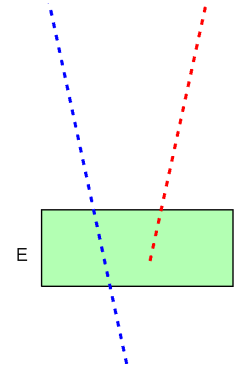

Fig. 7.1. A single-detector telescope measures the total kinetic energy of stopping ions (red) and the energy loss of penetrating ions (blue), which is much lower. The latter are (incorrectly) assumed to be rare. Access geometry is somewhat controlled by shielding (not shown) and a permanent magnet may be included to sweep away electrons, or to measure electrons by comparing detectors with and without magnets.

Electrons are particularly difficult to measure since they do not travel in straight lines, but suffer numerous large-angle scatters. The best remedy is extensive instrument calibration before launch.

Single-element and other limited telescopes are sometimes flown on deep-space missions where weight and power are severely limited and where SEPs are not the primary objective. Unfortunately, these low-priority hitchhikers may even be turned off during transit to the mission destination to save resources, greatly decreasing their value.

7.2 E vs. E Telescopes

These telescopes consist of at least three active detector elements. Particles enter the first detector, penetrate into the second, and stop before entering the third anti-coincidence detector. The separation of the first two detectors, and their areas, determine the instrument geometry-factor. The detector thicknesses determine the minimum and maximum energy according to the range-energy relation in Si (*e.g.* Hubert, Bimbo, and Gauvin 1990). Front detector thicknesses of 10 – 20 μm set a lower bound of ~1 MeV amu^{-1}, depending upon species. Total thicknesses of D+E of up to 10 cm of Si are used for energies ~200 MeV amu^{-1}. The energy range can be extended to above ~400 MeV amu^{-1} by observing the *change* in dE/dx between D and E, if penetrating ions are measured. The concept of a two-element telescope is shown in Figure 7.2.

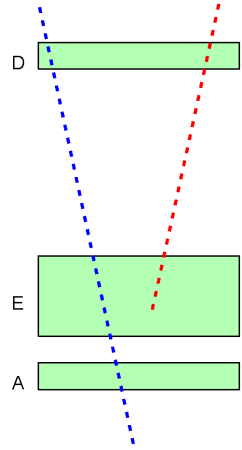

Fig. 7.2. A minimal *E vs. E* or two-dimensional telescope requires coincidence of signals from the D and E elements and no signal from the A element to define stopping (red) ions. "Matrix" plots of pulse-heights of D *vs.* E are used to resolve elements and measure their energies (see Figure 7.3). The anti-coincidence element or inert shielding may surround the telescope.

Most of the particle telescopes flown in space are of this general type, although multiple detectors may be used in place of the D and E elements. Early telescopes used plastic scintillator or even gas drift chambers, but most telescopes of the last 20 years are "solid state" Si detectors which have extremely high resolution and *stability*, *i.e. their response does not change at all during several decades of operation*.

Anti-coincidence detectors were sometimes wrapped around the whole telescope. However, at the high rates in a large SEP event these may be recording particles nearly all the time, and insure that the telescope is effectively turned off.

A geometry factor defined by surfaces S_1 and S_2 is

$$A\Omega = \iint_{S_1} dS_1 \iint_{S_2} dS_2 \frac{(\mathbf{n}_1 \cdot \mathbf{r})(\mathbf{n}_2 \cdot \mathbf{r})}{r^4} \qquad (7.2)$$

where $\boldsymbol{n}_1$ and $\boldsymbol{n}_2$ are unit vectors normal to the surface elements dS_1 and dS_2, respectively and $\boldsymbol{r}$ is the vector distance between them. Geometry factors are usually calculated numerically.

7.2.1 An Example: LEMT

Response of a telescope with a thin front detector, the *Low-Energy Matrix Telescope* (LEMT) on the *Wind* spacecraft (von Rosenvinge *et al.* 1995), is shown in Figure 7.3. LEMT has three important virtues, large geometry (51 cm^2 sr), broad element coverage (He – Pb at ~2 – 20 MeV amu^{-1}), and, equally important, the author is familiar with it. Each LEMT consists of a domed array of 16 D-detectors 18 μm thick, followed by a large 1-mm-thick E-detector with coarse 5 × 5 position sensing and an anticoincidence detector (see von Rosenvinge *et al.* 1995).

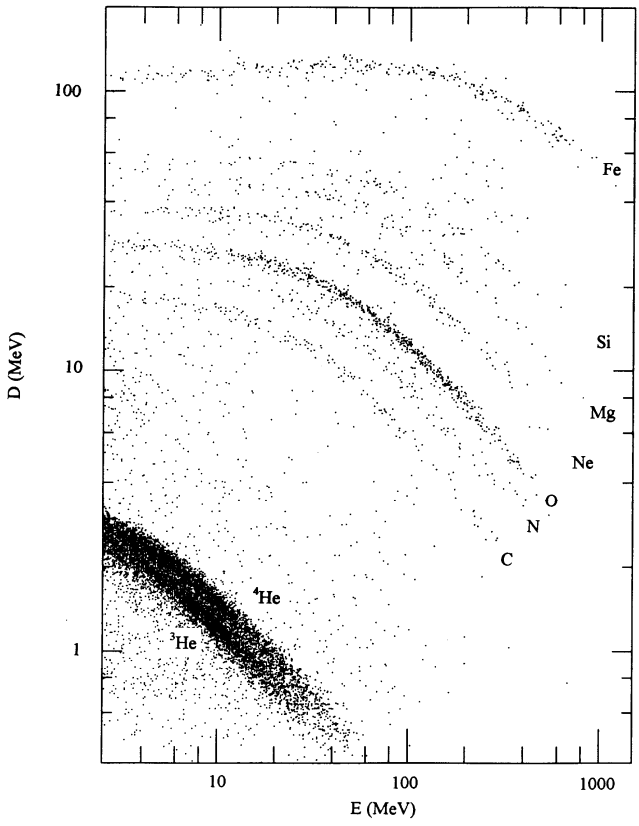

Fig 7.3. Response of the LEMT telescope to ions from a small ^{3}He-rich event in 1995 is shown with "tracks" of species indicated. The telescope has only modest resolution of He isotopes. The track of O is heavily populated by anomalous cosmic rays during this period near solar minimum (see Reames *et al.* 1997)

Particles entering LEMT are corrected for angle of entry, mapped in a log *D vs.* log *E* space, like that of Figure 7.3, and binned onboard according to particle species and energy interval (see Reames, Ng, and Berdichevsky 2001). The right-hand ends of the particle tracks, especially noticeable for C, N, and O, occur just before the ions have enough energy to begin to penetrate into the anticoincidence detector.

In the region of the rarer elements with $Z \geq 34$, "priority" measurements of individual ions are rare enough to be telemetered for later analysis. The performance of LEMT at high Z is shown in Figure 7.4.

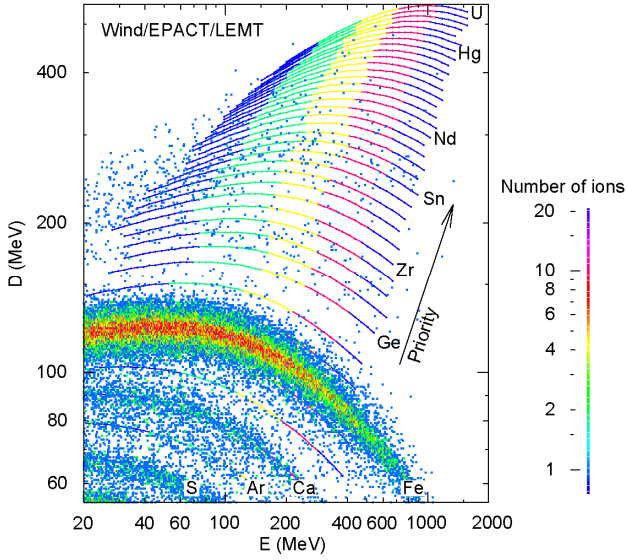

Fig. 7.4. High-Z response of LEMT is shown where resolution (*i.e.* track width) is comparable with that at Fe. Energy varies along each calibration curve from left to right, from 2.5 to 10 MeV amu^{-1}.

While the error at high Z is 2 to 3 units, the resolution is adequate to show bands of enhanced abundances, such as that between Ge and Zr and the band near Sn, that reflect an abundance maximum at $50 \leq Z \leq 56$. The absolute locations of the reference curves of the elements were calibrated prior to launch using accelerator beams of He, C, O, Fe, Ag, and Au (see von Rosenvinge *et al.* 1995). By measuring at low energy with a fairly large geometry factor, LEMT can move up the steep energy spectra to get a rough measure of the abundances of the rare elements with $34 \leq Z \leq 82$. For results of these measurements see Figures 4.7 and 4.9.

7.2.2 Isotope Resolution: SIS

Accuracy can be affected by thickness variations and sec θ variations by particle trajectories inclined by an angle θ to the telescope axis. Both of these may be reduced by accurately measuring sec θ using two sets of x and y strip detectors (*e.g.* Stone *et al.* 1998). The additional detector thickness required for these measurements raises the energy threshold above ~10 MeV amu^{-1}, depending upon particle species, but also permits isotope resolution up to Fe – an important tradeoff. Figure 7.5 shows the resolution of Ne isotopes by the *Solar Isotope Spectrometer* (SIS) on the *Advanced Composition Explorer* (ACE) in two different SEP events. Isotopic abundances show the same A/Q variations we have seen in element abundance enhancements in both impulsive and gradual SEP events. Here, however, there is no question about the average value of Q, which we expect to be the same for all isotopes of an element.

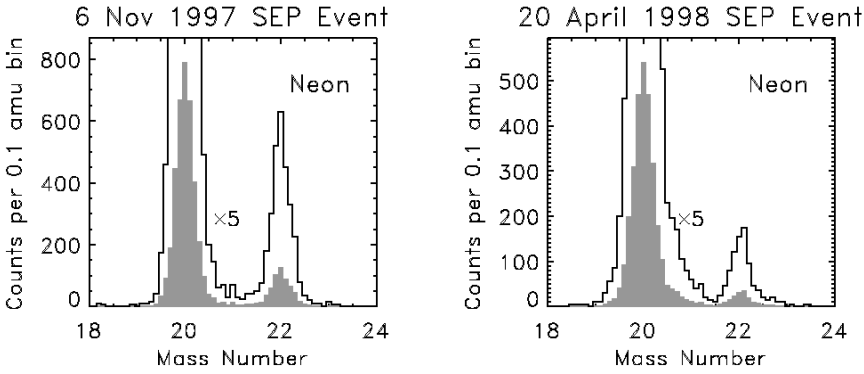

Fig. 7.5. Panels show the resolution of Ne isotopes by the SIS telescope in two SEP events. Histograms are also shown enhanced by a factor of 5 to clarify ^{22}Ne measurement (Leske *et al.* 2007). Isotope measurements show *A/Q* enhancements like those seen in element abundances.

7.3 Time-of-Flight *vs.* E

Measurement of a particle's time of flight over a fixed distance determines its velocity. If the particle subsequently stops in a Si detector its total kinetic energy can be measured, and the pair of measurements determines the particle mass. The design of the *SupraThermal Energetic Particle* (STEP) system flown on the *Wind* and STEREO spacecraft is shown in Figure 7.6.

Fig. 7.6. The STEP telescope measures time of flight *vs.* energy (see text; von Rosenvinge *et al.* 1995).

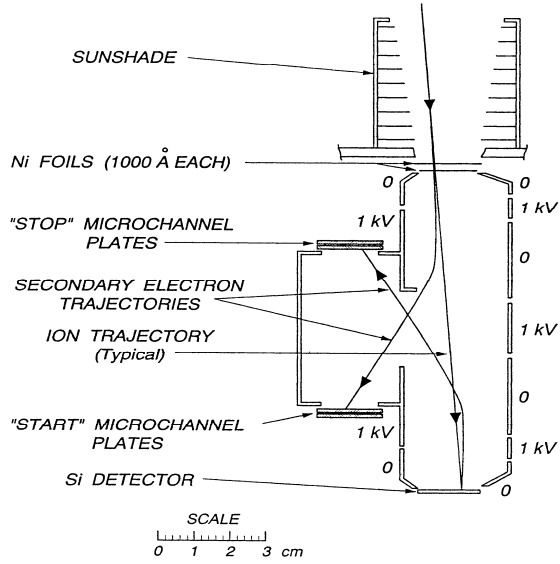

A particle penetrating the entrance Ni foil in STEP may knock off ~4 – 30 electrons that are accelerated and deflected by the 1 kV electric field into the "start"

microchannel plates that multiply the signal by ~100. If the particle then enters the Si detector, backscattered electrons are accelerated into the "stop" microchannel plates, and energy is measured in the Si detector. The time between the start and stop signals, 2 – 100 ns, is processed by a time-to-amplitude converter (TAC). The TAC and energy signals are combined into a weighted analog sum that assigns a priority that controls further processing. Heavies, with A > 4, are assigned the highest priority, He next, and then H.

The response of STEP to a small ^{3}He-rich SEP is shown in Figure 7.7.

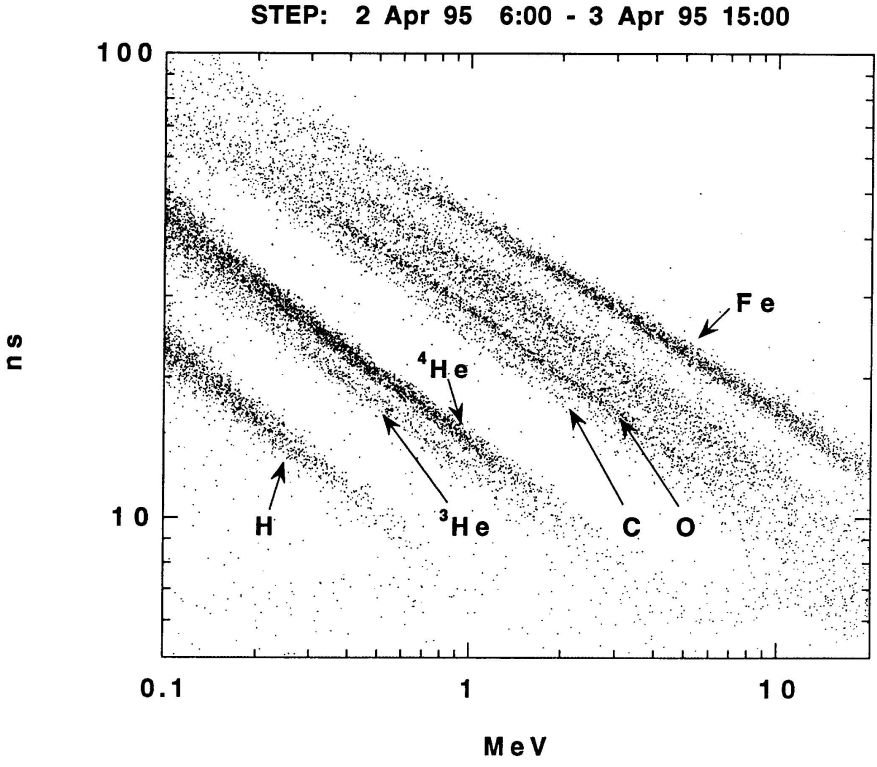

Fig. 7.7. The response of the STEP telescope shows the time-of-flight (ns) *vs.* the total kinetic energy (MeV) for a sample of ions during a small ^{3}He-rich SEP event (see von Rosenvinge *et al.* 1995; Reames *et al.* 1997).

The resolution using this technique can be greatly improved by adding an additional timing plane, using electrostatic mirrors to reflect the electrons, and using microchannel plates with position-sensing anodes. This was done for the ULEIS instrument on the ACE spacecraft (Mason *et al.* 1998). This instrument produced the resolution seen in Figure 4.16.

7.4 NOAA/GOES

The *Geostationary Operational Environmental Satellites* (GOES), operated by the *National Oceanic and Atmospheric Administration* (NOAA), are a series of satellites intended to give continuous time coverage of the space environment. A new GOES spacecraft with equivalent capabilities is launched every few years.

Energies of interest for SEP observations are proton energies in five channels from 4 to 500 MeV measured by two-element telescopes behind different thicknesses of shielding in the *Energetic Particle Sensor* (EPS). In addition, the *High Energy Proton and Alpha Detector* (HEPAD) adds a Cherenkov detector to measure protons in the intervals 350 – 420, 420 – 510, 510 – 700, and >700 MeV. These are extremely useful high-energy measurements. GOES data since 1986 are available at http://satdat.ngdc.noaa.gov/sem/goes/data/new_avg/ (although the web site has been known to change). Note that the low-energy channels of the EPS should *not* be used for onset timing since they are contaminated by higher-energy particles. Geometry factors for high-energy particles are too uncertain to allow channel differences to exclude all contamination in EPS. However, GOES provides an excellent synoptic summary of SEP events (see Figure 5.1) and the >700 MeV channel may be a better indicator of a high-energy protons than neutron monitors (Thakur *et al*. 2016).

GOES also provides 1 – 8 Å soft X-ray peak intensities that is a classic measure of heating in solar flares. The X-ray "CMX class" specifies the decade of X-ray peak intensity with C*n* for $n \times 10^{-6}$ W m^{-2}, M*n* for $n \times 10^{-5}$ W m^{-2}, and X*n* for $n \times 10^{-4}$ W m^{-2} (*e.g.* see Figure 4.13).

7.5 High-Energy Measurements

Ground-level neutron monitors have provided the historic information on SEPs above ~0.5 GeV by observing the products that rain down from nuclear interactions of energetic protons with atomic nuclei of the upper atmosphere. When the signal from the SEPs can be seen above the background produced by galactic cosmic rays we have a ground-level event (GLE). However, many GLEs rise less than 10% above background, providing rather poor information on timing.

As noted previously, high-energy protons are often strongly beamed along the interplanetary magnetic-field line, so a particular neutron monitor on Earth sees an intensity maximum when its asymptotic look direction is aligned with that field. Since the field direction can vary, neutron monitors often see sudden increases or decreases, or even multiple peaks and valleys of intensity as their look direction scans across the pitch-angle distribution as the interplanetary magnetic-field direction swings around. Nevertheless, integrating over an event at multiple stations can produce creditable spectra, that compare well with those from GOES and IMP, as obtained by Tylka and Dietrich (2009) and shown in Figures 6.2 and 6.3. This was a significant advance in high-energy spectra.

Two newer instruments, the *Payload for Antimatter Exploration and Light-nuclei Astrophysics* (PAMELA) mission and the *Alpha Magnetic Spectrometer*

(AMS) are large complex instruments that were justified and funded for particle physics and cosmology, which may also prove useful for high-energy SEP measurements. These instruments use transition-radiation detectors, time-of-flight detectors, a permanent magnet and tracking system, Cherenkov systems, and calorimeters to measure each incident particle. They were designed to search for antimatter, such as anti-helium, strange quark matter, and dark matter.

The PAMELA satellite is in a near-polar, 70^{o}-inclination, orbit. It can measure protons and He above about 80 MeV amu^{-1} and reported spectra for the 13 December 2006 SEP event (Adriani *et al.* 2011) and for several events in 2010 – 2012 (Bazilevskaya *et al.* 2013). AMS is on the *International Space Station*. It can measure protons and isotopes of light ions above about 200 MeV amu^{-1}.

While these instruments must deal with geomagnetic-field limitations, as neutron monitors do, they can directly measure spectra and abundances and represent a great improvement in the accuracy of measurements at high energies.

7.6 Problems and Errors

The single most difficult problem in measuring SEPs is exploring rare species and small events while still dealing with the high intensities in large events. Most high-resolution instruments fail or degrade during periods of *high SEP intensity*.

Early instruments sampled particles randomly and sent the measurements to the ground for analysis. However, since telemetry was slow and the H/O ratio can exceed 10^4 at fairly high energies, H and He consumed all the telemetry and heavy ions were almost never seen. Later instruments incorporated priority schemes to distinguish H, He, and "heavies" and selectively telemetered them at different priorities, keeping track of the number received onboard for re-normalization. Most modern instruments determine particle species and energy and bin them onboard in most cases. The higher onboard processing rates have allowed geometry factors to profitably expand, improving statistics and observing rare species.

As rates increase, the first problem to solve involves "dead-time corrections." An instrument cannot process a new particle while it is still busy processing the previous one. Knowing the processing times, these corrections are usually already made while calculating intensities. However, it does make a difference whether the telescope has become busy because too many high-energy particles traverse the anticoincidence detector, or because too many low-energy particles are striking the front detector. Some instruments can determine coincidence and priority at high rates before they decide to perform the slower pulse-height analysis; they can handle much higher throughput. Instruments that must pulse-height analyze every above-threshold signal in every detector are more limited in speed, by factors of 10 or more, since many of the pulse heights are not of interest; perhaps they do not even meet the coincidence conditions.

Eventually, problems come from multiple particles in the telescope within the resolution time. A proton stops in the back detector and triggers the coincidence while a low energy Fe stops in the front detector, or while an energetic He or

heavier ion crosses the front detector at some large angle. Background in LEMT during the first day of the Bastille-Day SEP event on 14 July 2000 is shown in Figure 7.8. Background stretches all the way up the ordinate in the 2< E < 20 MeV band. Calibration curves that are shown have omitted the 2.5 – 3.3 MeV amu^{-1} interval which would extend into this band. The added background not only contaminates measurements but also reduces the time available for real particles. Fortunately this is a rare problem for LEMT and it fails quite gracefully in this case, *i.e.* abundances and spectra above 3.3 MeV amu^{-1} are still quite useful.

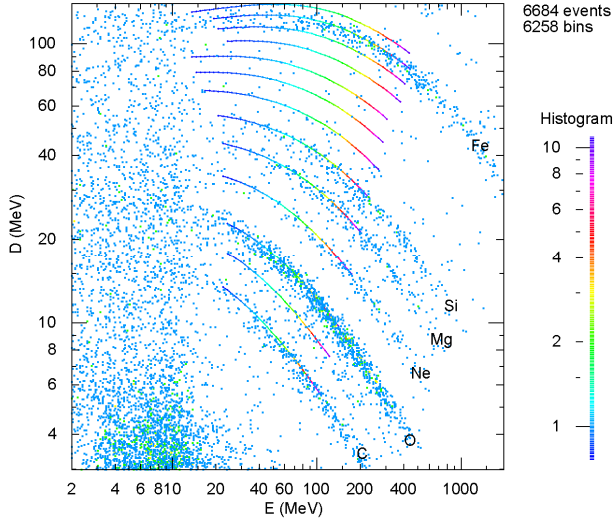

Fig. 7.8. Sampled response of LEMT is shown during the first day of the Bastille-Day event, 14 July 2000. Calibration curves are only shown from 3.3 – 10 MeV amu^{-1}, to emphasize the band of background covering the region where the 2.5 – 3.3 MeV amu^{-1} interval would be. Compare the region 2 < E < 20 MeV with that in Figure 7.3.

The upper limit of E of the background band in LEMT occurs because it is difficult for a proton, the most abundant species, to deposit more than 10 or 15 MeV into the E detector before penetrating into the anticoincidence detector.

One easy way to detect background is to check for unrealistic abundances, such as measurable ratios F/O or B/O. *If you discover something really unusual, it is wise to check the pulse-height matrix before publishing your new finding*.

Different instruments have different problems and some have interesting solutions. Some early instruments suffered gain changes in large events so the particle tracks moved around with time. *Many* instruments saturate at high particle rates, the smaller, faster instruments on GOES and *Helios* do not. ULEIS has a restricting aperture that can be rotated into place to reduce intensities. Other telescopes turn off detector elements to reduce their geometry factor.

The data base for many measurements from many spacecraft, including SEP intensities, is http://cdaweb.gsfc.nasa.gov/sp_phys/. Generally, however, pulse-height data are not widely available, since the more-extensive data and specialized processing and software required are only developed by the instrument teams. This software is generally not modified to keep up with evolution of computer hardware and operating systems.

References

Adriani, O., Barbarino, G. C., Bazilevskaya, G. A., Bellotti, R., Boezio, M., Bogomolov, E. A.; Bonechi, L., Bongi, M., Bonvicini, V., Borisov, S., *et al.*, Observations of the 2006 December 13 and 14 solar particle events in the 80 MeV n^{-1} – 3 GeV n^{-1} range from space with the PAMELA detector, Astrophys. J. **742**, 102 (2011)

Bazilevskaya, G. A., Mayorov, A. G., Malakhov, V. V., Mikhailov, V. V., Adriani, O., Barbarino, G. C.; Bellotti, R., Boezio, M., Bogomolov, E. A., Bonechi, L., *et al.*, Solar energetic particle events in 2006-2012 in the PAMELA experiment data, J. Physics: Conf. Series, **409**, 012188 (2013) DOI: 10.1088/1742-6596/409/1/012188

Hubert, F., Bimbot, R., Gauvin, H., Range and stopping-power tables for 2.5–500 MeV/nucleon heavy ions in Solids, Atom. Dat. Nucl. Dat. Tables **46**, 1 (1990)

Leske, R.A., Mewaldt, R.A., Cohen, C.M.S., Cummings, A.C., Stone, E.C., Wiedenbeck, M.E., von Rosenvinge, T.T., Solar isotopic composition as determined using solar energetic particles, Space Sci. Rev. **130**, 195 (2007)

Mason, G. M., Gold, R. E., Krimigis, S. M., Mazur, J. E., *et al.*, The Ultra-Low-Energy Isotope Spectrometer (ULEIS) for the ACE spacecraft, Space Sci. Rev. **86**, 409 (1998)

Paul, H., Schinner, A., Empirical stopping power tables for ions from ^{3}Li to ^{18}Ar and from 0.001 to 1000MeV/nucleon in solids and gases, Atom. Dat. Nucl. Dat. Tables **85**, 377 (2003)

Reames, D. V., Barbier, L. M., von Rosenvinge, T. T., Mason, G. M., Mazur, J. E., Dwyer, J. R., Energy spectra of ions accelerated in impulsive and gradual solar events, Astrophys. J. 483, 515 (1997)

Reames, D. V., Ng, C. K., Berdichevsky, D., Angular Distributions of Solar Energetic Particles , Atrophys. J. **550** 1064 (2001)

Stone, E. C., Cohen, C. M. S., Cook, W. R., Cummings, A. C., Gauld, B., Kecman, B., Leske, R. A., Mewaldt, R. A., Thayer, M. R., Dougherty, B. L., *et al.*, The Solar Isotope Spectrometer for the Advanced Composition Explorer, Space Sci. Rev. **86** 357 (1998)

Thakur, N., Gopalswamy, N., Mäkelä, P., Akiyama, S., Yashiro, S., Xie, H., Two exceptions in the large SEP events of solar cycles 23 and 24, Solar Phys. **291**, 513 (2016)

Tylka, A. J., Dietrich, W. F., A new and comprehensive analysis of proton spectra in ground-level enhanced (GLE) solar particle events, in *Proc. 31st Int. Cos. Ray Conf* , Lódz (2009), http://icrc2009.uni.lodz.pl/proc/pdf/icrc0273.pdf

von Rosenvinge, T. T., Barbier, L. M., Karsch, J., Liberman, R., Madden, M. P., Nolan, T., Reames, D. V., Ryan, L., Singh, S., Trexel, H., The Energetic Particles: Acceleration, Composition, and Transport (EPACT) investigation on the *Wind* spacecraft, Space Sci. Rev. **71** 152 (1995)

8. Summary and Conclusions

What is our current understanding of solar energetic particles (SEPs)?

1. All acceleration of the SEPs that we see in space occurs on *open* magnetic field lines**.** We also see γ rays and neutrons from nuclear reactions on closed field lines in solar flares, but no products of these nuclear reactions are ever seen in space. Neither the primaries nor the secondaries can escape from flares.
2. There are two SEP acceleration sites: *solar jets* and *CME-driven shock waves*. A) Impulsive SEP events, accelerated at solar jets, appear to involve two physical mechanisms, magnetic reconnection and wave-particle resonant absorption. Both produce striking, and identifiable, relative enhancements of abundances of chemical elements and isotopes. B) For gradual SEP events the dominant mechanism is acceleration by CME-driven shock waves, but the seed population may be complex and abundances are also modified by transport in this case.
3. *Impulsive SEP events* are small and brief. Solar jets, where acceleration occurs, are associated with slow, *narrow CMEs*. *Magnetic reconnection* in jets, sampling ions of 2 – 4 MK plasma in active regions, cause abundance enhancements rising as a steep *power law in A/Q* by factors up to ~1000 from He to Pb. *Wave-particle resonance* causes large, but variable, *enhancements in* $^3He/^4He$ by factors up to 10,000 and may sometimes cause rounded, steep, low-energy spectra of ions with gyro-frequencies near the second harmonic of the ^{3}He gyro-frequency. The waves may be generated by the copious streaming electrons that also produce type III radio bursts. Acceleration may occur below 1.5 R_S and ions may traverse enough material to attain equilibrium Q, but not enough to lose energy or disrupt the strong A/Q dependence that is seen.
4. *Gradual SEP events* are large, energetic, and intense, and have long durations and broad spatial extent approaching ~180°. They are associated with *fast*, *wide CMEs* that drive shock waves that accelerate ions from ambient coronal plasma of ~0.8 – 1.6 MK in ~69% of the events. In 24% of gradual events the shock waves pass through solar active regions where they sample a 2 – 4 MK seed population that includes ambient plasma laced with residual suprathermal ions from *multiple* small solar jets. The location of high-energy spectral breaks or knees depends upon both shock properties and A/Q of the ion species, causing complex abundance variations at high energies. Shock waves begin to form near 1.5 R_S, accelerating electrons that produce type II radio bursts; acceleration of SEPs begins above the magnetic loops by 2 – 6 R_S, depending upon longitude around the CME. The early shock acceleration of type II electrons may begin on closed magnetic loops.
5. *Self-amplified Alfvén waves become increasingly important in larger gradual SEP events.* Pitch-angle scattering by proton-amplified waves limits particle intensities at the *streaming limit*, alters initial element abundance ratios after onset, rapidly broadens angular distributions, and even flattens low-energy spec-

tra during the early intensity-plateau period. Preferential scattering of ions with lower *A/Q* during transport causes regions of relative *A/Q*-dependent abundance enhancements or depletions in space that evolve with time. This Q-dependence allows determination of the source plasma temperature. In contrast, non-relativistic electrons and particles from small impulsive SEP events travel scatter free.

6. Can we always distinguish impulsive and gradual events? Usually, but *not always*. Shocks often reaccelerate residual impulsive suprathermal ions with pre-enhanced abundances. Usually these are diluted by inclusion of ambient coronal plasma which moderate the enhancements, but not always. A few percent of SEP events, called "impulsive" because of their high Fe/O enhancement, for example, may actually have undergone reacceleration by a shock wave. However, our goal is not just to label each SEP event by type, but to understand the underlying physics.
7. Non-thermal event-to-event *variations* in abundances are *much smaller in gradual than in impulsive* SEP events, even when both sample active-region plasma. The seed population for shock acceleration in active regions must consist of a mixture of ambient plasma and residual suprathermal ions from *multiple* impulsive SEP events. Active regions can produce a profusion of multiple small jets (nanojets?) that provide a persistent, long-lived, and recurrent supply of ^{3}He-rich, Fe-rich energetic ions from jet sources that are too small to be resolved into individual SEP events. These are sampled by shock waves passing above active regions.
8. Reservoirs are large volumes of adiabatically-trapped SEPs seen late in gradual events. Particles are magnetically trapped between the CME and the Sun. Intensities of all species and energies are spatially uniform but all decrease with time as the trapping volume expands. Early workers mistook this slow decline as slow spatial diffusion. Reservoirs probably provide the energetic particles that slowly precipitate to produce long-duration, spatially-extensive, energetic γ-ray events when they scatter into the magnetic loss cone and interact in the denser corona below.
9. In large events, CMEs capture the largest share of magnetic energy released at the Sun and SEPs can acquire as much as ~15% of a CME's energy.

Thus, much of the mystery of SEP origin seems to be resolved. This progress has come almost entirely from the direct measurement of SEPs in space, especially from their abundances. The story is complex. It involves acceleration and reacceleration of ions that, nevertheless, carry measurable properties of their convoluted histories. We have identified the physical mechanisms that contribute to particle acceleration. What remains is to understand their detailed interplay. What parameters determine when and where each mechanism operates, and how can we predict their onset, their magnitude and their outcome?